

THIS REPORT HAS BEEN DELIMITED
AND CLEARED FOR PUBLIC RELEASE
UNDER DOD DIRECTIVE 5200.20 AND
NO RESTRICTIONS ARE IMPOSED UPON
ITS USE AND DISCLOSURE.

DISTRIBUTION STATEMENT A

APPROVED FOR PUBLIC RELEASE;
DISTRIBUTION UNLIMITED.

UNCLASSIFIED

AD _____

*Reproduced
by the*

ARMED SERVICES TECHNICAL INFORMATION AGENCY
ARLINGTON HALL STATION
ARLINGTON 12, VIRGINIA



DECLASSIFIED
DOD DIR 5200.9

UNCLASSIFIED

Armed Services Technical Information Agency

Because of our limited supply, you are requested to return this copy WHEN IT HAS SERVED YOUR PURPOSE so that it may be made available to other requesters. Your cooperation will be appreciated.

AD

46351

NOTICE: WHEN GOVERNMENT OR OTHER DRAWINGS, SPECIFICATIONS OR OTHER DATA ARE USED FOR ANY PURPOSE OTHER THAN IN CONNECTION WITH A DEFINITELY RELATED GOVERNMENT PROCUREMENT OPERATION, THE U. S. GOVERNMENT THEREBY INCURS NO RESPONSIBILITY, NOR ANY OBLIGATION WHATSOEVER; AND THE FACT THAT THE GOVERNMENT MAY HAVE FORMULATED, FURNISHED, OR IN ANY WAY SUPPLIED THE SAID DRAWINGS, SPECIFICATIONS, OR OTHER DATA IS NOT TO BE REGARDED BY IMPLICATION OR OTHERWISE AS IN ANY MANNER LICENSING THE HOLDER OR ANY OTHER PERSON OR CORPORATION, OR CONVEYING ANY RIGHTS OR PERMISSION TO MANUFACTURE, USE OR SELL ANY PATENTED INVENTION THAT MAY IN ANY WAY BE RELATED THERETO.

Reproduced by
DOCUMENT SERVICE CENTER

88503

AERO REPORT 853

AD No. 4935
ASTIA FILE COPY

NAVY DEPARTMENT
THE DAVID W. TAYLOR MODEL BASIN
AERODYNAMICS LABORATORY
WASHINGTON 7, D.C.

WIND-TUNNEL TESTS OF A 1/48-SCALE MODEL OF THE XZS24-1
AIRSHIP WITH VARIOUS TAIL CONFIGURATIONS

PART I - LONGITUDINAL AND DRAG CHARACTERISTICS

by

Arnold W. Anderson and Samuel J. Flickinger, Jr.

TED No. TMB AD-3110
(Formerly DE-3110)

"This document contains information affecting the national defense of the United States within the meaning of the Espionage Laws, Title 18, U.S. C., Sections 793 and 794. The transmission or the revelation of its contents in any manner to an unauthorized person is prohibited by law."

"Reproduction of this document in any form by other than naval activities is not authorized except by special approval of the Secretary of the Navy or the Chief of Naval Operations as appropriate."

8

September 1954

NAV 8 9 1954

54AA

72247

CONFIDENTIAL

BEST AVAILABLE COPY

**NOTICE: THIS DOCUMENT CONTAINS INFORMATION AFFECTING THE
NATIONAL DEFENSE OF THE UNITED STATES WITHIN THE MEANING
OF THE ESPIONAGE LAWS, TITLE 18, U.S.C., SECTIONS 793 and 794.
THE TRANSMISSION OR THE REVELATION OF ITS CONTENTS IN
ANY MANNER TO AN UNAUTHORIZED PERSON IS PROHIBITED BY LAW.**

Reproduced
FROM LOW CONTRAST COPY.

TABLE OF CONTENTS

	Page
SUMMARY	1
INTRODUCTION	2
MODEL	3
TESTS	5
RESULTS	7
DISCUSSION	8
LONGITUDINAL STABILITY	9
LONGITUDINAL CONTROL CHARACTERISTICS	17
HINGE-MOMENT CHARACTERISTICS	20
REFERENCES	22

Table

PRINCIPAL MODEL CONSTANTS USED IN DATA REDUCTION FOR THE 1/48-SCALE MODEL XZS2G-1 AIRSHIP	1
COMPARISON OF THEORETICAL AND MEASURED LIFT CHARACTERISTICS FOR VARIOUS TAIL CONFIGURATIONS OF THE 1/48-SCALE MODEL XZS2G-1 AIRSHIP	2
ELEVATOR EFFECTIVENESS OF VARIOUS TAIL CONFIGURATIONS ON A 1/48-SCALE MODEL XZS2G-1 AIRSHIP	3
EFFECT OF ELEVATOR DEFLECTION UPON THE CHARACTERISTICS OF A 1/48-SCALE MODEL XZS2G-1 AIRSHIP	4
COMPARISON OF CALCULATED AND EXPERIMENTAL VALUES OF HINGE MOMENTS FOR 1/48-SCALE MODEL XZS2G-1 AIRSHIP	5

Figure

PRINCIPAL DIMENSIONS OF THE 1/48-SCALE MODEL XZS2G-1 AIRSHIP	1
---	---

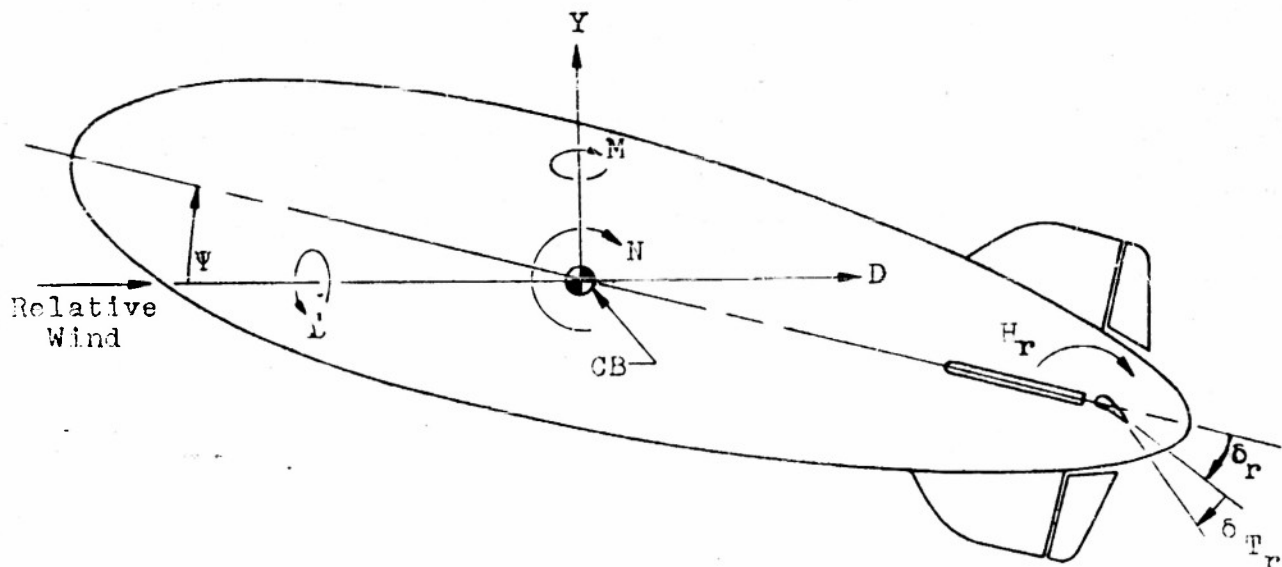
TABLE OF CONTENTS (Continued)

	Figure
PRINCIPAL DIMENSIONS OF THE CONVENTIONAL TYPE TAIL ON THE 1/48-SCALE MODEL XZS2G-1 AIRSHIP	2
PRINCIPAL DIMENSIONS AND ARRANGEMENT OF THE X-TAIL ON THE 1/48-SCALE MODEL XZS2G-1 AIRSHIP	3
PRINCIPAL DIMENSIONS AND ARRANGEMENT OF THE A-TAIL ON THE 1/48-SCALE MODEL XZS2G-1 AIRSHIP	4
PRINCIPAL DIMENSIONS OF THE HORIZONTAL H-TAIL ON THE 1/48-SCALE MODEL XZS2G-1 AIRSHIP	5
PARTIAL CROSS SECTION OF 1/48-SCALE MODEL XZS2G-1 AIRSHIP SHOWING FLEXURE-PLATE MOUNTING	6
CLOSE-UP OF UPPER SURFACE OF A-TAIL ON THE 1/48-SCALE MODEL XZS2G-1 AIRSHIP	7
PHOTOGRAPHS OF 1/48-SCALE MODEL XZS2G-1 AIRSHIP MOUNTED IN WIND TUNNEL FOR PITCH TESTS	8
SCHEMATIC DRAWING OF VARIOUS TAIL ARRANGEMENTS ON 1/48-SCALE MODEL XZS2G-1 AIRSHIP VIEWED FROM REAR	9
EFFECT OF COMPONENT PARTS ON LONGITUDINAL CHARACTERISTICS OF A 1/48-SCALE MODEL XZS2G-1 AIRSHIP	10
EFFECT OF ELEVATORS ON LONGITUDINAL CHARACTERISTICS OF A 1/48-SCALE MODEL XZS2G-1 AIRSHIP	11
EFFECT OF X-TAIL DIHEDRAL ON LONGITUDINAL CHARACTERISTICS OF A 1/48-SCALE MODEL XZS2G-1 AIRSHIP	12
EFFECT OF ELEVATOR AND TAB ON LONGITUDINAL CHARACTERISTICS OF A 1/48-SCALE MODEL XZS2G-1 AIRSHIP	13
EFFECT OF TAB DEFLECTION ON LONGITUDINAL CHARACTERISTICS OF A 1/48-SCALE MODEL XZS2G-1 AIRSHIP	14

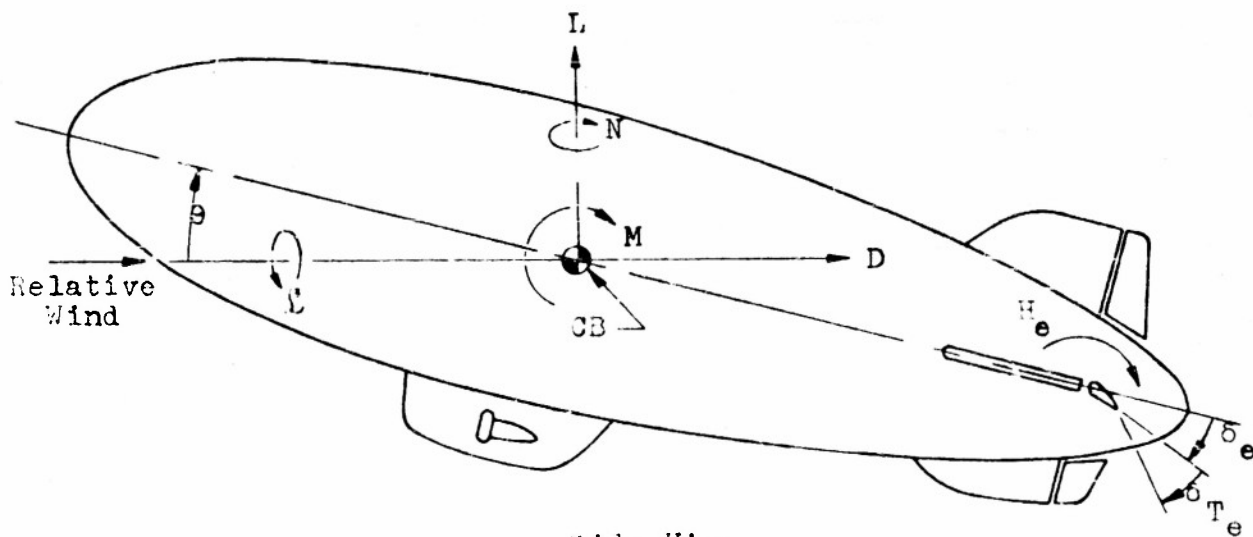
TABLE OF CONTENTS (Concluded)

	Figure
VARIATION OF WETTED-AREA COEFFICIENT WITH REYNOLDS NUMBER FOR SEVERAL CONFIGURATIONS OF A 1/48-SCALE MODEL XZS2G-1 AIRSHIP	15
COMPARISON OF BODY GEOMETRY OF SEVERAL AIRSHIP ENVELOPES	16
VELOCITY OF AIR IN BOUNDARY LAYER OF AN AIRSHIP	17
PITCHING MOMENT DIRECTLY ATTRIBUTABLE TO THE TAIL OF AN AIRSHIP	18
PITCHING MOMENT DUE TO TAIL ON A 1/48-SCALE MODEL XZS2G-1 AIRSHIP	19
TAIL-LIFT COEFFICIENTS FOR THE VARIOUS TAILS ON A 1/48-SCALE MODEL XZS2G-1 AIRSHIP	20
VARIATION OF DRAG WITH PITCH FOR TRIM CONDITION OF A 1/48-SCALE MODEL XZS2G-1 AIRSHIP	21
VARIATION OF LIFT WITH PITCH FOR TRIM CONDITION OF A 1/48-SCALE MODEL XZS2G-1 AIRSHIP	22
PITCHING MOMENT DUE TO ELEVATOR DEFLECTION ON A 1/48-SCALE MODEL XZS2G-1 AIRSHIP	23
ELEVATOR ANGLE REQUIRED FOR TRIM ON A 1/48-SCALE MODEL XZS2G-1 AIRSHIP	24
VARIATION OF ELEVATOR HINGE-MOMENT COEFFICIENT WITH δ_e VERSUS PITCH ANGLE ON A 1/48-SCALE MODEL XZS2G-1 AIRSHIP	25
ELEVATOR FLOATING ANGLE ON A 1/48-SCALE MODEL XZS2G-1 AIRSHIP	26
ELEVATOR HINGE MOMENT REQUIRED FOR TRIM ON A 1/48-SCALE MODEL XZS2G-1 AIRSHIP	27
VARIATION OF ELEVATOR HINGE-MOMENT COEFFICIENT WITH S_T VERSUS PITCH ANGLE ON A 1/48-SCALE MODEL XZS2G-1 AIRSHIP	28

Positive Directions of Axes, Forces, Moments, and
Angular Displacements are Shown by Arrows



Top View



Side View

Axis	Force in pounds	Force Coefficient	Moment in pound-feet	Moment Coefficient
D	D	$C_S = D/q(\text{Vol.})^{2/3}$	L (rolling)	$C_l = L/q(\text{Vol.})$
Y	Y	$C_{SS} = Y/q(\text{Vol.})^{2/3}$	M (pitching)	$C_m = M/q(\text{Vol.})$
L	L	$C_L = L/q(\text{Vol.})^{2/3}$	N (yawing)	$C_n = N/q(\text{Vol.})$
Hinge	-	-----	H (hinge)	$C_h = H/qS\bar{c}$

General Symbols

Vol.	volume of main envelope in cubic feet
q	dynamic pressure ($\rho V^2/2$) in pounds per square foot
V	airspeed in feet per second
V_1	airspeed in knots
R	Reynolds number $\rho V(\text{Vol.})^{1/3}/\mu$
ρ	mass density of air in slugs per cubic foot
μ	absolute coefficient of viscosity of air in pound-second per square foot
CB	center of buoyancy
SR	slenderness ratio
\bar{c}	root-mean-square chord of control surface aft of hinge line in feet
S_e, S_r	control surface area (including hinge overhang) in square feet
S_t	horizontal tail area outside envelope in square feet
S_v	vertical tail area outside envelope in square feet
S_T	tab area in square feet
W	surface area in square feet
C_w	wetted-area coefficient D/qW
R	main envelope
C	car with cylindrical radome attached
C_E	car with elliptical radome
H	horizontal tail
V	vertical tail

54AA

72247

Angular Settings

θ	angle of pitch in degrees (angle between the airship reference line and the projection of the relative wind vector on the plane of symmetry of the airship)
ψ	angle of yaw in degrees (angle between relative wind vector and plane of symmetry of the airship)
δ	angle of control surface deflection in degrees, measured in a plane perpendicular to the hinge line
Γ	dihedral angle in degrees (angle between airship horizontal plane of symmetry and the plane of the tail surface)

Subscripts

e	elevator
r	rudder
t	tail
T	tab
C	conventional tail arrangement
X	X-tail arrangement
A	inverted Y-tail arrangement
H	H-tail arrangement
RL	lower vertical fin removed

AERODYNAMICS LABORATORY
DAVID TAYLOR MODEL BASIN
UNITED STATES NAVY
WASHINGTON, D. C.

WIND-TUNNEL TESTS OF A 1/48-SCALE MODEL OF THE XZS2G-1
AIRSHIP WITH VARIOUS TAIL CONFIGURATIONS

PART I - LONGITUDINAL AND DRAG CHARACTERISTICS

by

Arnold W. Anderson and Samuel J. Flickinger, Jr.

SUMMARY

A series of tests has been conducted to determine the aerodynamic characteristics of several types of tail configurations when mounted on a given airship envelope. The tests included force-coefficient results on the entire model due to model pitch, elevator deflection, and elevator-tab deflection. Elevator-hinge-moment data were also taken for the above variables.

The results indicated that all tail configurations contribute approximately the same increment to stability for the entire range of pitch investigated. The H-tail configuration of the complete airship had approximately 35 percent more drag near zero yaw, as compared to other tail configurations. All tail-elevator combinations were capable of trimming the model when the moments due to engine thrust and differences

CONFIDENTIAL

between center of gravity and center of buoyancy are neglected, with the H-tail configuration requiring a 20° elevator deflection and the A-tail requiring a 10° elevator deflection. These were the maximum and minimum deflections required for the tails investigated.

Stick-free elevator angles remained within a limit of $\pm 3.5^\circ$ throughout most of the pitch range investigated for all tail configurations.

INTRODUCTION

The XZS2G-1 airship configuration was established using the results from a series of airships that were previously tested at the Taylor Model Basin (Reference 1). The Bureau of Aeronautics in Reference 2 requested that the Model Basin investigate the controllability and stability of the airship to develop the optimum empennage arrangement. The current designation of the XZS2G-1 airship (formerly the XZP and ZP5K airship) was assigned by Reference 3.

This report presents the results of the longitudinal tests conducted on a 1/48-scale model of the XZS2G-1 airship, with an envelope slenderness ratio of 4.17. These tests were made to investigate the aerodynamic characteristics of four basic tail-envelope configurations and the effect on these characteristics of two car-radome combinations. The discussion of results is rather lengthy but was felt to be necessary as the data are of interest for general application as well as for specific

application on the model investigated. The tests were conducted between the dates of 21 April and 9 May 1952. Advance copies of the data were furnished to interested parties, including the Bureau of Aeronautics representatives, soon after completion of the tests.

MODEL

The 1/48-scale model of the XZS2G-1 Airship was designed and built at TMB from drawings furnished by the Goodyear Aircraft Corporation. Previous tests (Reference 1) indicated that force results could be very erratic if the model was too small, but excessive tunnel blockage would result if the model was too large. Therefore, a compromise of 1/48-scale was chosen.

The principal-dimension drawings of the model and a sketch of the internal mounting are shown in Figures 1 through 6. Principal dimensions are shown in Table 1. Photographs of the model mounted in the tunnel in various configurations are shown in Figures 7 and 8. The fuselage-form equation is as follows:

$$Y = R \left[1.02062 - 0.21263 \frac{x}{a} \right] \sqrt{1 - \left(\frac{x}{a} - 0.2 \right)^2}$$

where

- Y envelope radius at distance x
- R maximum envelope radius
- a envelope half length
- x distance from maximum-diameter section
(negative when forward)

To meet the test requirements a hollow fuselage was built using rib formers at several stations and mahogany planking. Two ribs near the center of the fuselage were equipped with thin stainless-steel webs which acted as flexure plates for making drag tests and also provided a means of attaching the model to a rigid strut used in force tests.

The tails (Figure 9), car, and elliptical radome were readily removable. There were two radomes tested, a cylindrical and an elliptical. The tails were attached to the model by means of steel pins which mated with a steel ring built as an integral part of the main fuselage. The tails could then be positioned at any of several prepared locations around the envelope, thus providing a rigid assembly for the tails and also maintaining a smooth external envelope surface.

The tails were built of mahogany and had variable-incidence, plain flaps and trimmer-type trailing-edge tabs. Ball bearings were used at the hinges of those flaps (Figure 9) on which hinge moments were to be read, and pin hinges were used on the other flaps. The incidence of the tabs was changed by bending the soft steel pins which were used as tab hinges. All flap and tab angles were set with templates.

The car was constructed in duplicate with one model used for drag and force tests and one used for pressure tests. On the latter car a cylindrical radome was separately removable.

TESTS

The tests were conducted in the TMB 8- by 10-foot Wind Tunnel 2, which is an atmospheric, closed throat, return-type tunnel.

Two phases were included in the model tests. One phase, a drag-Reynolds-number investigation, was directed toward obtaining an accurate value of model drag for several configurations at 0° pitch and yaw, for a range of Reynolds numbers. The other phase, a stability investigation, was directed toward finding the variation of forces and moments on the model throughout a range of pitch and yaw at a constant Reynolds number.

It was necessary in the drag-Reynolds-number investigation to use a support system with a minimum amount of interference. To provide this, a sting type of support system was used which entered the model from the rear. The sting was supported on the tunnel floor through a series of spiderlike legs and attached to the model through the diaphragms shown in Figure 6. This allowed freedom of movement of the model along the sting or drag axis. The model was set at 0° pitch and yaw for the drag tests. Drag forces were measured by means of a previously calibrated beam which had two strain gages attached to it. Model configurations investigated during the drag tests included bare envelope; envelope with car; and the several combinations of envelope, car, and tail.

The stability investigation was conducted using a single support. The model was mounted on its side and pitched in a horizontal plane. In general, each tail type was investigated to find the following values:

1. Contribution to model longitudinal stability with the car on and off
2. Elevator effectiveness with car on and off
3. Elevator effectiveness when operating with a trimmer-type tab on a 1:1 elevator/tab ratio, with car on
4. Tab effects on aerodynamic coefficients at elevator deflections of 0° and 20°
5. Variation of elevator hinge moment for the various model, elevator, and tab deflections

The effect on model characteristics of changing tail dihedral angle was investigated for the X-tail configuration. Two dihedral angles, 45° and 37.5° with respect to a line perpendicular to the plane of symmetry, were investigated. These angles were set by rotating the tail about the longitudinal center line of the model. Elevator effectiveness was investigated for both angles.

The drag-Reynolds-number tests were conducted through an airspeed range of 17.3 knots to 112.0 knots corresponding to Reynolds numbers from 1,000,000 to 6,700,000, based on a model length of 5.87 feet rather than $(\text{volume})^{1/3}$.

The force tests were conducted at a dynamic pressure of 50.0 pounds per square foot which corresponds to an airspeed of approximately 123 knots and a Reynolds number of approximately 2,330,000, based on a value of 1.85 feet for (volume)^{1/3}.

The range of angular variables investigated was as follows:

$$\theta = \pm 15^\circ$$

$$\delta_e = 0^\circ \text{ to } 30^\circ$$

$$\delta_{T_e} = 0^\circ \text{ to } 40^\circ$$

RESULTS

The test data are presented in the form of plots showing the variation of force and moment coefficients (see notation) with pitch angle in Figures 10 through 14 and the variation of wetted-area coefficient with Reynolds number in Figure 15. The test results are presented in Figures 16 through 28 as various cross plots based on the test data or theoretical considerations.

Principal model constants used in data reduction are given in Table 1. A schematic drawing showing positive deflection of flaps and tabs when acting as control surfaces is shown in Figure 9.

Two tunnel corrections were added to the drag-Reynolds-number test data. They include a buoyancy and a blockage and wake correction. The corrections are defined as follows:

$$\Delta C_{W_{buoy}} = 0.0010$$

$$C_{W_{true}} = 0.987 (C_{W_{tun}} + \Delta C_{W_{buoy}}) \quad (\text{Reference 4})$$

where $C_{W_{tun}}$ is wetted-area coefficient based on original drag measured in tunnel (see notation sheet).

Three corrections were added to the force data. They include tare and interference corrections, a buoyancy correction and a blockage and wake correction.

$$C_S = 0.987 (C_S' + 0.0058 + \text{tare and interference})$$

where 0.987 is the wake and blockage factor, C_S' is uncorrected tunnel coefficient, and 0.0058 is the buoyancy correction. All data have been transferred to a center-of-buoyancy location 45.7 percent of the fuselage length aft of the nose.

The model nomenclature used is given in the notation.

DISCUSSION

The discussion that follows includes a commentary on three aspects of the XZS2G-1 airship tests with several tail surfaces. These are longitudinal stability, longitudinal control, and control hinge moments. There is some degree of similarity between tails and there are certain data available from which calculated comparisons can be made. The comparisons with calculated data are made to verify the applicability of these results. Where disagreement is found, an explanation is sought;

where no outside data are available for direct application, some analysis is sought through theory. It is felt that some additional value can be given to the results, other than direct application to the envelope form used, by divorcing and analyzing the effect of each tail on the model coefficients. Also, comparison of the tail parameters with previous tests or theory will tend to give a designer more confidence in calculated parameters if there is good agreement.

LONGITUDINAL STABILITY -- The old question is here raised again: How much tail area should be added to an envelope to obtain a given value of static longitudinal stability? Three values are required for a solution: horizontal-tail lift-curve slope, dynamic pressure in the vicinity of the tail, and angle of attack of the tail surface. The lift-curve slope will be compared and reconciled with calculated values from various sources and the references will be cited in the discussion. Munk (Reference 5) has pointed out that it is impossible to arrive at a definite conclusion as to the value of the latter two parameters. Methods that have been used in the past will be pointed out here, and will be explained and references cited in the discussion.

Tail Dynamic Pressure and Angle of Attack -- The dynamic pressure acting on the tail surface can be approximated very closely using Millikan's boundary-layer equations, Reference 6, if the static pressure variation on the envelope

in the vicinity of the tail is known. This, however, has to be found experimentally. The angle of relative wind acting on the tail is dependent on sidewash due to the fuselage. It is impossible to predict the value of sidewash, but this can also be found experimentally by varying the fin angles for a series of runs. (See Figure 9 of Reference 7 for magnitude of sidewash.) Neither the pressure tests nor the various fin-setting tests were attempted on the model. It is possible, however, using the data from previous tests of a similar nature, to estimate fairly accurately the thickness of the boundary layer in the vicinity of the tails. References 8 and 9 show the boundary-layer thickness with position downstream on a model airship. However, geometric similarity in the vicinity of the tail seems to be most closely approximated by the short body of Reference 9 as shown in Figure 16. The parameters $\frac{r}{r_0}$ and $\frac{a}{L}$ were chosen as the important geometric characteristics, as the boundary-layer thickness in the vicinity of the tail has been found to be most closely related to these parameters (References 8 and 9). The thickness is not a function of Reynolds number (Reference 10) for the Reynolds number of these tests.

It is assumed that the velocity profile in the boundary layer varies as the one-seventh power (turbulent flow) of the ratio of the distance to the point of interest (measured perpendicular to the envelope) over the total boundary-layer thickness times free-stream velocity. If this is true, a profile similar

to that shown in Figure 17 probably exists near the airship in the vicinity of the model tails. The value of 1.4 inches for thickness of the boundary layer was arrived at using Figure 4 of Reference 8 and Figure 6 of Reference 9.

Now the question of the effect of the boundary layer on the stability of the airship still exists. It is assumed that the slope of the lift curve and center of pressure of the tail sections exposed to the boundary layer are the same as those not exposed to the boundary layer. The percentage change in $\frac{\partial C_m}{\partial \theta}$ for the airship is indicated in the table below, using an average of 0.88 times free-stream velocity for the velocity in the boundary layer.

Tail	Percentage Change
C	- 9.3
X	- 9.3
A	- 7.8
H	-10.5

With the small differences in slopes between tails shown above, a discussion intended for comparison of the merits of each tail can neglect the boundary-layer effects.

Lift-Curve Slopes of Tails -- As explained in the model description, several types of tails were investigated, some of which were set at large dihedral angles. The question immediately arises, on a test of this nature, of how a change in tail dihedral angle would affect the model stability. Neglecting secondary effects, the following facts are known: the true angle

of attack of the lifting surface is approximately equal to the model angle of attack times the cosine of the dihedral angle, Γ ; and the component of tail-lift force which contributes to model stability is equal to the lift in a plane perpendicular to the chordal plane times the cosine of the dihedral angle. It is now evident that the contribution to stability which is directly attributed to the tail varies approximately as $\cos^2 \Gamma$. This neglects the change in tail aspect ratio with Γ .

As stated above, the cosine-squared rule applies; however, with the addition of the tail, the change in model pitching moment is not entirely due to the tail forces (Reference 11). The pressure increments on the tail tend to carry over onto the fuselage. The ratio of ΔC_m due to the tail forces to total ΔC_m due to installation of the tail is shown in Figure 18, which was calculated using the values shown in Figure 14 of Reference 11. The information in Figure 18 is particularly applicable to a conventional type of tail, but in this analysis has been applied directly to all the tail data except the H-type tail, where the following empirical formula was applied:

$$C_m \text{ (due directly to H-tail)} = \Delta C_{m_H} - (1.00 - \Delta C_{m_p}) \Delta C_{m_C}$$

where

$$\Delta C_{m_H} = C_{m_{B(HV)_H}} - C_{m_B} \quad (\text{Figure 10d})$$

ΔC_{m_p} is given in Figure 18

$$C_{m_C} = C_{m_{B(HV)_C}} - C_{m_B} \quad (\text{Figure 10a})$$

This formula was applied to compensate for end plating.

In Figure 19 is shown the total change in pitching moments with the addition of each tail for both the car-off and car-on configurations. Comparison reveals small differences due to the car. Applying the data of Figure 18 to Figure 19, one obtains the dashed lines representing that portion of the model pitching moment which is due directly to the tail forces. Using these data, the actual lift coefficients were calculated and are presented in Figure 20. The tail-lift coefficients were calculated assuming free-stream velocity and an area equal to the tail area extending beyond the envelope line multiplied by $\cos^2 \Gamma$. The aerodynamic center of the tail was assumed to fall at Station 63.5, which is at the trailing edge of the stabilizer. This is not strictly true but was considered sufficiently accurate for comparative purposes. Sidewash effects were not negligible as shown in Figure 9 of Reference 7, but they were omitted in these results.

H. R. Lawrence has presented a means of computing the lift-curve slope of low-aspect-ratio wings in Reference 12. Using Figure 2 of Lawrence's paper, we can estimate the approximate slope for surfaces tested without end plates. It is necessary, however, in order to make the comparison, to compute the aspect ratio of the tails. In most aircraft work it is assumed that the lift continues through the fuselage. Figure 18, however, indicates that a varying ratio of the load is carried by the portions of the tail included inside the fuselage.

For purposes of estimation it will be assumed that the tail aspect ratio is equal to $\frac{b^2}{S}$ where b is the geometric distance between tips and S is the total projected tail area between tips as shown in Table 2. The value of dC_L/da for the H-tail was obtained from Reference 13. As seen from the table, there is no duplication in aspect ratio for the various tail models investigated. Reference 14 indicates that the lift-curve slope increases with aspect ratio in agreement with theory. In those tests, however, all tails were of the conventional type.

As mentioned previously, a portion of the moment attributed to the tail is carried by the fuselage owing to a pressure carry-over from the tail. With a conventional-type tail this effect is the same for both positive and negative angles and its value is known from the NACA tests (Figure 18).

When this same tail is rotated 45° , two counteracting effects come into play. First, the effective aspect ratio of the tails is decreased, which would tend to decrease the lift-curve slope. Secondly, there was the assumption in converting the change in model pitching moment to tail-lift coefficient, that a certain percentage of the pitching-moment change was due directly to the tails. The basis for this assumption is already known. With fins projecting out at 45° to the horizontal, there is a strong possibility that the fuselage no longer acts as a partial end plate. It is possible that a larger portion of the tail pressure forces are actually carried over onto the fuselage.

This effect would tend to counteract the decrease in aspect ratio mentioned earlier. The reader should remember that the pressure carry-over for this case, as in the conventional type, is the same for both positive and negative angles of attack.

The Λ -type tail has an aspect ratio between that of the other two tails. It is unsymmetrical about the horizontal center line of the model. From the standpoint of aspect ratio, a lift-curve slope somewhere between that of the first two tails mentioned is dictated. Considering position of the tail on the fuselage, advantages have been gained over the conventional tail from a standpoint of pressure carry-over. However, the lift curve may not be symmetrical around the zero angle of pitch, depending on the relative effectiveness with which positive and negative pressures carry over onto the envelope. Also, for the negative model angles, the tail may be partially shielded by the envelope.

A comparison of predicted and actual lift-curve slopes of the tails shown in Table 2 indicates quite a margin of error in the cases of the conventional and Λ -type tails. The predicted results are definitely high as they assume that those portions of the tail passing through the fuselage carry a load approximately proportional to their area. The conventional tail deviated farthest from the predicted slope, with the Λ -tail coming next and finally the X-tail, which is in fairly good agreement. The Λ -tail curve is not symmetrical but shows a

tendency for decreasing slope in the negative range of angles (Figure 20). The direct comparison of slopes in this region should not be made as the tail forces on the Λ -type tail were difficult to estimate..

In the H-type tail, there apparently was a poor flow condition or premature stall due to low Reynolds number. At the low angles it seemed to meet predicted slope but as the angle of pitch increased above 4° , the tail lift-curve slope decreased to a value which is about equal to that of the other tails (Figure 20). For other reasons also, to be mentioned later, this design did not seem satisfactory.

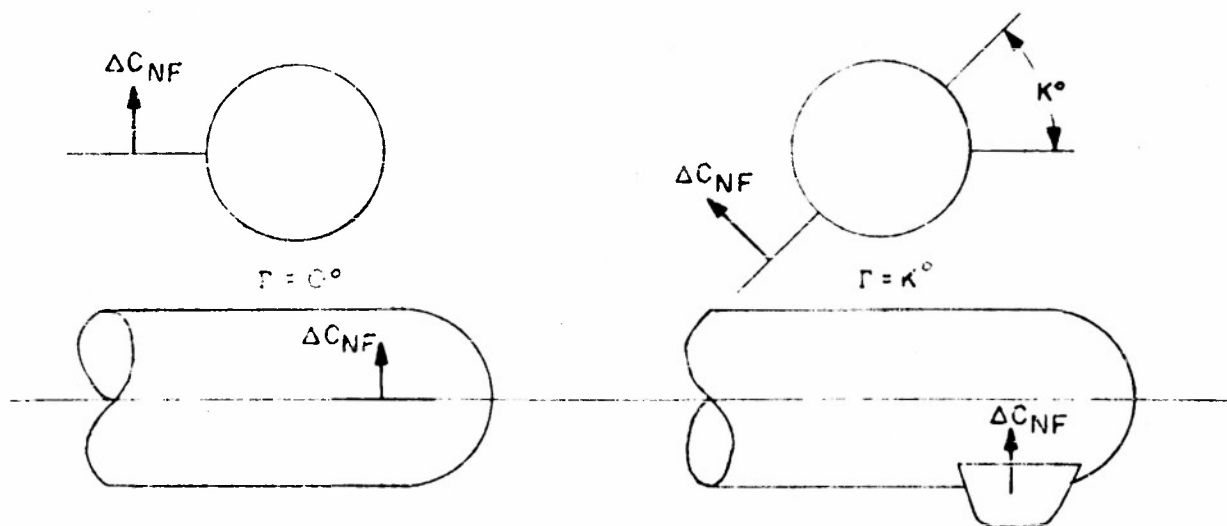
Cross plots of the drag and lift on the model for the trimmed condition are presented in Figures 21 and 22. The drag plots indicate little difference between the various configurations. The Λ -type tail has the least drag throughout the range investigated. In the lift plot the Λ -type tail configuration has the largest value of $\partial C_L / \partial \theta$. From a comparison of only these two plots, the Λ -type tail seems best suited from an aerodynamic point of view.

Tail Dihedral-Angle Effects == In Figure 12 the results of a test to investigate the effect of dihedral are presented. The ratio of the changes in pitching-moment slope with the addition of the tails should vary directly as $\cos^2 \Gamma$. This was not the case, however, for the X-tail investigated. The pitching-moment slope did not drop off as fast as $\cos^2 \Gamma$, which indicates that other factors were coming into play.

LONGITUDINAL-CONTROL CHARACTERISTICS -- The tail configurations tested were able to trim the model over a range of pitch angles. This does not mean, however, that the same condition would be true on the full-scale airship. Two factors not considered here are the difference in location between center of gravity and center of buoyancy and the effect of engine thrust.

Theoretical Consideration -- The ratio of elevator area to total tail area was constant for all tails and was equal to 0.268. For a constant ratio of elevator to total tail area, the effectiveness of the elevators to produce pitching moment with change in elevator angle depends on total tail area, dihedral angle of tail, aspect ratio of the tail, tail end plating, and pressure-carry-over effects.

The effect of dihedral on the longitudinal-control power is shown in the sketch below.



The ΔC_{NF} in the sketch signifies the change in lifting-surface normal force with elevator deflection. The change is the same for both cases, but only that portion of the normal force in the vertical plane actually contributes to a change in pitching moment. It is self-evident, then, that the elevator power varies as $\cos \Gamma$.

The effect of tail aspect ratio on elevator power can be better understood by defining the change in air flow with elevator deflection. Elevator deflection serves the same purpose as changing tail incidence. With a fixed ratio of elevator area to tail area, this change in tail incidence with elevator deflection is a fixed percentage of elevator deflection. From the above, the deflection relation of elevator power to aspect ratio can be recognized. End plating the tail surface has the same effect as increasing the aspect ratio.

Experimental Results -- Basically, the geometry of the X- and C-type horizontal tails is the same. Considering one individual surface, we can see that for the same elevator deflection, the contribution to pitching moment for the two tails differs by a factor $\cos \Gamma$. For the X-tail, this amounts to a reduction in moment contribution of 0.707. However, if the total tail area is doubled (as it is for the X-tail) the real change in moment with elevator deflection should be 1.41 times greater for the X-tail than for the conventional tail. Referring to Figure 23, it is evident that the ratio is even greater than this for most elevator deflections. Although the

real reason for this is not known, there is a possibility that the pressure carry-over mentioned in a previous discussion comes into play here again.

The elevator tests of Figure 12, however, show that for the X-tail configuration at two dihedral angles, the change in pitching moment with elevator deflection compares almost perfectly with the cosine rule.

For the Λ -tail, the results indicate that the ratio of cosines does not hold. The moments are too large when compared to the conventional tail and too small when compared to the X-type of tail.

In Figure 5-33 of Reference 15 is shown a curve of the expected ratio $d\alpha_t/d\delta_e$ as a function of S_e/S_t where

α_t	tail angle of attack for zero lift
δ_e	elevator deflection
S_e	elevator area
S_t	total tail area

All the data points for the tails investigated fall below the curve shown in Figure 5-33 of Reference 15 except those for the X-tail. The experimental and expected values of $d\alpha_t/d\delta_e$ are shown in Table 3.

In Table 4 are presented some of the effects on the model forces and pitching moment due to elevator deflection.

In Figure 24 is presented a plot of elevator angle required for trim on the model, as tested. The slope of the curves, $\partial \delta_{e(\text{trim})} / \partial \theta$, is a measure of tail ability to trim. The larger the slope of the curves in Figure 24, the slower the tail is in acting to overcome the adverse pitching moment on the model. The conventional tail is most undesirable in this respect and the X-type is the most desirable for small angles of pitch. However, with increase in pitch, the H-type tail shows little tendency to change slope and consequently requires the largest elevator deflection for trim at the higher angle of pitch. For configurations other than the H-type tail, the slope $\partial \delta_{e(\text{trim})} / \partial \theta$ passes through zero and becomes negative. For the zero slope point the Λ -type tail requires an zero elevator deflection of only 10° when the tab deflection is 0° . A comparison can also be seen in Figure 24 of the effect on elevator angles required for trim when the tab is being used as a trimmer.

HINGE-MOMENT CHARACTERISTICS -- In Figures 11, 13, and 14 is shown the variation of elevator hinge moment with pitch angle for the conventional, X-type, and H-type tails. No hinge moments were recorded on the Λ -type tail for this series of tests.

The elevator hinge moment was investigated for several conditions: variation with elevator deflection, 0° tab; variation with elevator and tab deflected in opposite directions on a one to one ratio; and variation with tab deflection, 0° and 20° elevator.

In Figure 25 is shown the variation of hinge moment with elevator deflection through the angle-of-pitch range.

The solid line indicates the actual variation which was found in the tests while the broken line indicates what is probably the true variation of $\partial C_{h_e} / \partial \delta_e$. The discrepancy was caused by the model support-strut wake. The tail surface was in the direct wake of the strut in the region where the broken line differs from the solid line.

In Table 5 is shown a comparison of experimental and calculated (Reference 15, pages 275 and 276) variation of the hinge moments for the models tested. The discrepancies are probably caused by model inaccuracies such as leakage around the tabs, which were not sealed, and no effective end plating at the elevator-fuselage juncture.

All models indicate an almost constant stick-free elevator floating angle as shown in Figure 26.

In Figure 13 is presented the test results of the trim-tab-effectiveness tests, when the tab is deflected in the opposite direction to the elevator. In Figure 27 are presented the cross plots of the results from Figures 11 and 13. The cross plots indicate that the tab is overeffective when deflected on a 1:1 ratio and results in a near or actual control-force reversal at small δ_e . A more suitable ratio would be 1:2.

In Figure 28, is presented a series of cross plots of tab data showing the variation of $\partial C_{h_e} / \partial \delta_{T_e}$ for various

angles of pitch. The results from tab tests indicate that the tab effectiveness is a function of elevator loading.

Aerodynamics Laboratory
David Taylor Model Basin
Washington, D. C.
September 1954

REFERENCES

1. Broberg, Ralph F. and Anderson, Arnold W.: Wind-Tunnel Force and Moment Tests of Three Related 1/72-Scale Models of the ASW Airship. (U. S.) TMB Report 746. Aero Report 797, December 1950. 9 1. illus.
2. BuAer ltr Aer-DE-31 Serial 53261 dated 29 May 1951 on TED No. TMB DE-3110.
3. Memorandum for Aerodynamics Laboratory Files dated 28 April 1954.
4. Glauert, H.: Wind Tunnel Interference on Wings, Bodies and Airscrews. (Gt. Brit.) ARC RandM. 1566, September 1933. 75 p. illus.
5. Munk, Max M.: Aerodynamics of Airships. (In Durand, W. F., ed.: Aerodynamic Theory. (Ger.) Springer, 1936, Vol. 6, pp. 32-48. Reprinted at California Institute of Technology by Durand Reprinting Committee, 1943.)
6. Millikan, Clark B.: The Boundary Layer and Skin Friction for a Figure of Revolution. ASME Transactions (U. S.), Vol. 54, 1932, pp.29-43. (APM 54-3)

7. McHugh, James G.: Pressure-Distribution Measurements at Large Angles of Pitch on Fins of Different Span-Chord Ratio on a 1/40-Scale Model of the U. S. Airship "Akron". (U. S.) NACA Report 604, 1937. 20 p. incl. illus.

8. Simmons, L. F. G.: Experiments Relating to the Flow in the Boundary Layer of an Airship Model. (Gt. Brit.) ARC R and M 1268. April, 1929. 7 p. illus.

9. Ower, E. and Hutton, C. T.: Investigation of the Boundary Layers and the Drags of Two Streamline Bodies. (Gt. Brit.) ARC R and M 1271. September, 1929. 18 p. illus.

10. Freeman, Hugh B.: Measurements of Flow in the Boundary Layer of a 1/40-Scale Model of the U. S. Airship "Akron" (U. S.) NACA Report 430, 1932. 15 p. incl. illus.

11. Freeman, Hugh B.: Pressure-Distribution Measurements on the Hull and Fins of a 1/40-Scale Model of the U. S. Airship "Akron." (U. S.) NACA Report 443, 1932. 15 p. incl. illus.

12. Lawrence, H. R.: The Lift Distribution on Low Aspect Ratio Wings at Subsonic Speeds. Jour. Aeronautical Sciences, Vol. 18, No. 10. October 1951, p. 685.

13. Bates, William R.: Collection and Analysis of Wind-Tunnel Data on the Characteristics of Isolated Tail Surfaces With and Without End Plates. (U. S.) NACA TN 1291, May 1947. 21 p. illus.

14. Rizzo, Frank: A Study of Static Stability of Airships. (U. S.) NACA TN 204 September 1924. 50 l. illus.

15. Perkins, Courtland D. and Hage, Robert E.: Airplane Performance Stability and Control. (U. S.) John Wiley and Sons, Inc. 1949. 493 p. illus.

TABLE 1

Principal Model Constants Used in Data Reduction
for a 1/48-Scale Model XZS2G-1 Airship

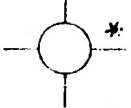
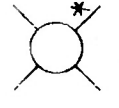
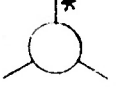
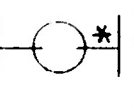
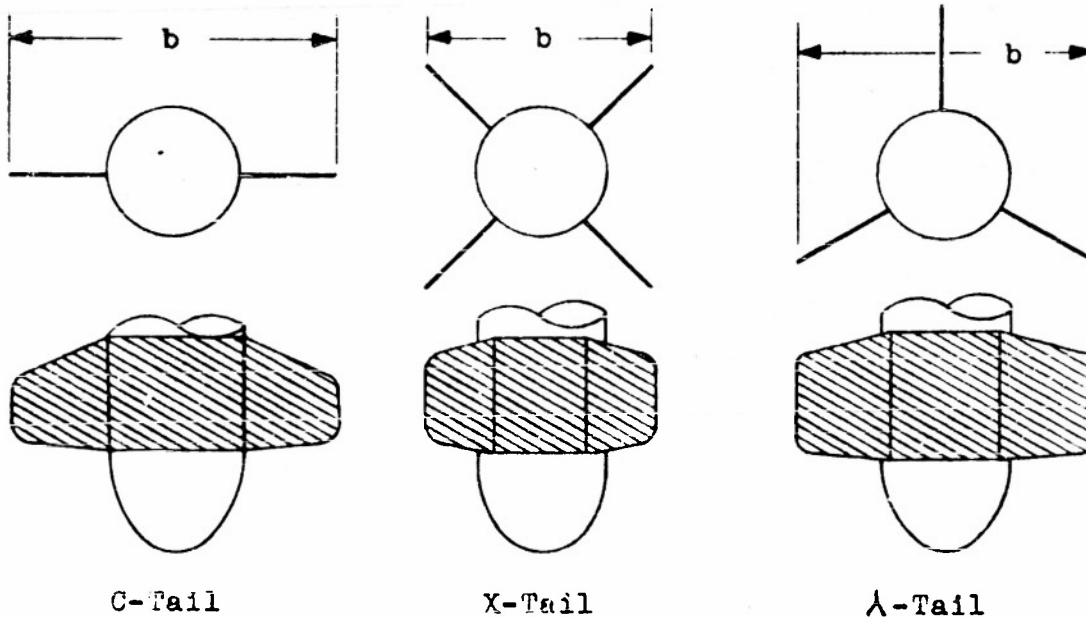
Item	C-type	X-type	A-type	H-type
Vol. in cubic feet	6.299	6.299	6.299	6.299
Vol. ^{2/3} in square feet	3.411	3.411	3.411	3.411
Vol. ^{1/3} in feet	1.847	1.847	1.847	1.847
W in square feet	20.203	20.203	20.203	20.203
Length in feet	5.873	5.873	5.873	5.873
S _e in square feet	0.070	0.070	0.098	0.052
\bar{c} in feet	0.158	0.158	0.181	0.118
Hinge moment measured on surface indicated by asterisk -- rear view				

TABLE 2

Comparison of Theoretical and Measured Lift Characteristics
for Various Tail Configurations of the
1/48-Scale Model XZS2G-1 Airship



Projected area shown crosshatched

Tail	Projected Area in ft ²	b^2 in ft ²	AR	dC_L/da per radian	
				Theoretical*	Measured**
C	1.226	2.28	1.86	2.35	1.43
X	0.866	1.14	1.32	1.80	1.78
Λ	1.382	2.00	1.45	1.95	1.57
H	1.028	2.10	2.04	3.44 [†]	3.84

* Reference 12, Figure 2

** From Figure 20

† Reference 13, Figure 47. If $\frac{S_{\text{endplate}}}{b} = 0.782$,
 $c_{l_a} = 6.08$, where c_{l_a} is the slope of section lift coefficient

TABLE 3

Elevator Effectiveness of Various Tail Configurations
on a 1/48-Scale Model XZS2G-1 Airship

$$\delta_{T_a} = 0^\circ$$

Configuration	$\frac{S_e}{S_t}$	$\frac{\Delta \alpha_t}{\Delta \delta_e}^*$	$\frac{d\alpha_t}{d\delta_e}^{**}$
C-type	0.267	0.25	0.46
X-type	0.267	0.50	0.46
λ -type	0.267	0.38	0.46
H-type	0.267	0.19	0.46

* Experimental average

** See Figure 5-33, Reference 14

TABLE 4

Effect of Elevator Deflection Upon the Characteristics
of a 1/48-Scale Model XZS2G-1 Airship

$$\theta = 0^\circ, \delta_{T_e} = 0^\circ$$

Configuration	δ_e in degrees	ΔC_m	ΔC_L	ΔC_S
B(HV) _C	10	0.034	0.030	0.0020
	20	0.076	0.062	0.0062
	25	0.092	0.073	0.0100
	30	0.096	0.082	0.0128
B(HV) _X	10	0.062	0.050	0.0045
	20	0.142	0.117	0.0177
	25	0.182	0.144	0.0282
	30	0.203	0.160	0.0378
B(HV) _Λ	10	0.054	0.043	0.0022
	20	0.113	0.093	0.0095
	25	0.142	0.115	0.0144
	30	0.162	0.130	0.0204
B(HV) _H	10	0.031	0.025	0.0013
	20	0.062	0.050	0.0038
	25	0.070	0.062	0.0100
	30	0.082	0.070	0.0123

TABLE 5

Comparison of Calculated and Experimental Values of Hinge

Moments for a 1/48-Scale Model XZS2G-1 Airship

$\theta = 0^\circ$

Configuration	$\frac{\partial C_{h_e}}{\partial \theta}$		$\frac{\partial C_{h_e}}{\partial \delta_e}$		$\left(\frac{\partial C_{h_e}}{\partial \delta_{Te}} \right)_{\delta_e = 0^\circ}$	
	Calculated	Experimental	Calculated	Experimental	Calculated	Experimental
BC(HV) C	-0.0003	0.0024	-0.0067	-0.0060	-0.0068	-0.0068
BC(HV) X	-0.0016	0.0000	-0.0100	-0.0072	-0.0067	-0.0080
BC(HV) A	-0.0013	----	-0.0096	-----	-0.0073	-----
BC(HV) H	-0.0014	0.0024	-0.0077	-0.0044	-0.0073	-0.0028

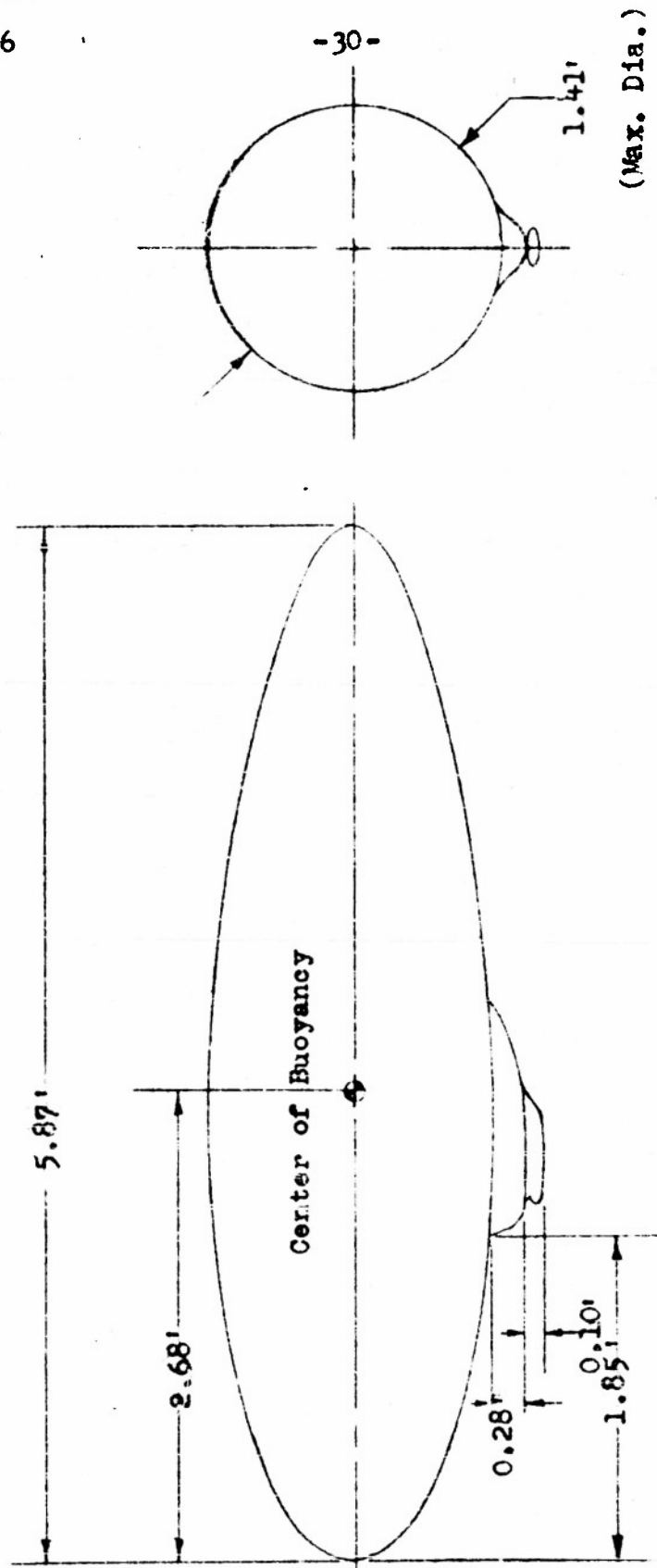


Figure 1 - Principal Dimensions of the Envelope of the
1/48-Scale Model XZS23-1 Airship

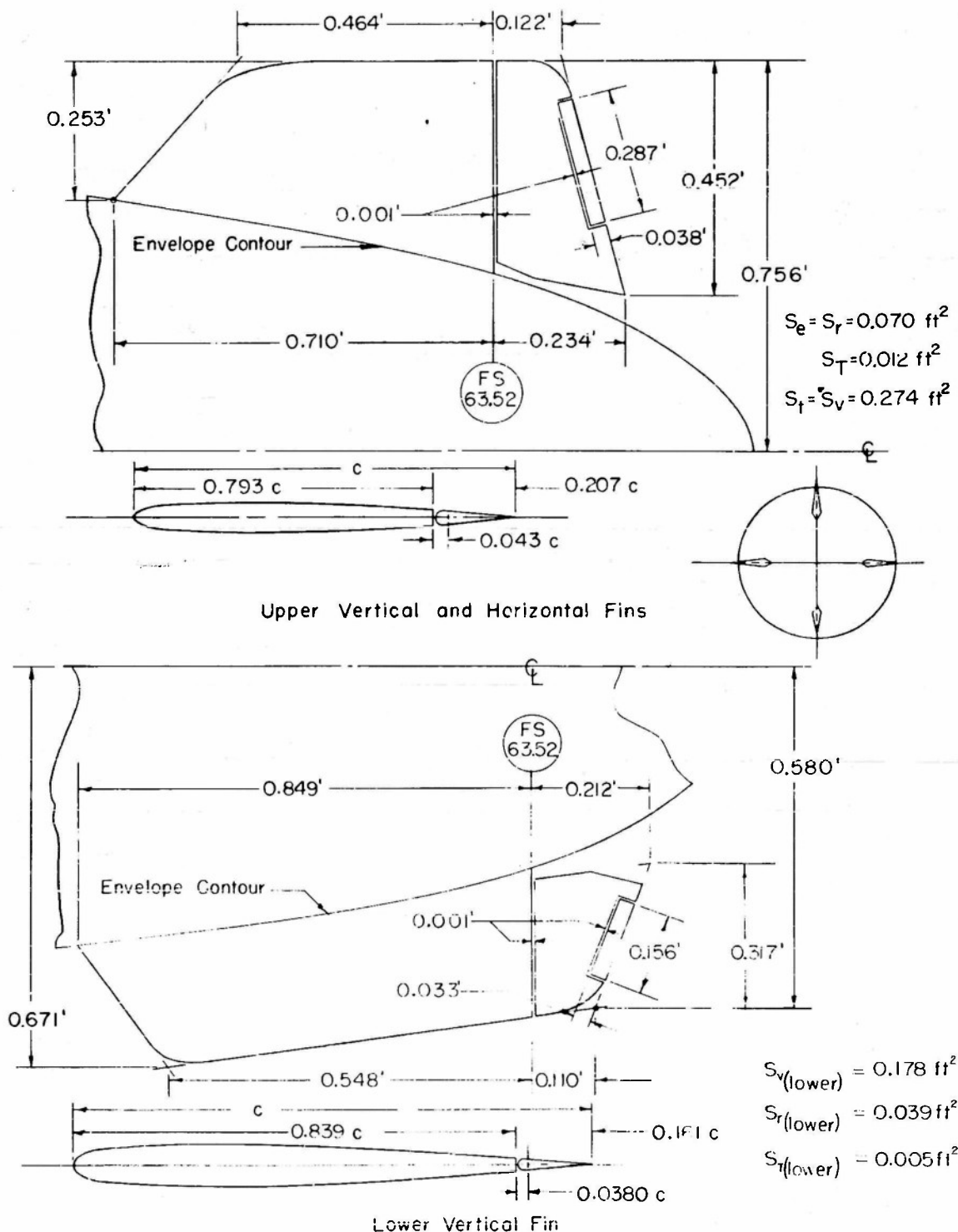
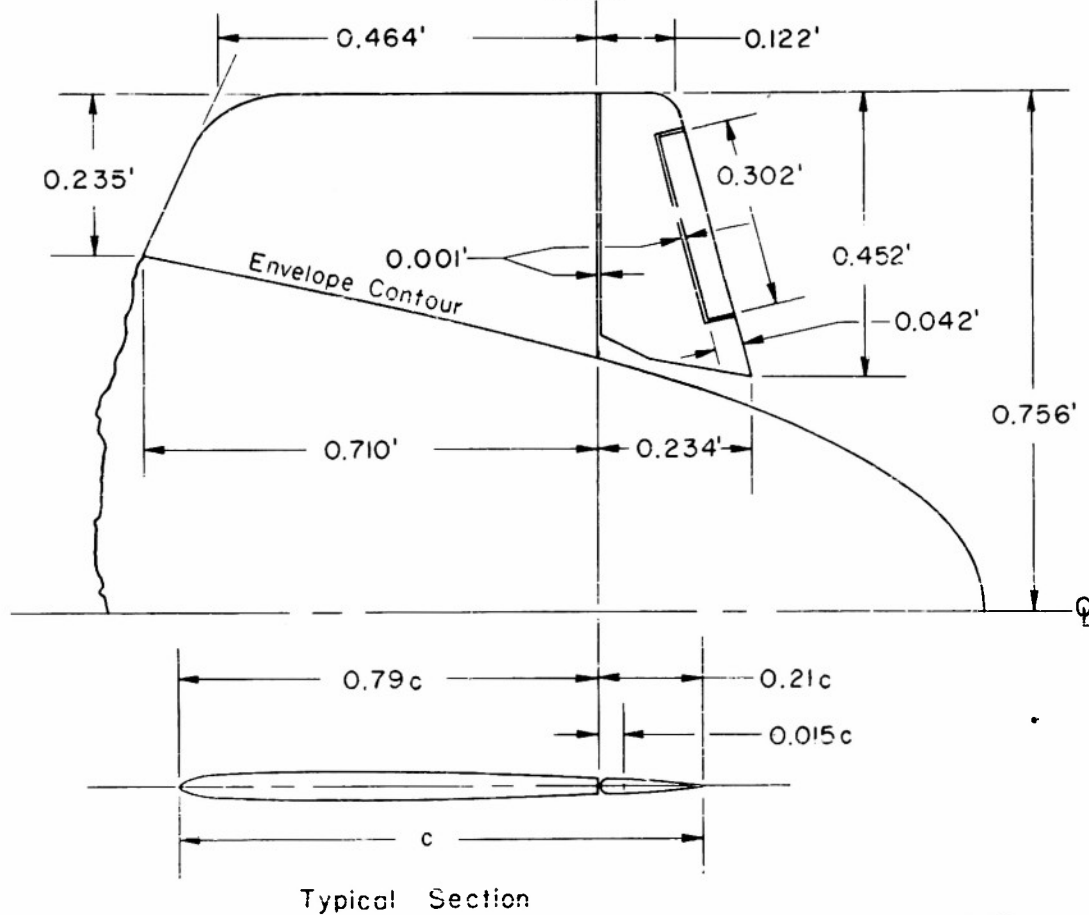


Figure 2 - Principal Dimensions of the Conventional Type Tail on the 1/48-Scale Model XZS2G-1 Airship



$$\bar{c} = 0.158 \text{ ft.}$$

$$S_e = S_r = 0.070 \text{ ft.}^2$$

$$S_T = 0.012 \text{ ft.}^2$$

$$S_f = S_v = 0.274 \text{ ft.}^2$$

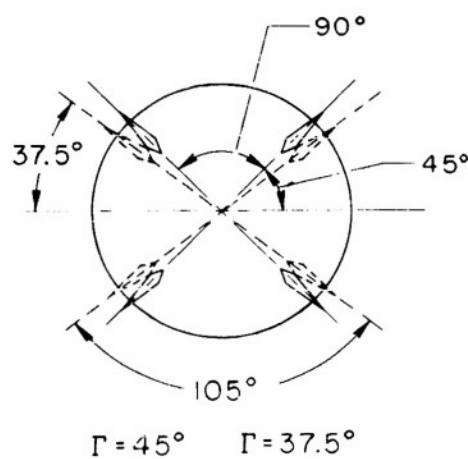


Figure 3 - Principal Dimensions and Arrangement of the X-Tail on the 1/48-Scale Model XZS2G-1 Airship

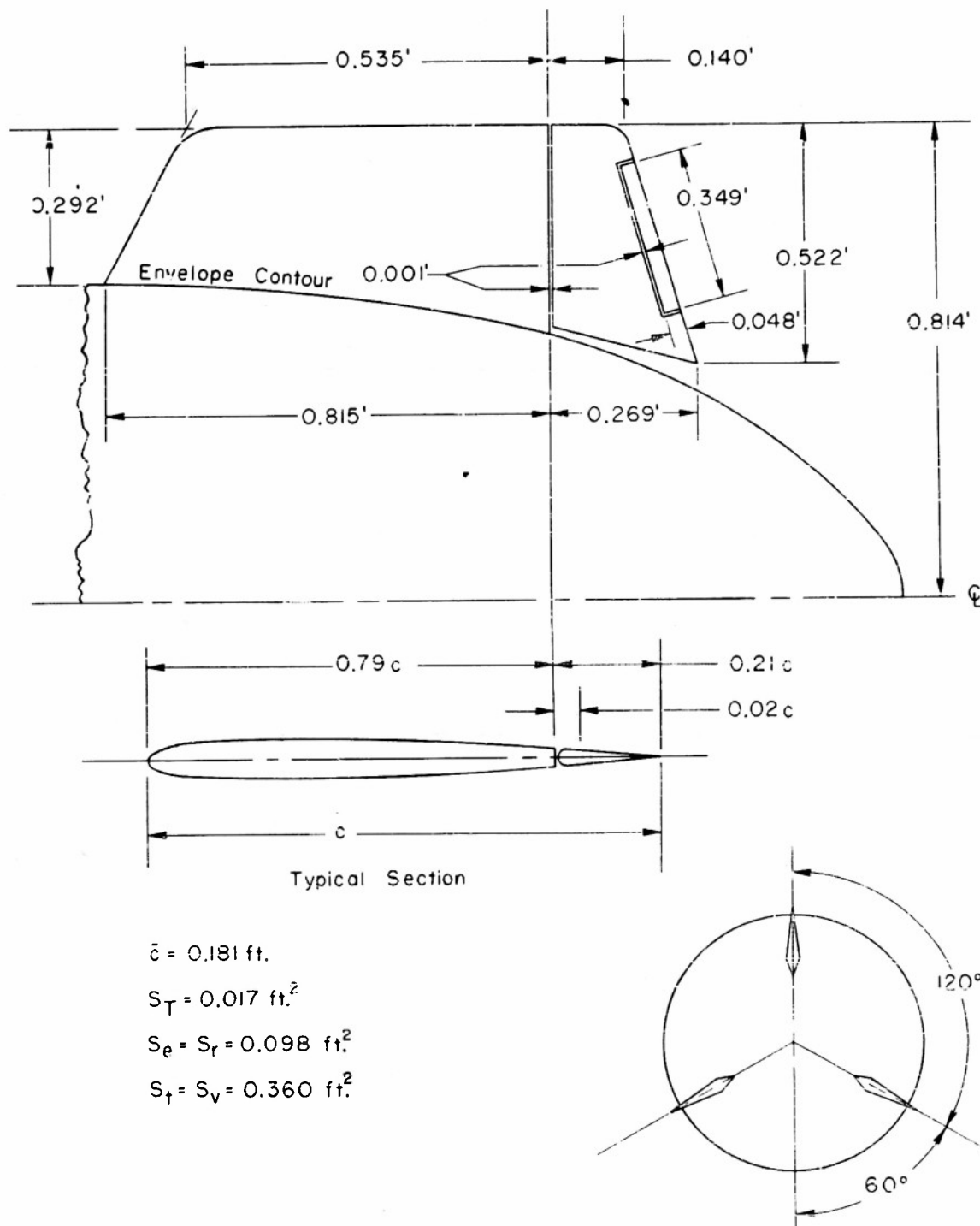


Figure 4 - Principal Dimensions and Arrangement of the λ -Tail on the 1/48-Scale Model XZS2G-1 Airship

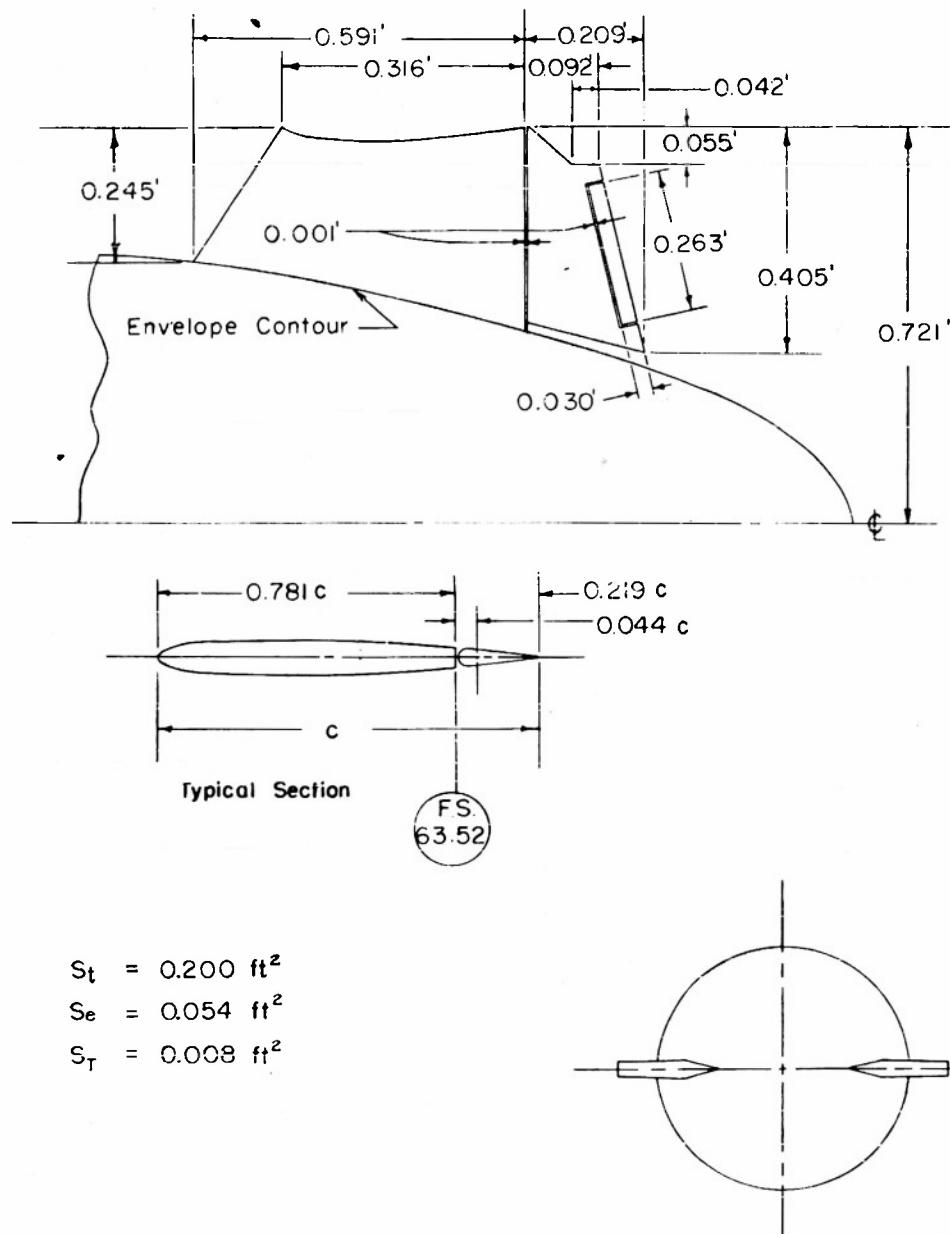


Figure 5 - Principal Dimensions of the Horizontal H-Tail on the
1/48-Scale Model XZS2G-1 Airship

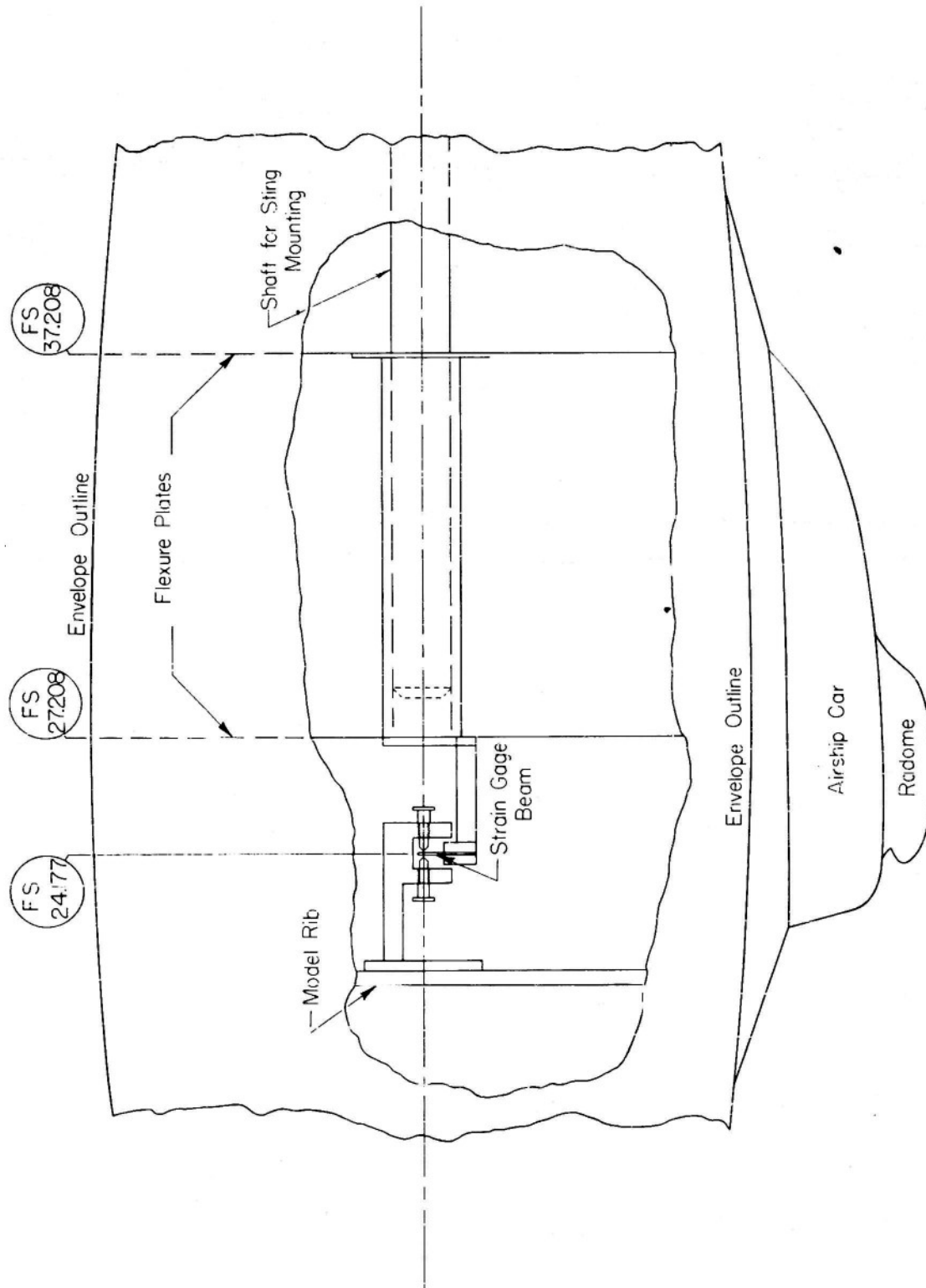


Figure 6 - Partial Cross Section of 1/48-Scale Model XZS2G-1 Airship Showing Flexure-Plate Mounting

CONFIDENTIAL



Figure 7 - Close-Up of Upper Surface of A-Tail on the
1/48-Scale Model XZS28-1 Airship

8 Dec 1952

NP21-51414

CONFIDENTIAL

CONFIDENTIAL

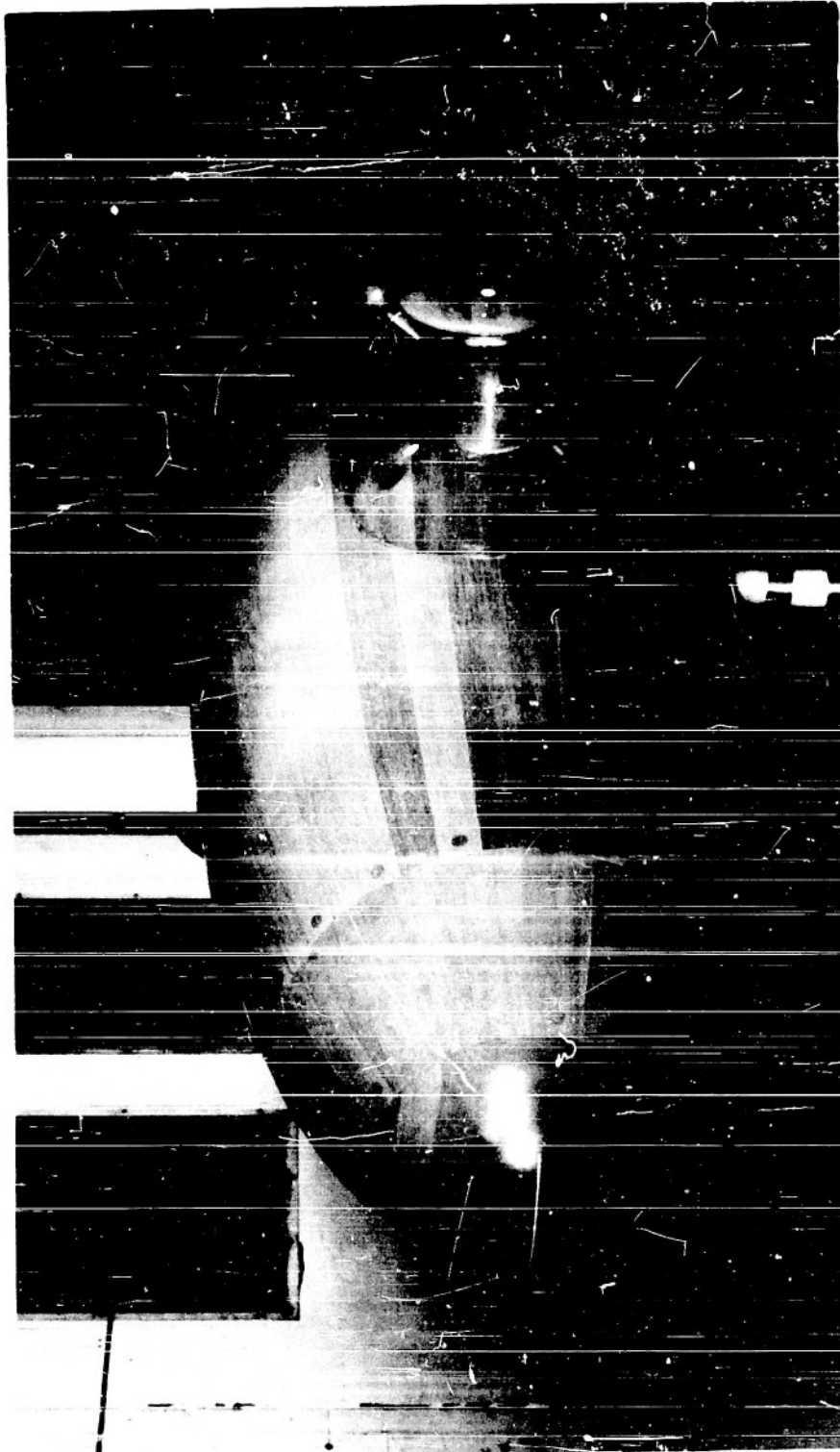


Figure 8 - 1/48-Scale Model XZS20-1 Airship Mounted
in Wind Tunnel for Pitch Tests

(a) Configuration BC_E(HV) X

14 May 1952

NP21-49334

CONFIDENTIAL

CONFIDENTIAL

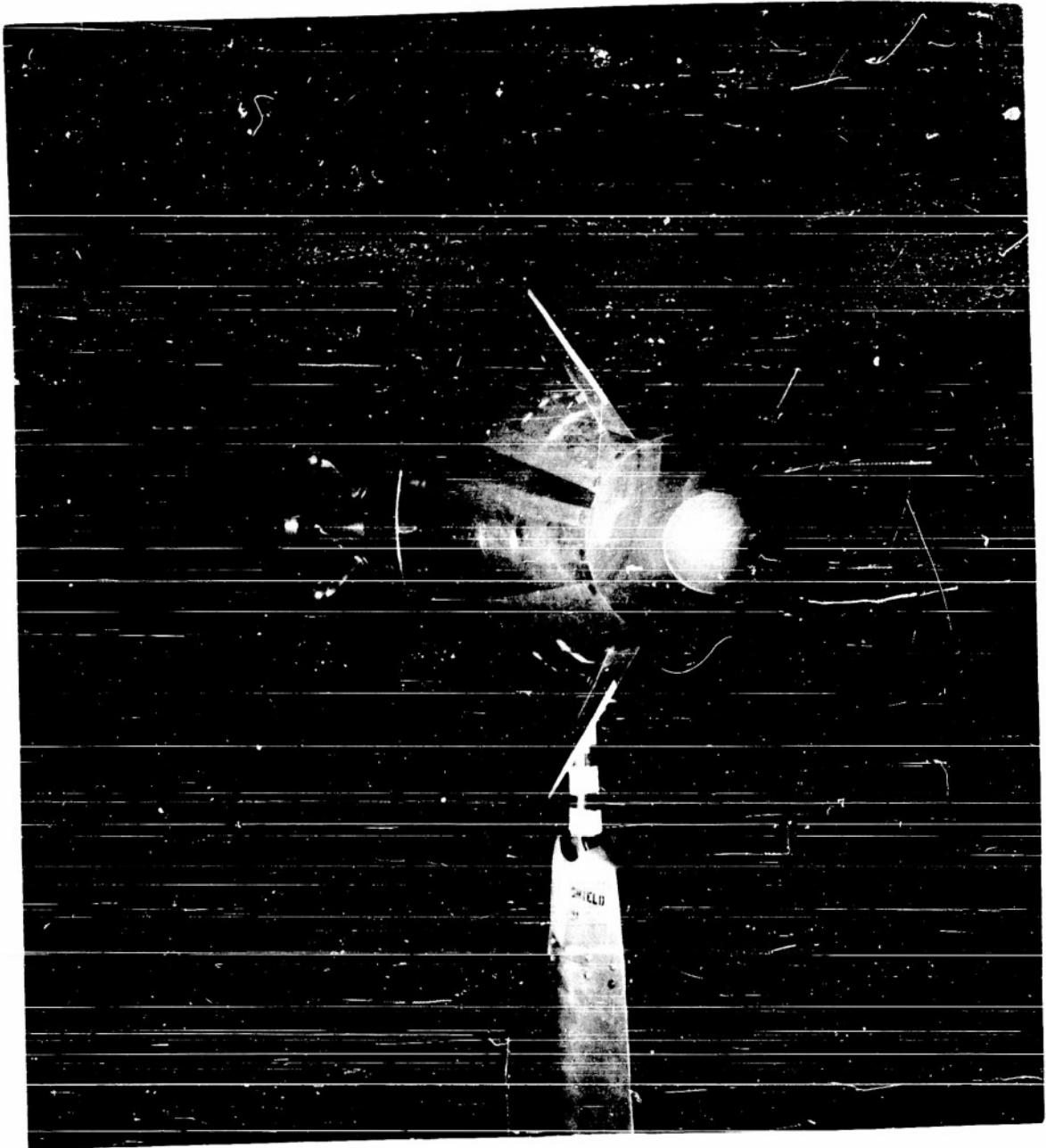


Figure 8 (Continued)
(b) Configuration BC(HV)₁

NP21-49331

14 May 1952

CONFIDENTIAL

CONFIDENTIAL



Figure 8 (Concluded)
(c) Configuration $BC(HV)_H$

NP21-49329

14 May 1952

CONFIDENTIAL

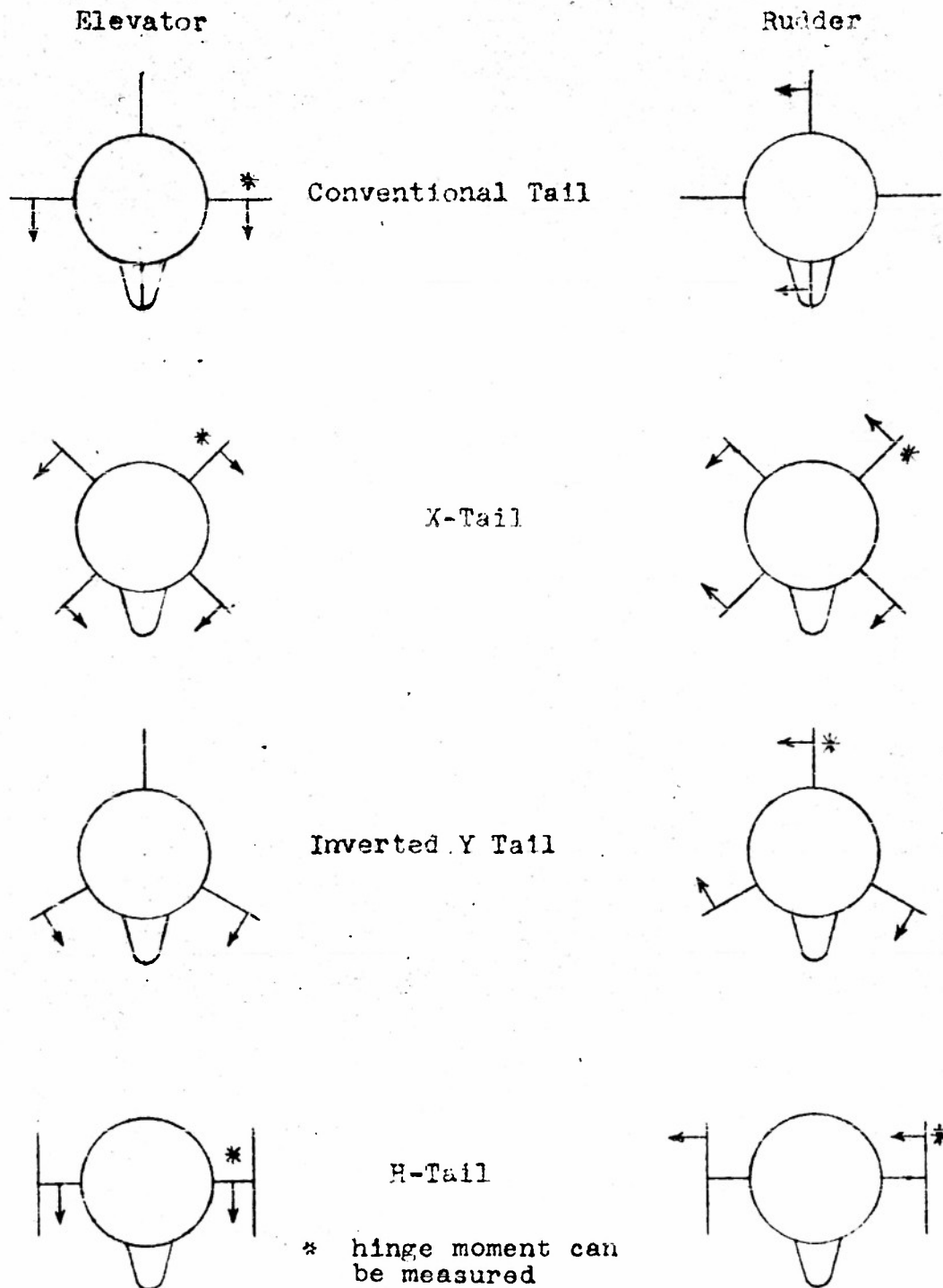


Figure 9 - Schematic Sketch of Various Tail Arrangements on 1/48-Scale Model XZS2G-1 Airship Viewed From Rear Showing Movement of Trailing Edge for Positive Deflection of Flaps and Tabs When Acting as Control Surfaces

JKM 5 May 52

AERO 866

CONFIDENTIAL

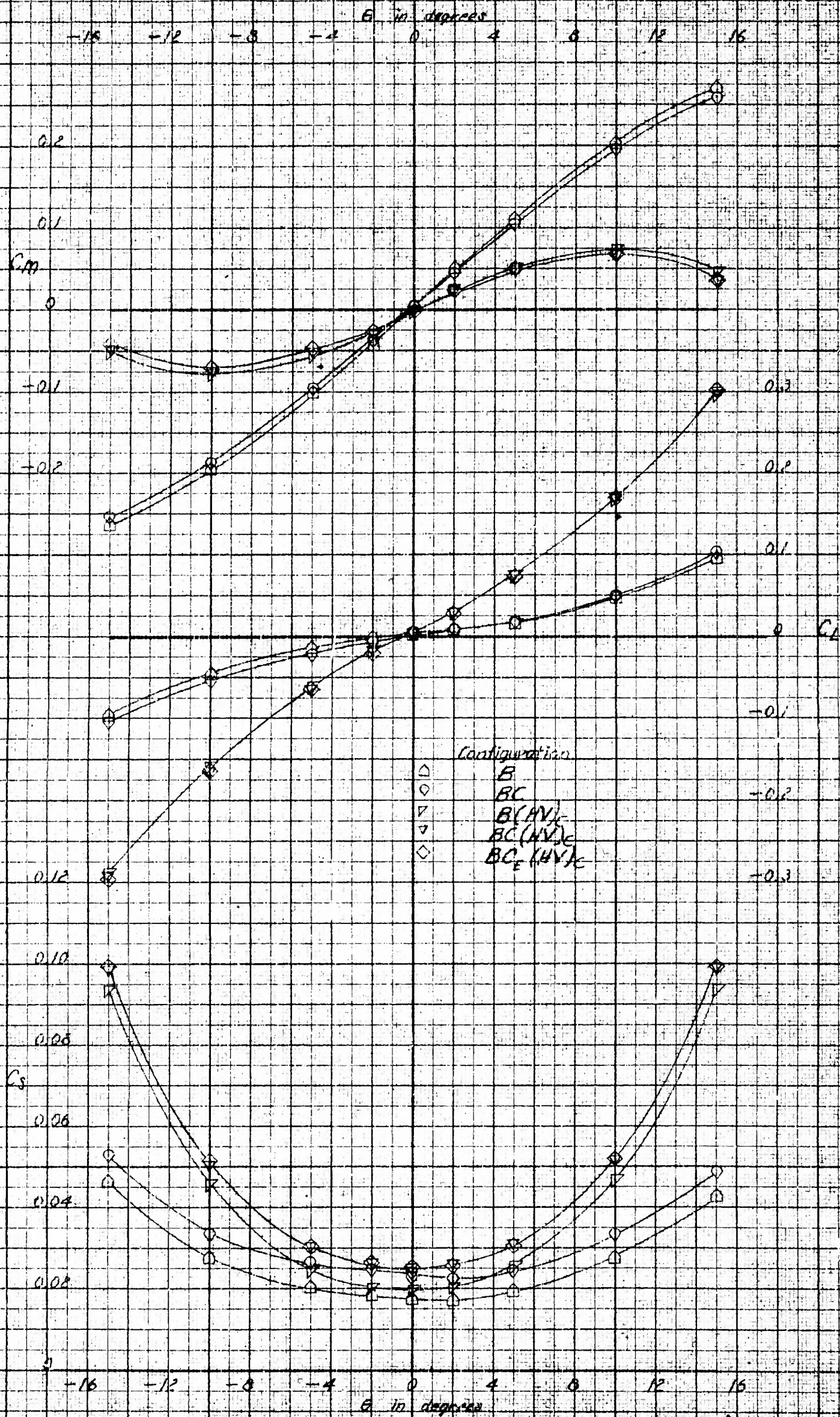


FIGURE 10

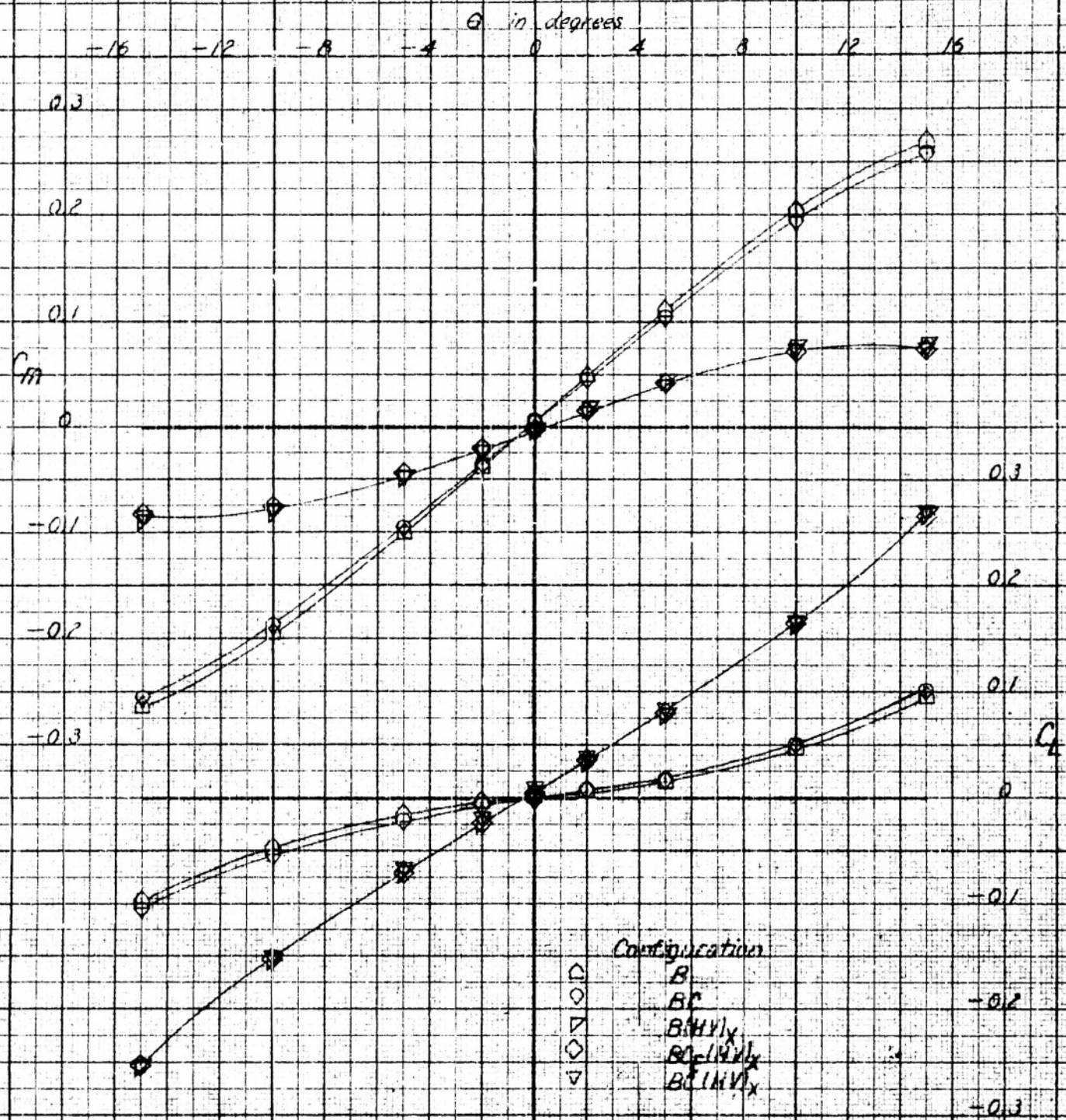
Figure 10 - Effect of Air Component Parts on Longitudinal Characteristics of a 1/48 Scale Model XZS26-L Airship
(a) Conventional Tail, $\delta_e = \delta_{Te} = 0^\circ$

CONFIDENTIAL

PM 1 May 52

AERO 865

CONFIDENTIAL



Configuration
B
BC
BHVLY
BCVLY
BCINVLY

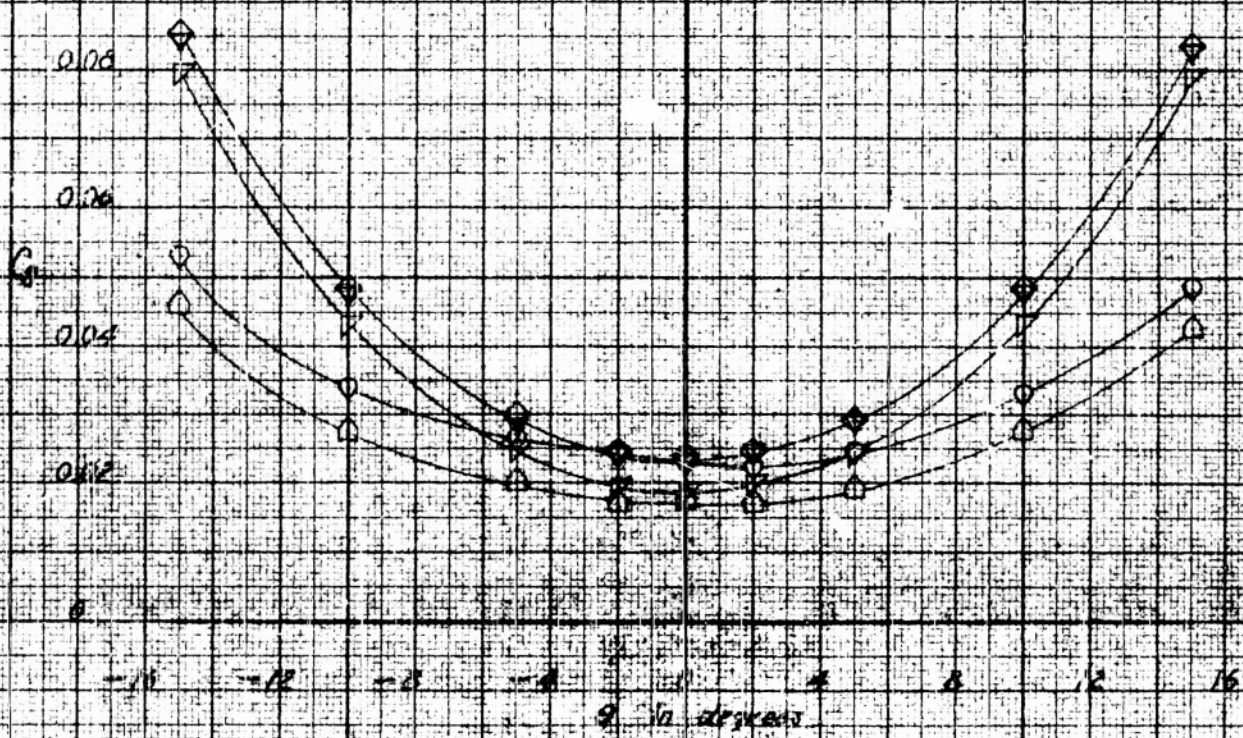


FIGURE 107 A

Figure 107 Continued
1000 ft/sec, $R_e = 5 \times 10^6$

CONFIDENTIAL

DE 6 May 1952

AERO 886

CONFIDENTIAL

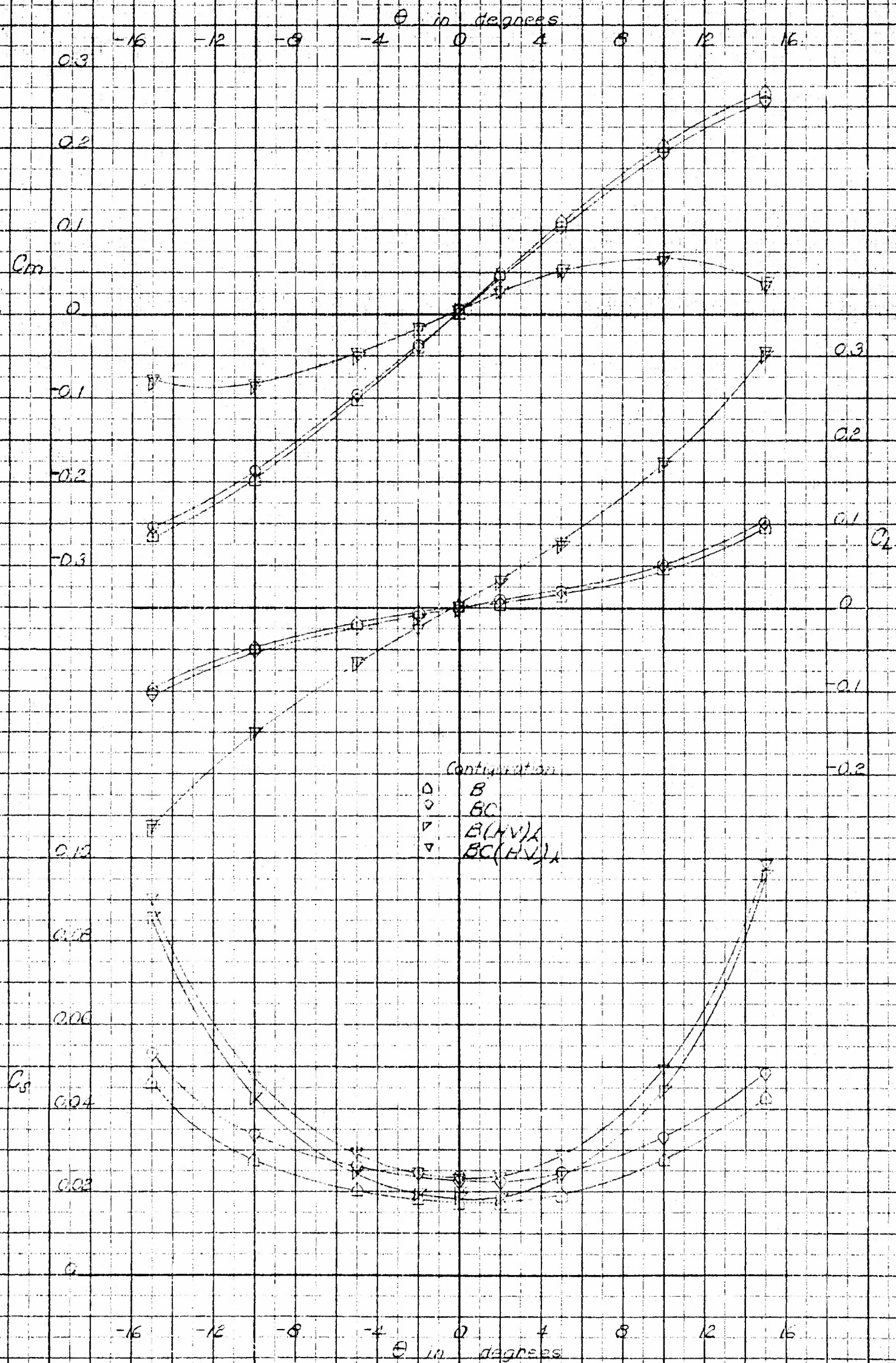


FIGURE 10C

Figure 10 (continued)
 (C) λ -Tail, $\delta_0 = \delta_{Te} = 0^\circ$

CONFIDENTIAL

CONFIDENTIAL

AERO 866

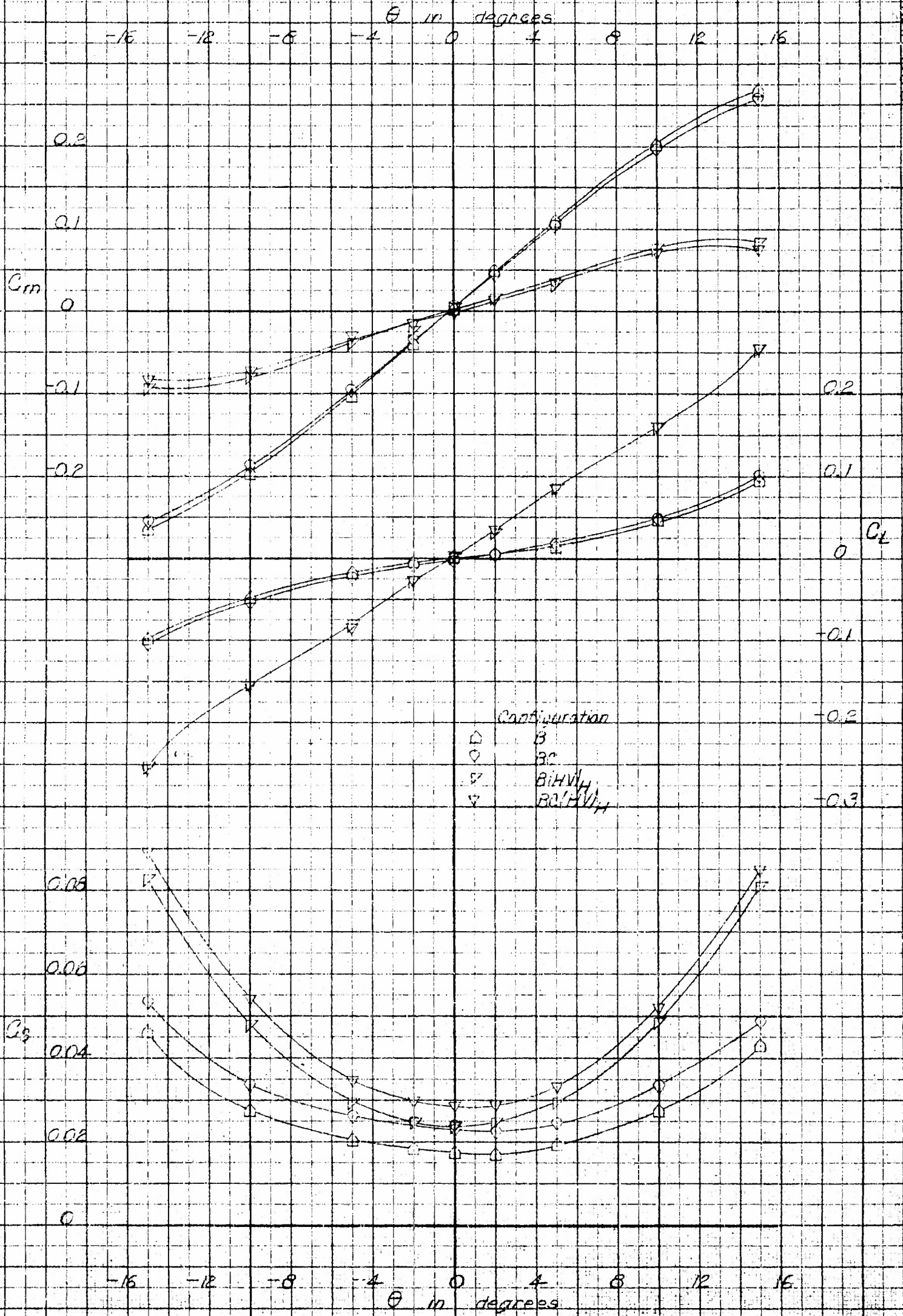


FIGURE 10A

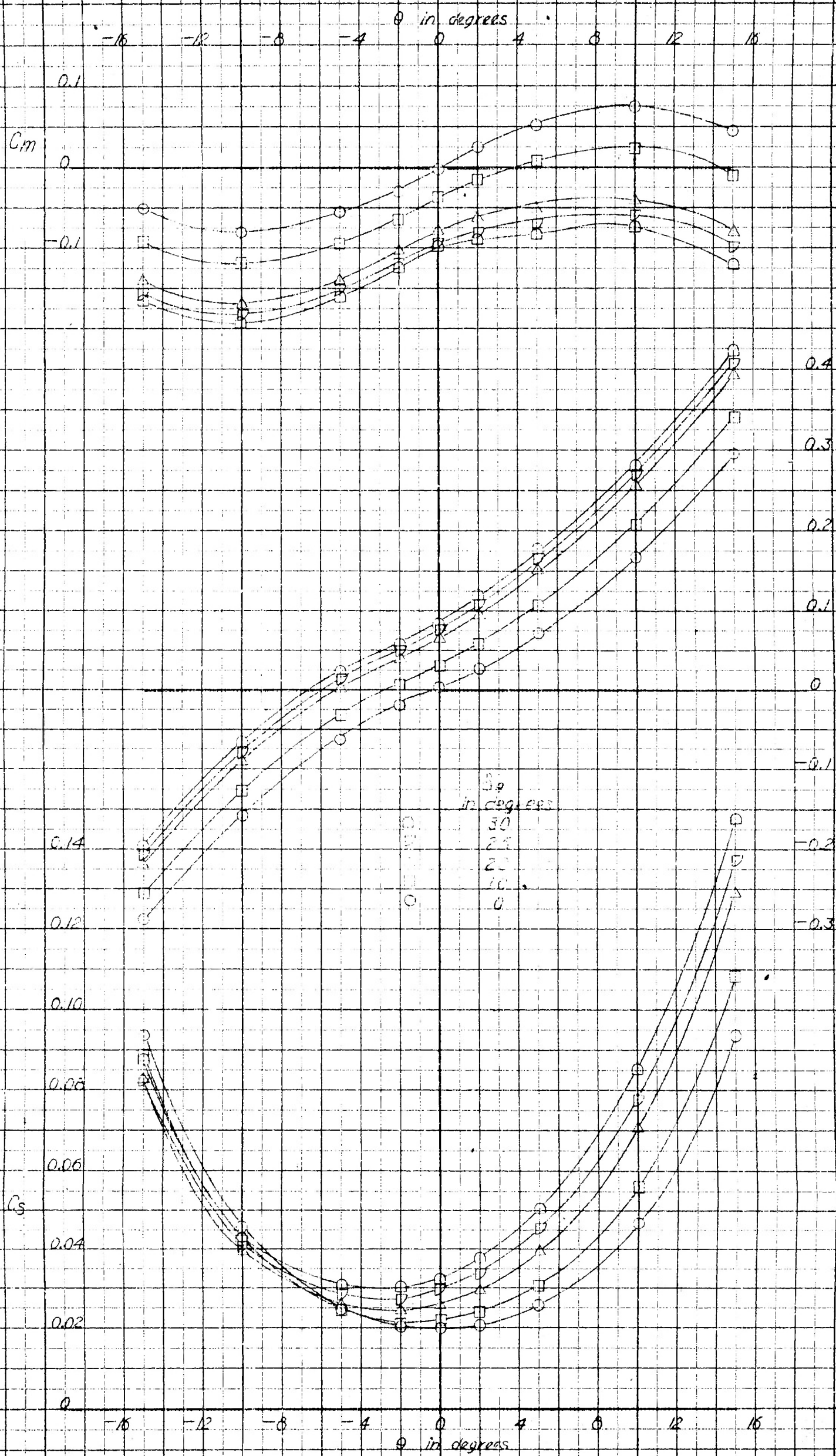
Figure 10 (Concluded)
101 H-Tail, $\delta_e = \delta_{T_e} = 0^\circ$

CONFIDENTIAL

44

CONFIDENTIAL

AERO 866



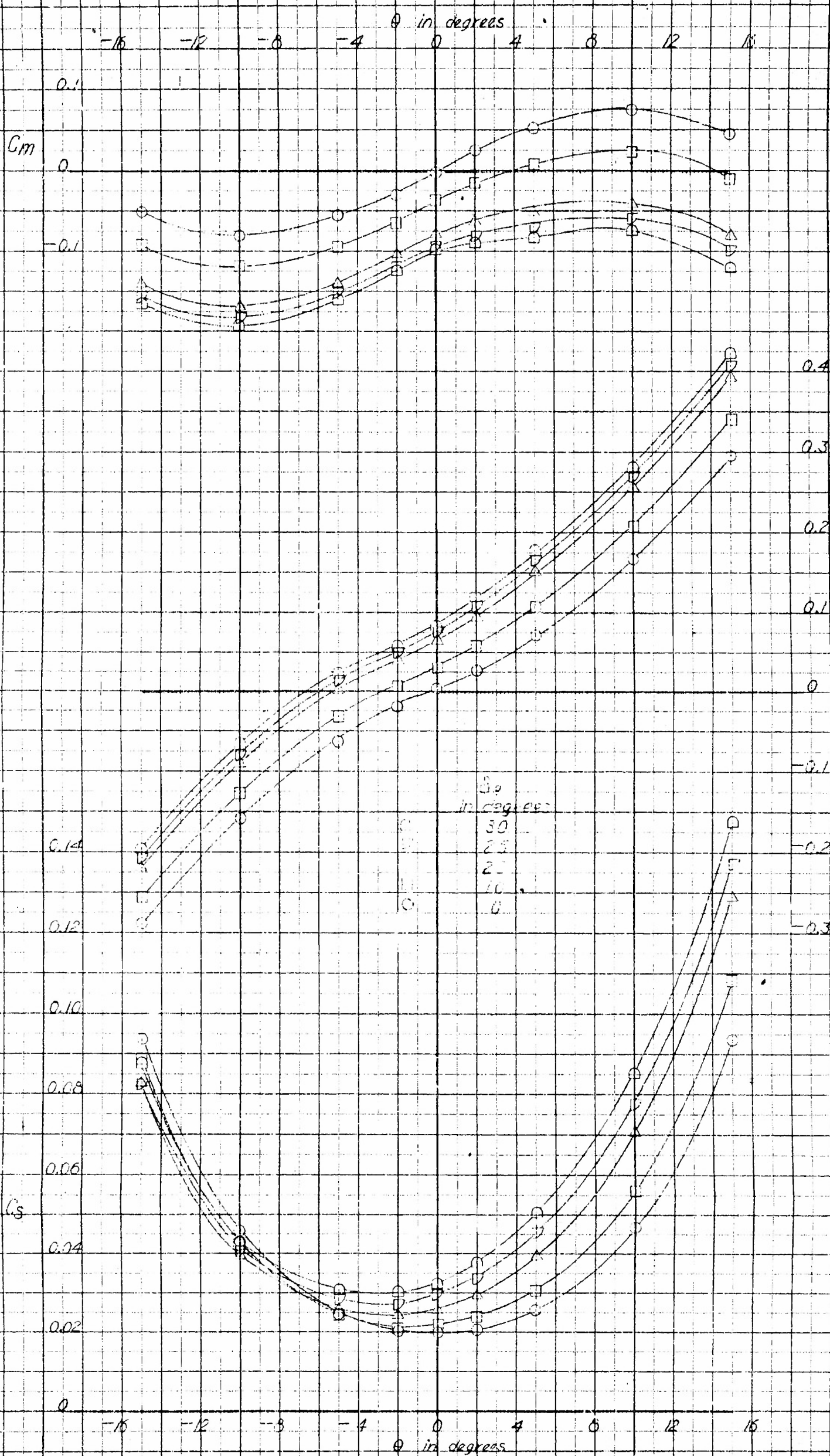
CONFIDENTIAL

Figure N-Effect of Elevators on Longitudinal Characteristics of a 1/48-Scale Model XZS20-1

CONFIDENTIAL

2

AERO 866



CONFIDENTIAL

Figure 11-Effect of Elevators on Longitudinal Characteristics of a 1/43-Scale Model XZS23-1
Aircraft

(a) Configuration B, $\delta_e = 0^\circ$

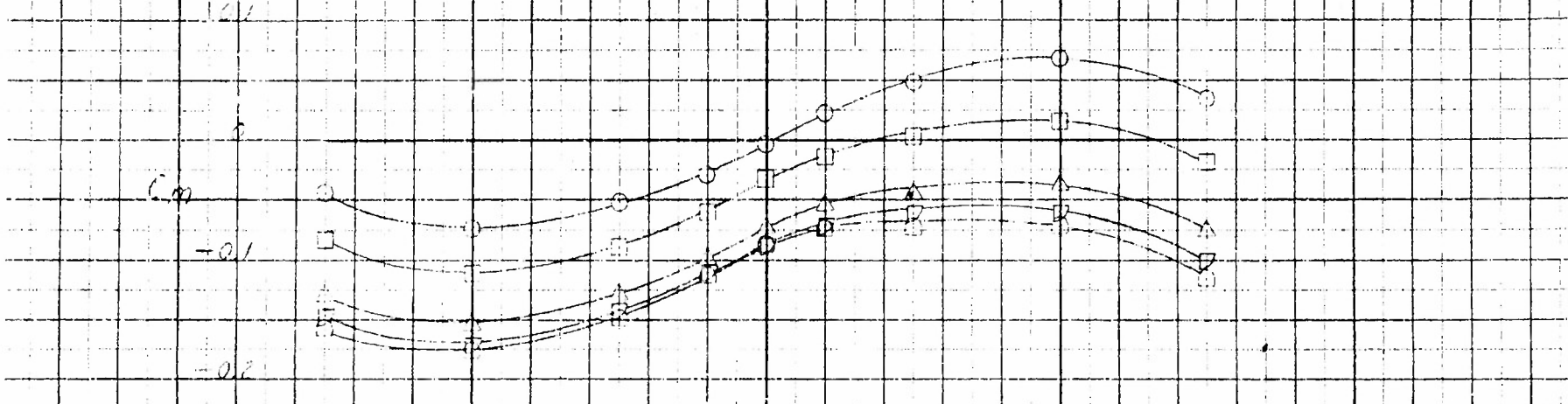
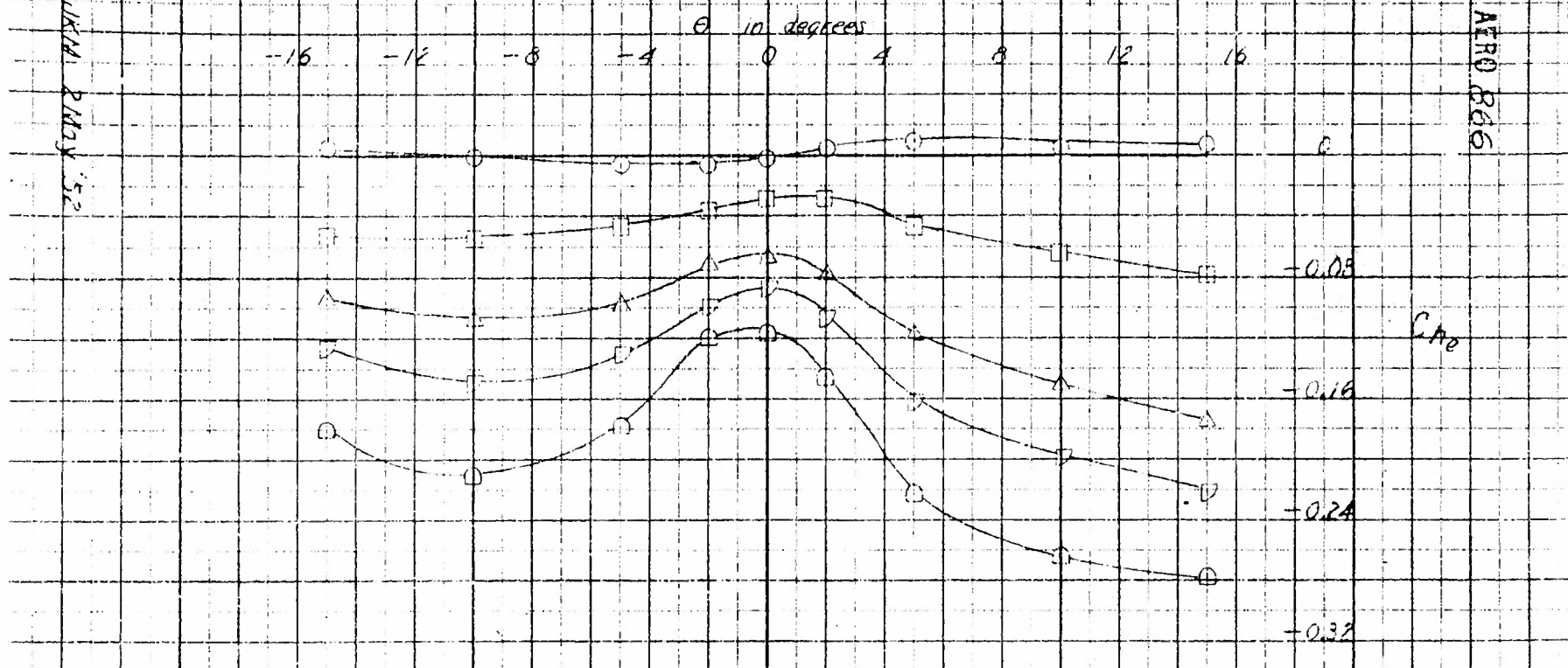
FIGURE 11-2

CONFIDENTIAL

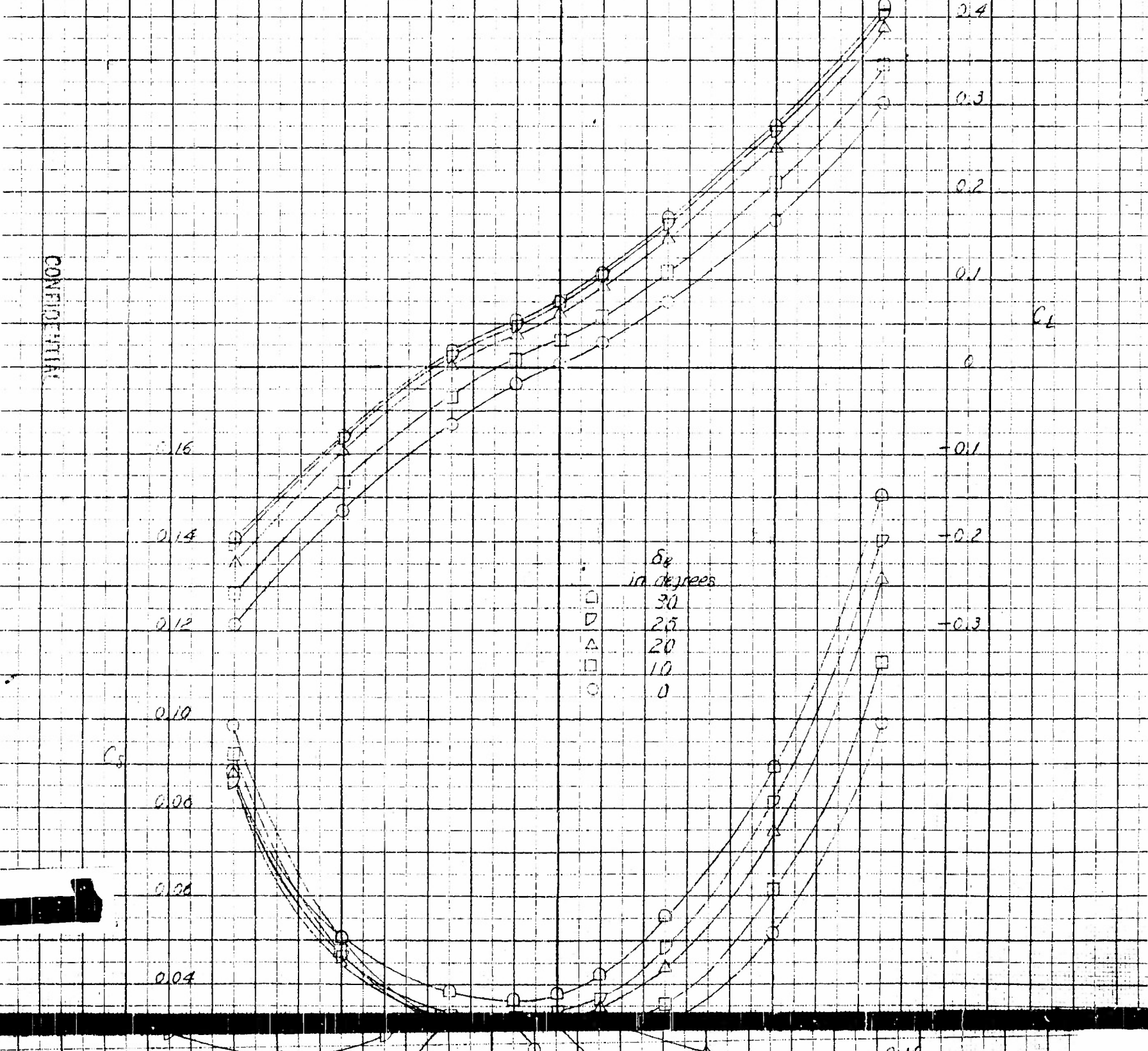
43-

WMA PMJ 52

ATRO 866



CONFIDENTIAL



2

CONFIDENTIAL

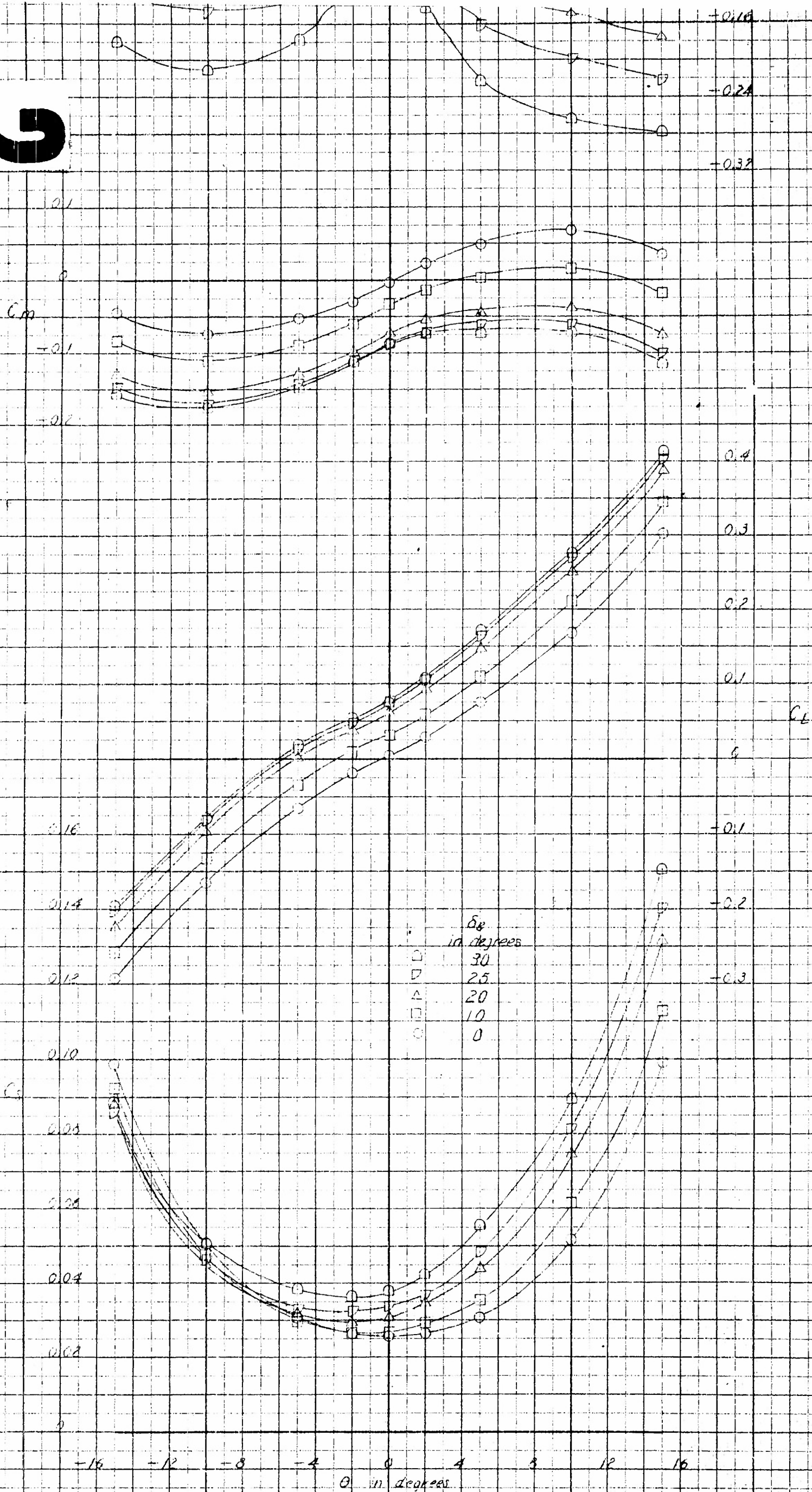


Figure 11 (Continued)
 (b) Configuration BCLH1c, $\delta_{T_e} = 0^\circ$

FIGURE 11b

CONFIDENTIAL

PC May '52

CONFIDENTIAL

URE 11

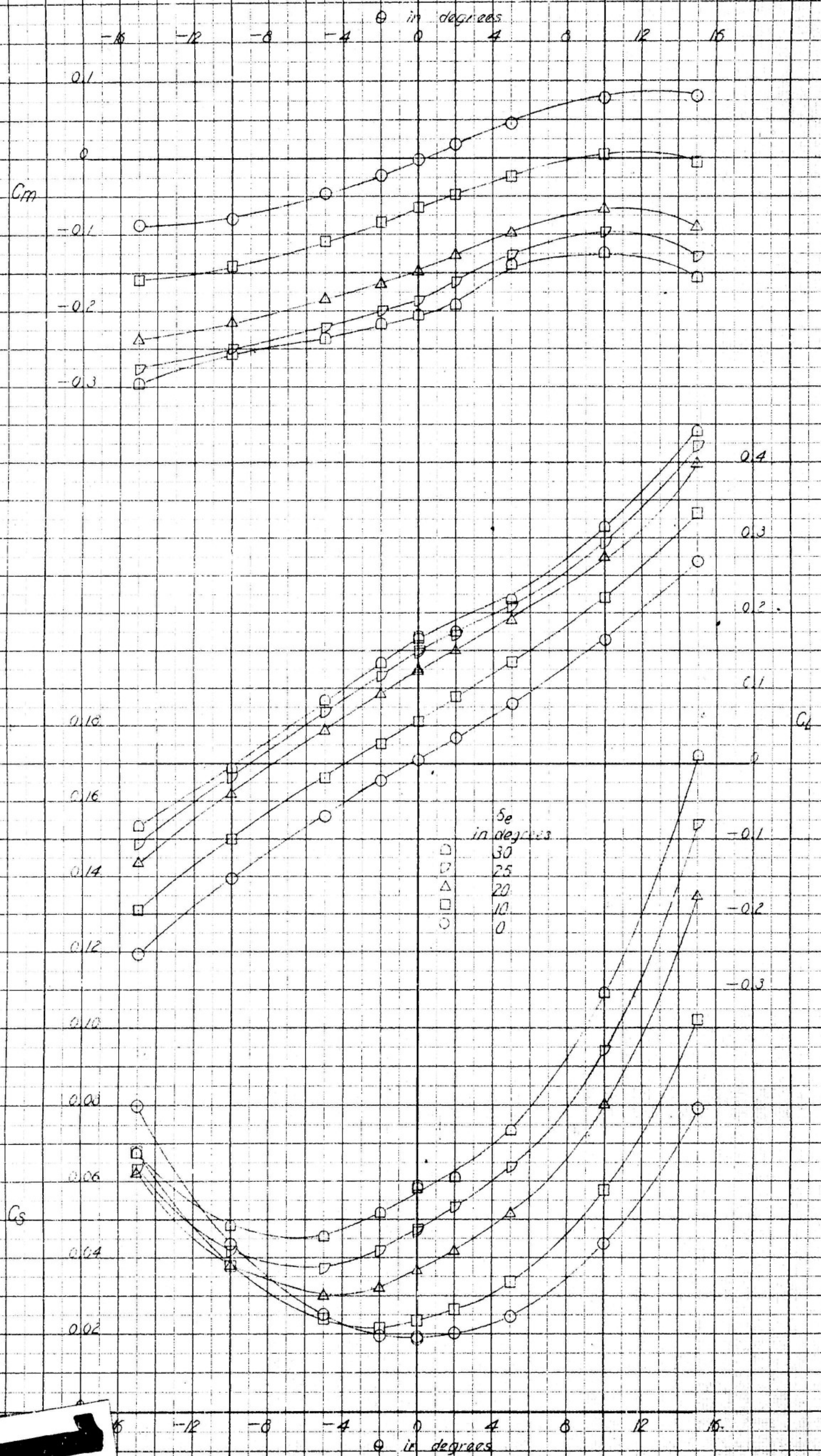
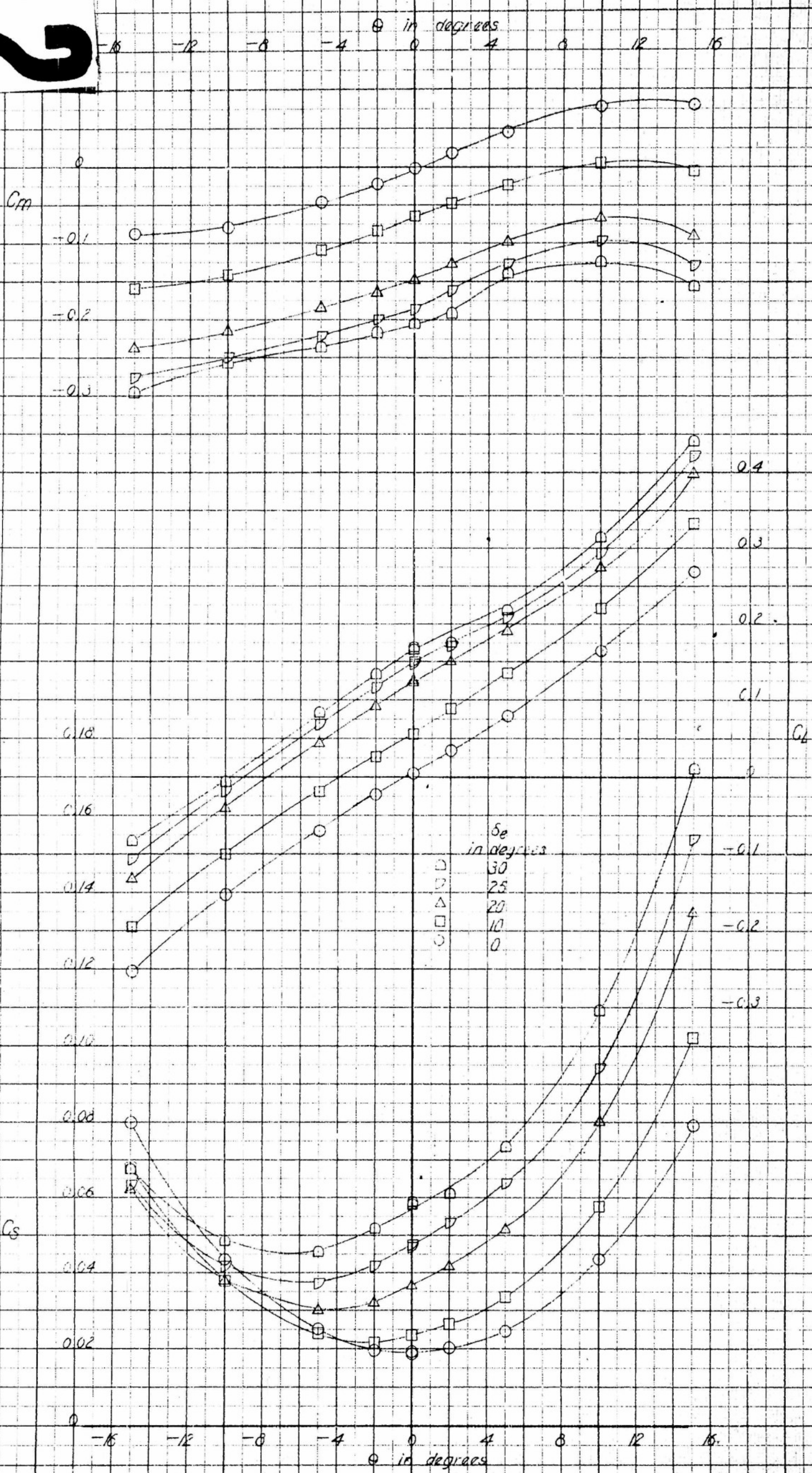


Figure 11 (Continued)

2

AERO 886



CONFIDENTIAL

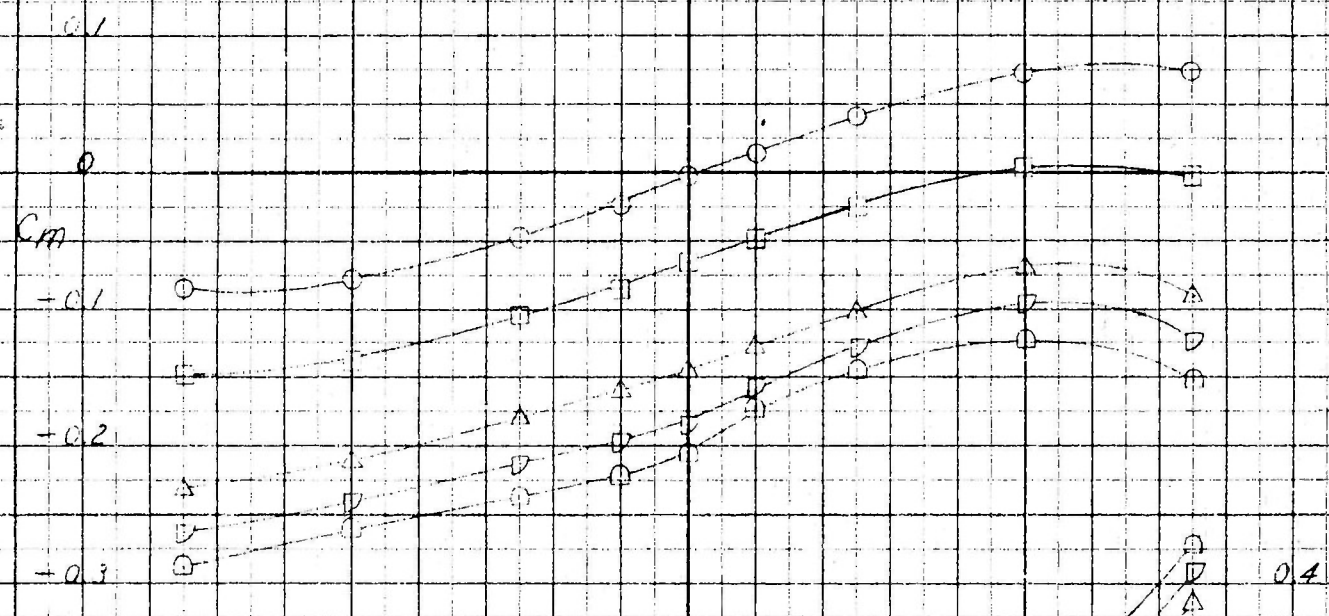
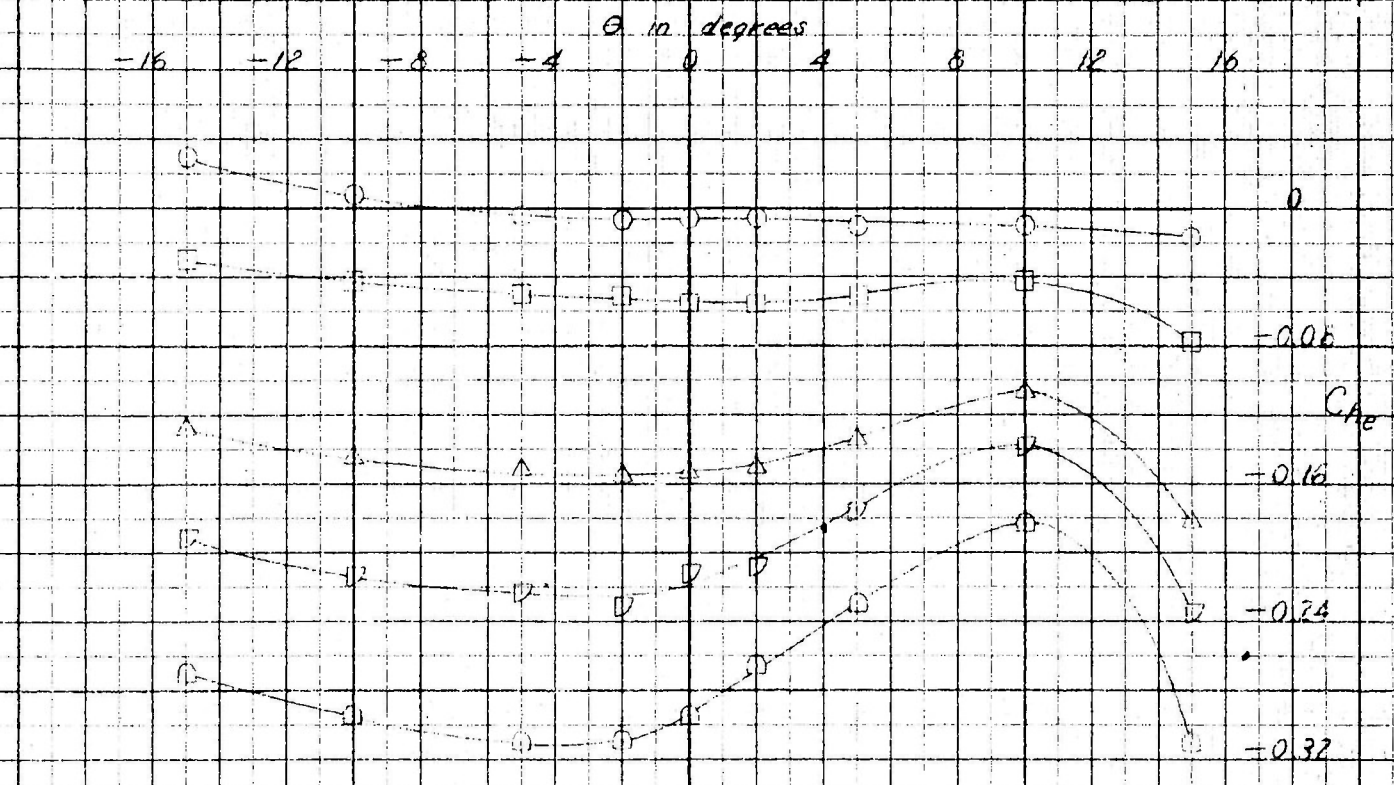
FIGURE 11C

Figure 11 (Continued)
 (c) Configuration B(HV)_x, $\delta_{TE} = 0^\circ$

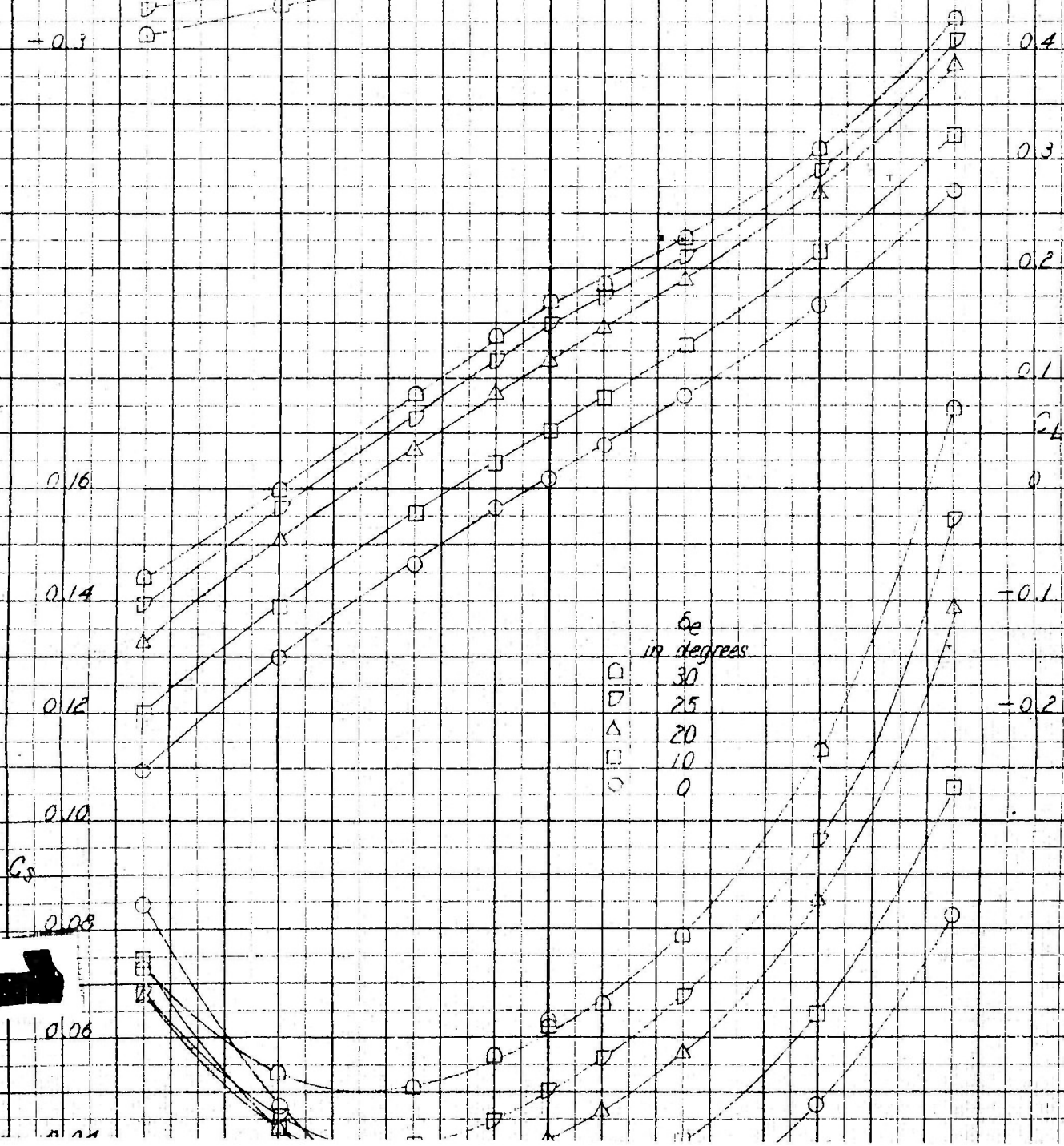
CONFIDENTIAL

15 MAY 52

ALFO 866



CONFIDENTIAL



2

CONFIDENTIAL

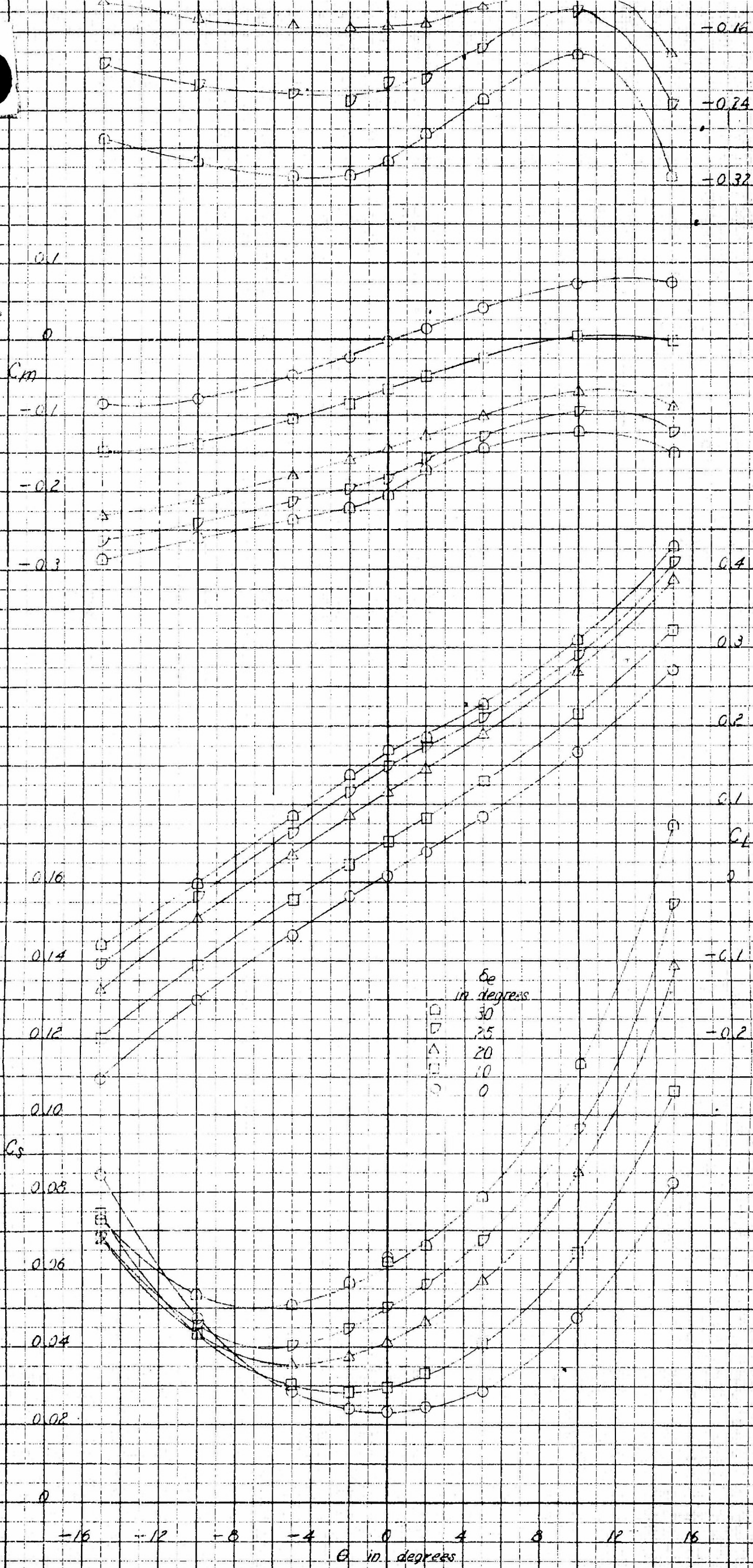


FIGURE 11d

Figure 11 (Continued)
(d) Configuration BCL(HV) χ , $\delta_{TE} = 0^\circ$

CONFIDENTIAL

PL 6 May 52

AIRFO B65

CONFIDENTIAL

CONFIDENTIAL

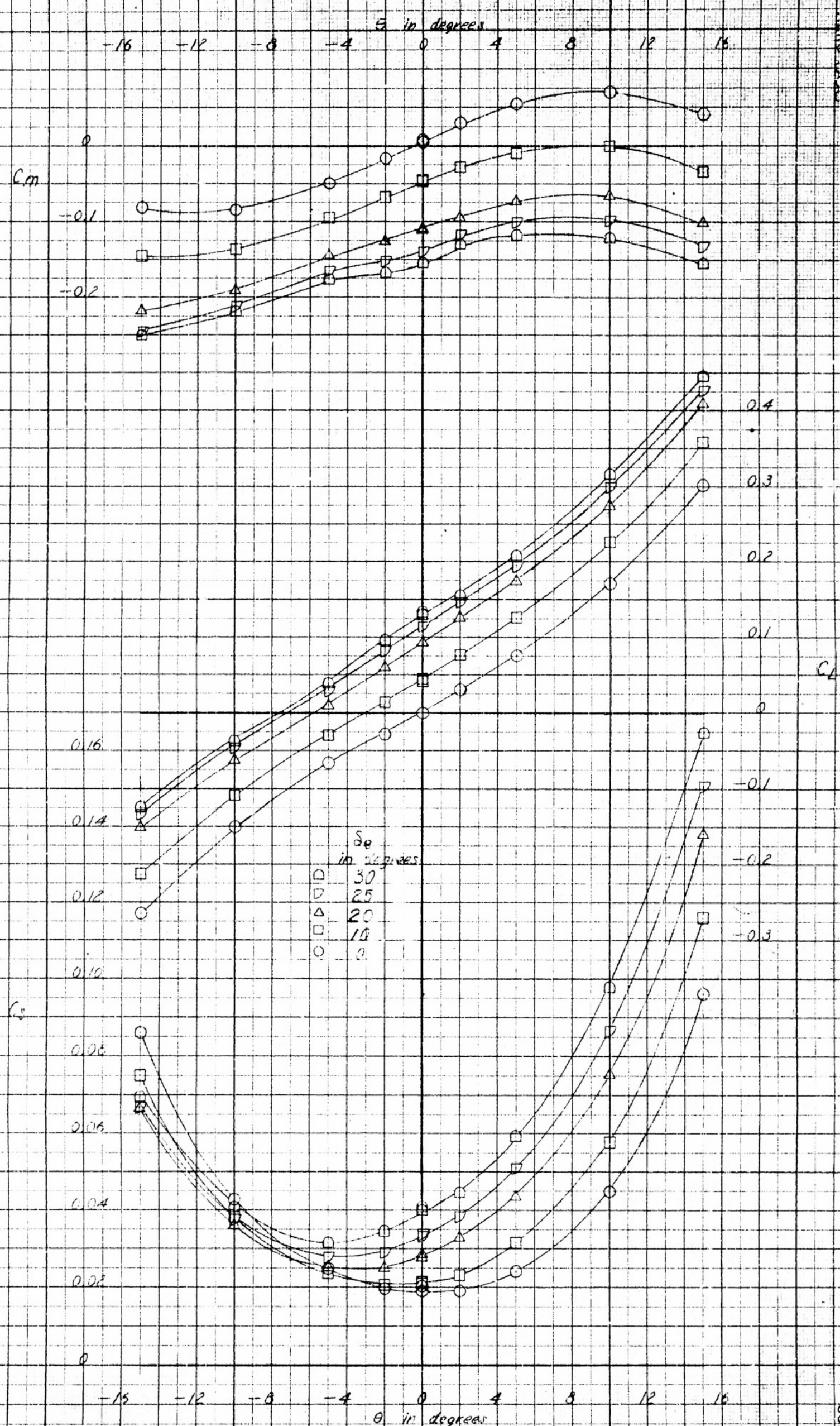


Figure 11 (Continued)

(e) Configuration B(HV)_k, $\delta_{Te} = 0^\circ$

FIGURE 11e

PA 541452

CONFIDENTIAL

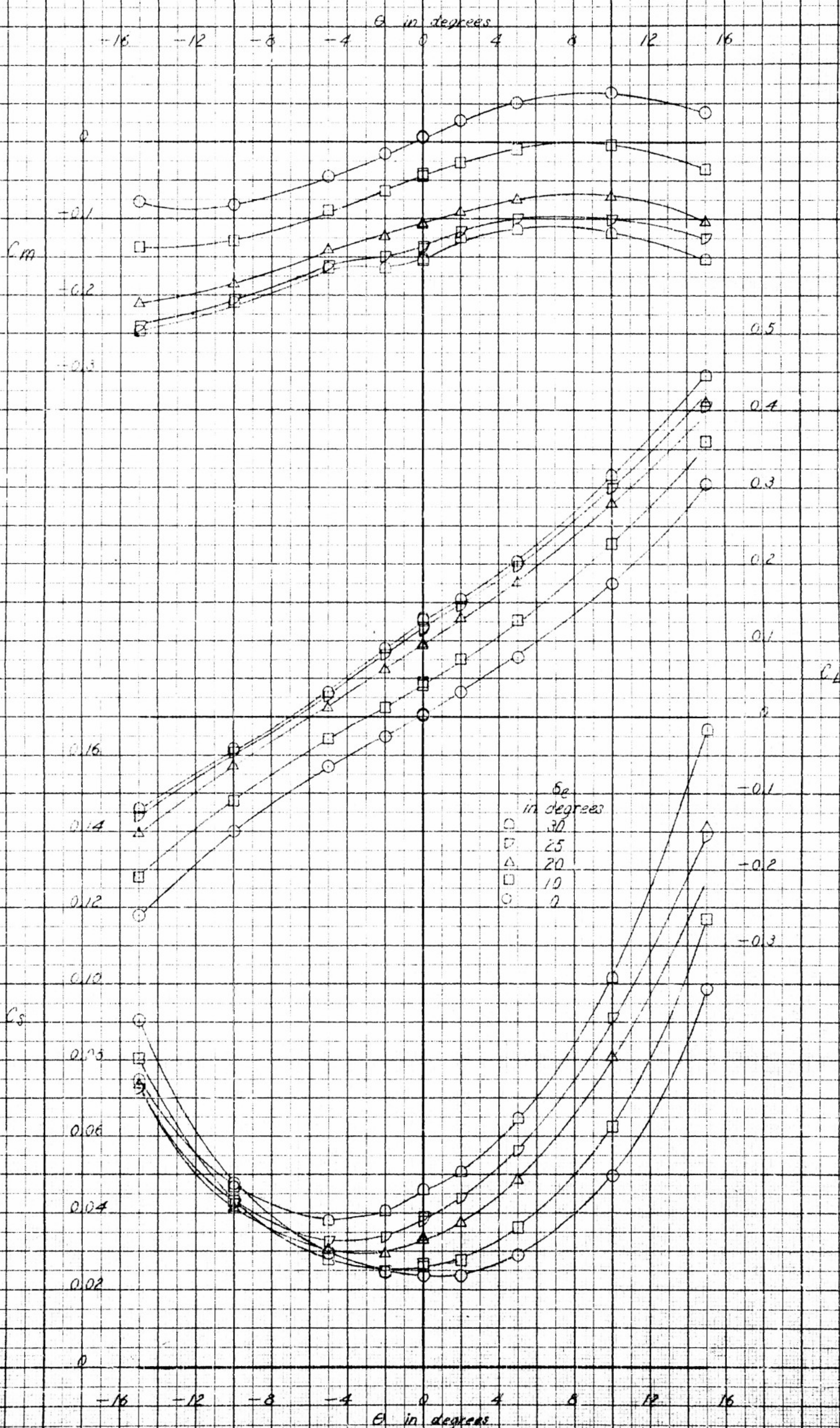


Figure 11 (Continued)

(A) Configuration B314V₁, $\delta_e = 0^\circ$

FIGURE 11

CONFIDENTIAL

AERO 866

JAN 12 1952

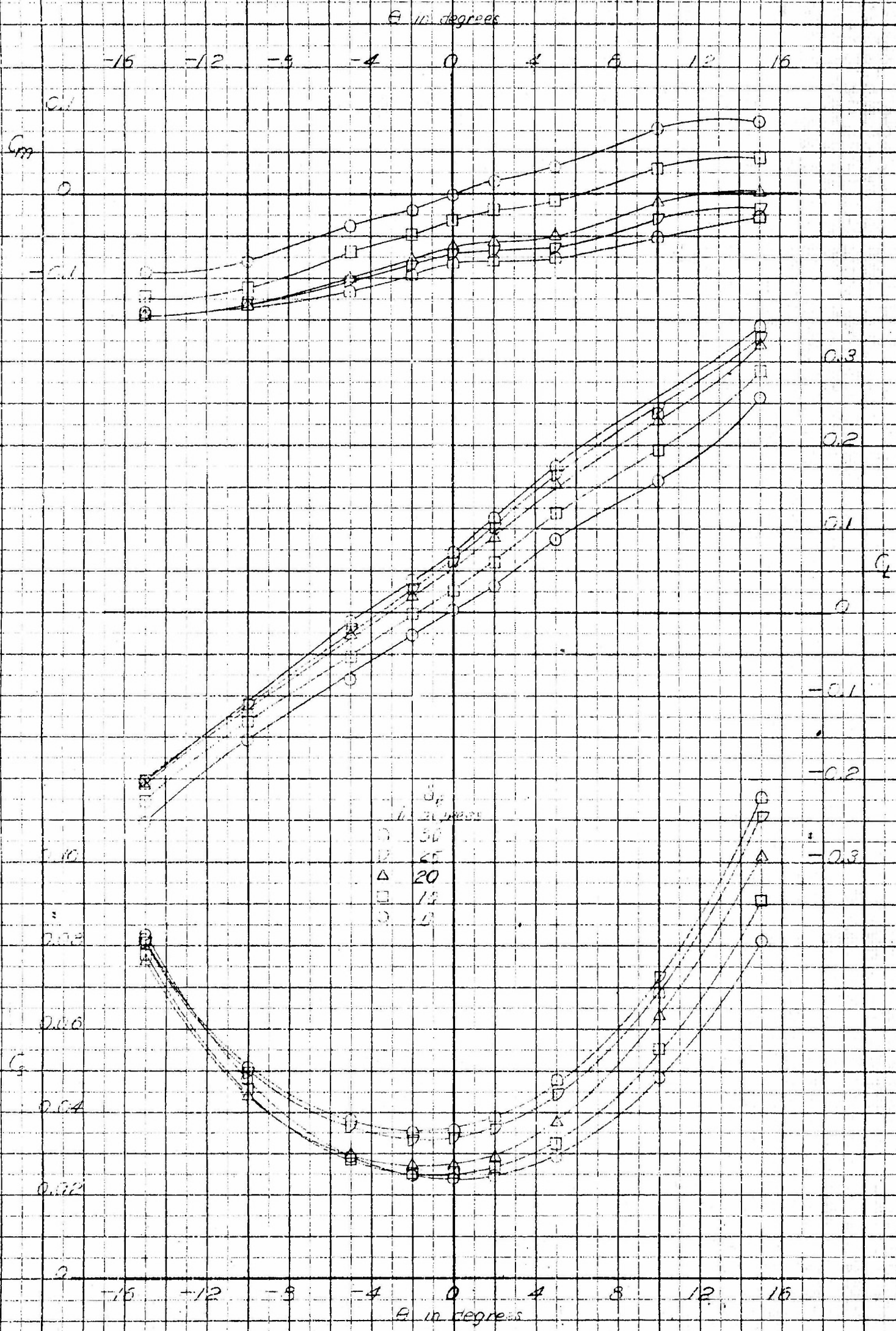


Figure 11 (Continued)

(g) Configuration B(IV) $\delta_{Te}=0^\circ$

FIGURE 11

CONFIDENTIAL

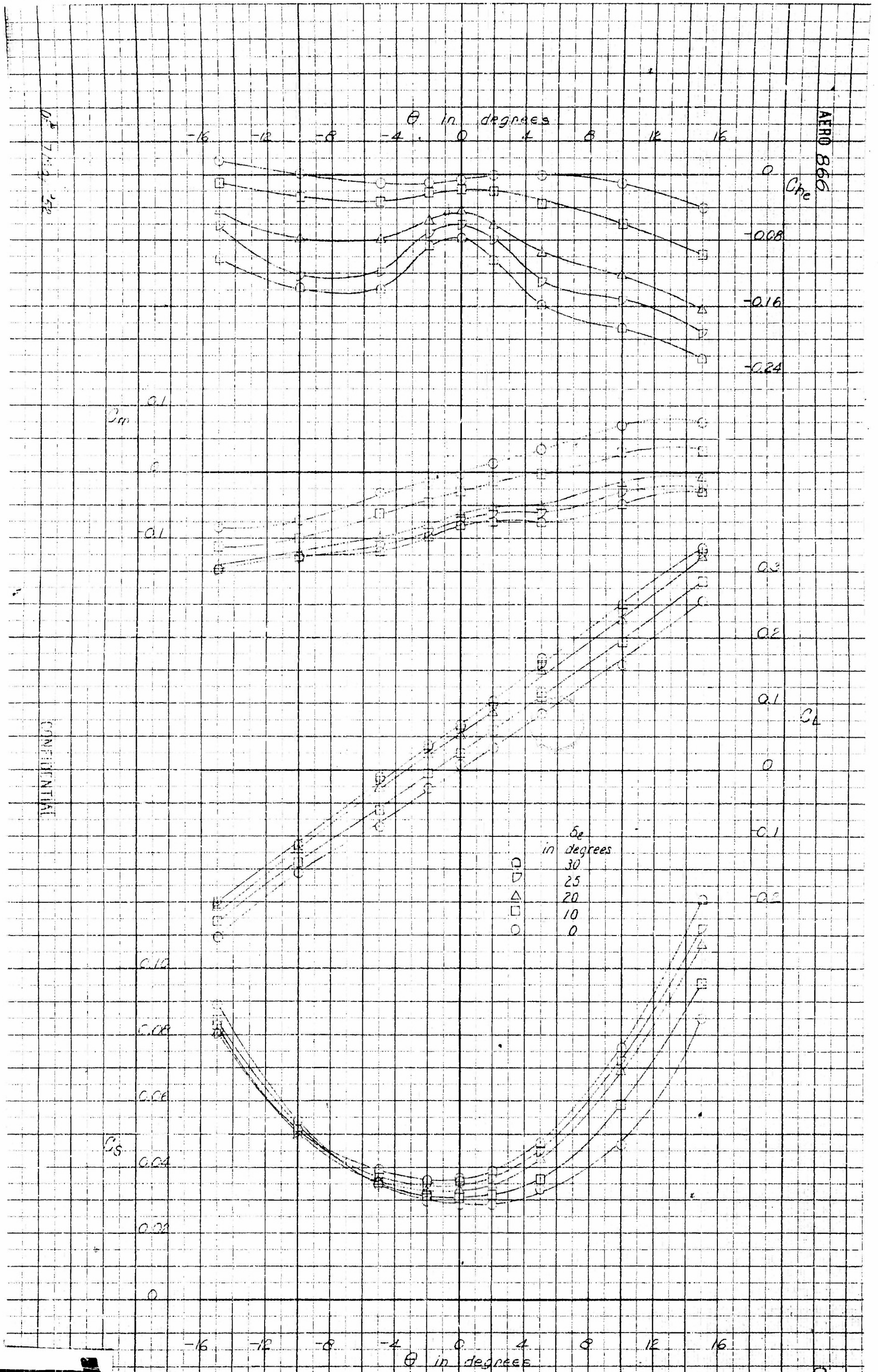


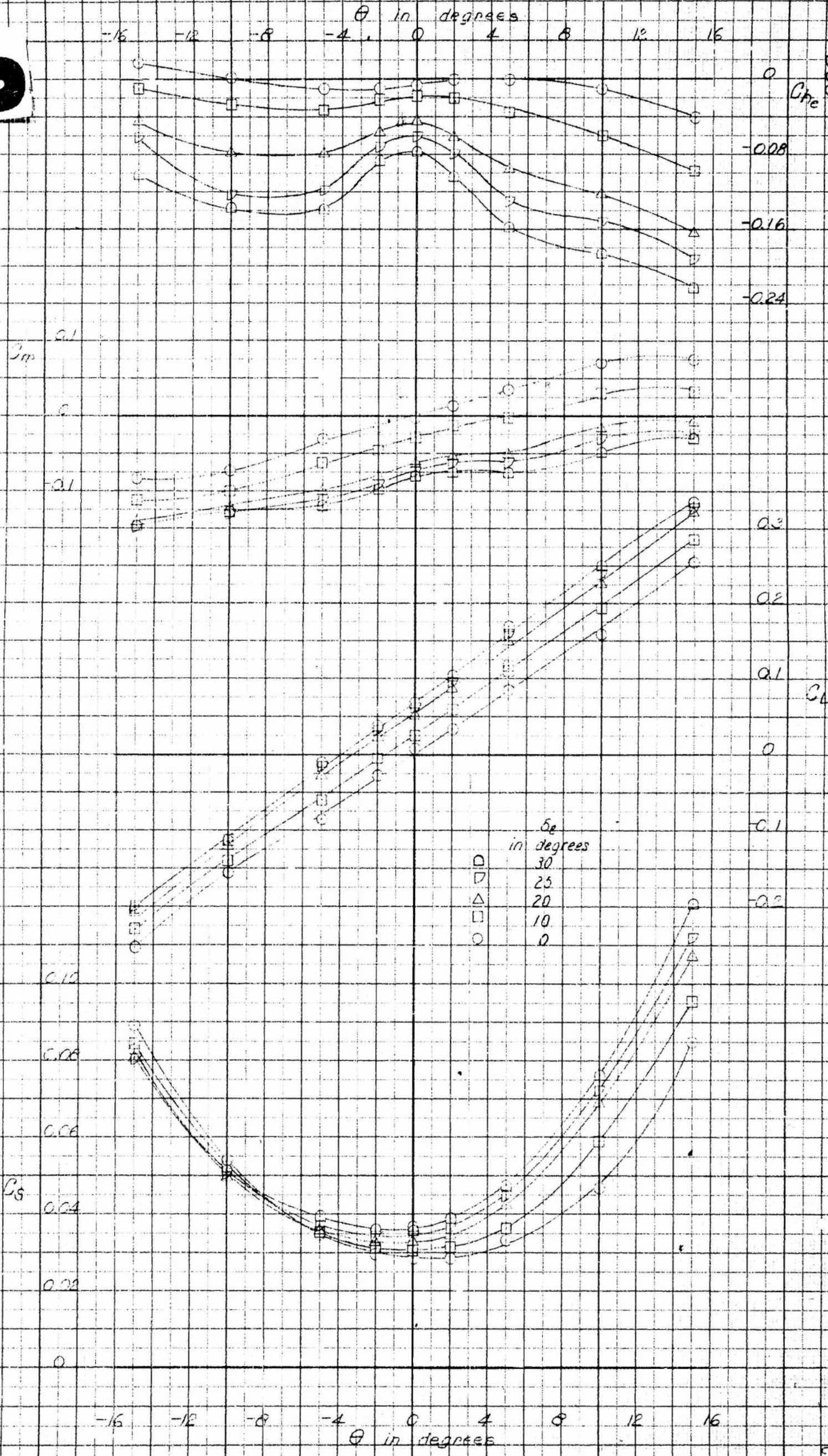
Figure 11 (Concluded)

(b) Configuration RC/411 $\delta = 0^\circ$

AERO 866

δ°

2



CONFIDENTIAL

FIGURE 11h

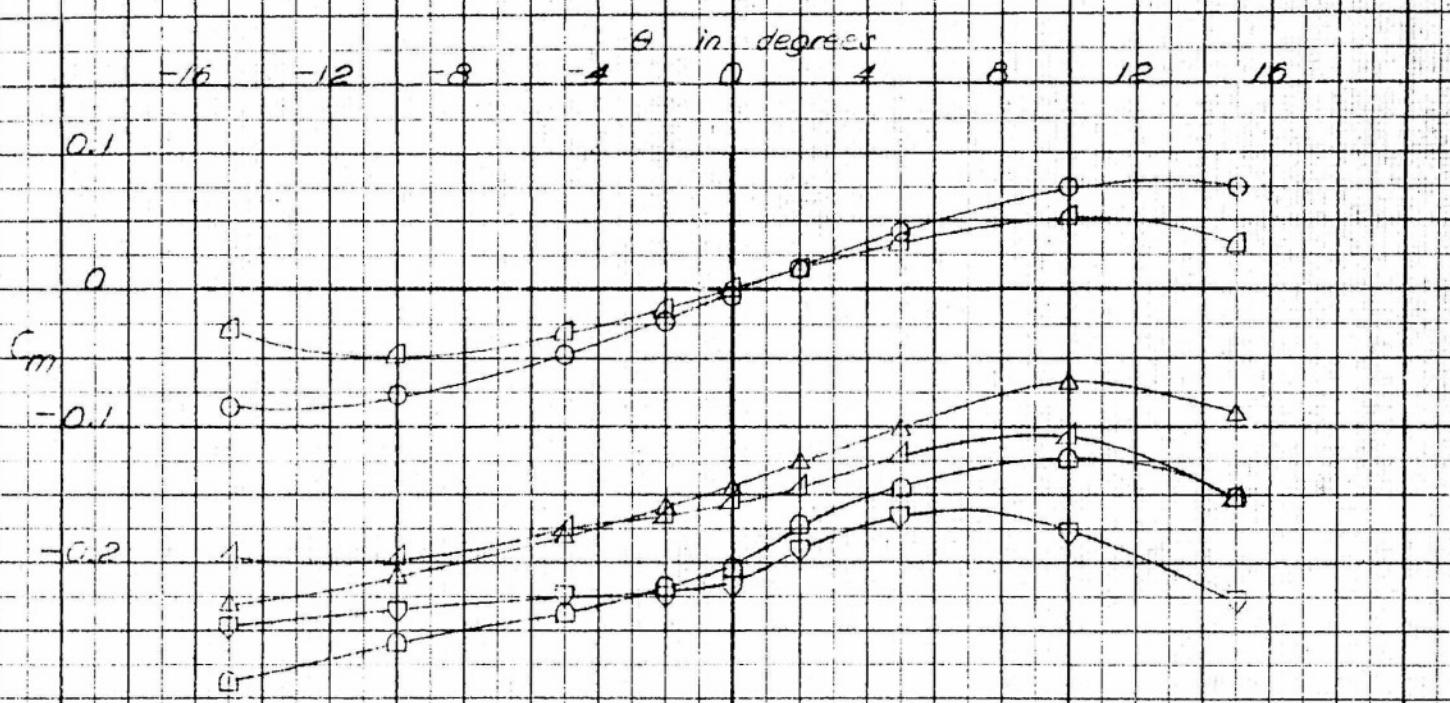
Figure 11 (Concluded)

In Configuration BC(HV)_H, $\delta_{Te} = 0^\circ$

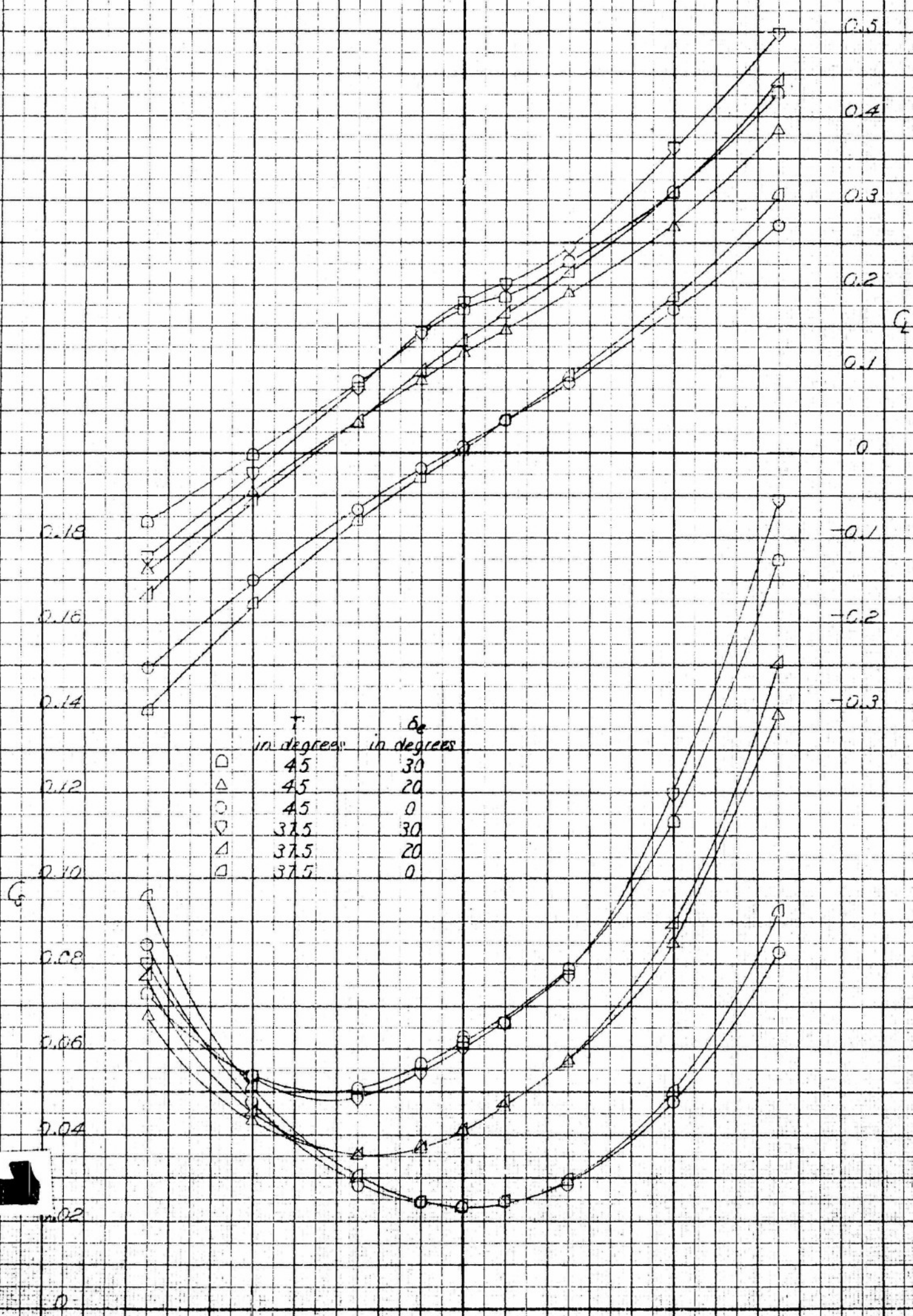
CONFIDENTIAL

16M 5 May 52

AERO 866



CONFIDENTIAL



	T in degrees	δ_e in degrees
\square	45	30
\triangle	45	20
\circ	45	0
∇	37.5	30
Δ	37.5	20
\diamond	37.5	0

CONFIDENTIAL

2

CONFIDENTIAL

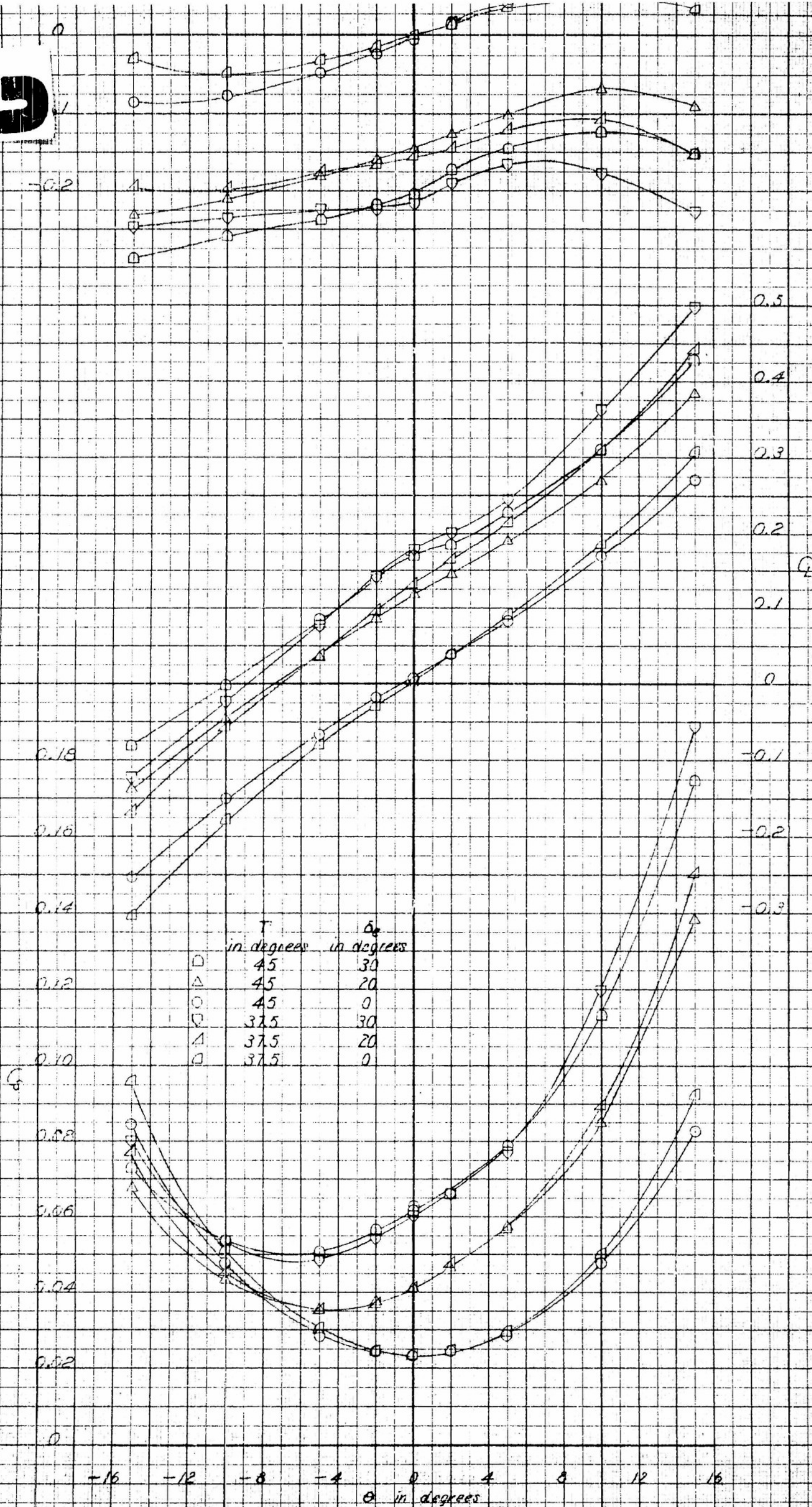


FIGURE 12

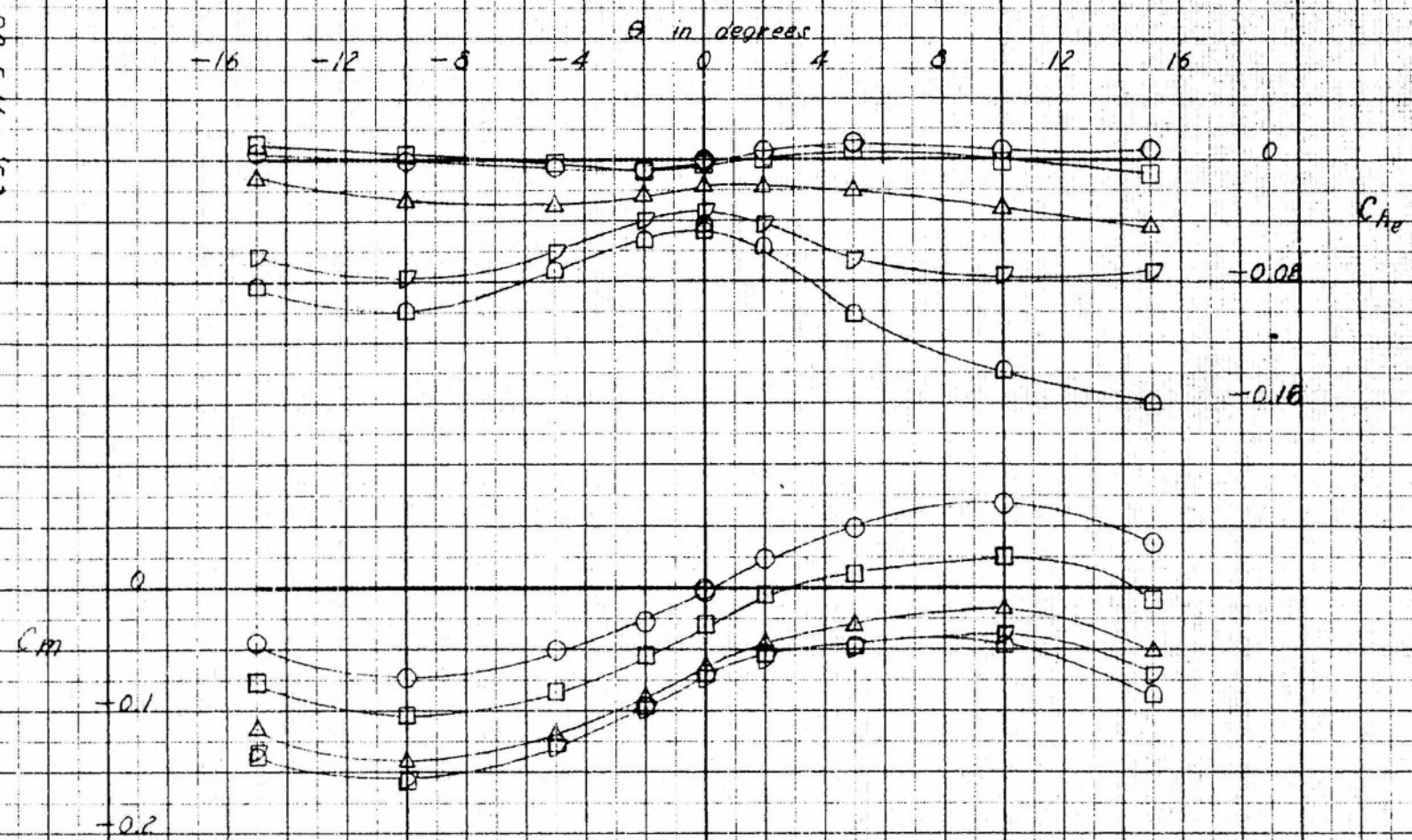
Figure 12 - Effect of X-Tail Dihedral on Longitudinal Characteristics of a 1/48 Scale Model XZS2B-1 Airship
Configuration BC(AV)X, $\delta_{T_e} = 0^\circ$

CONFIDENTIAL

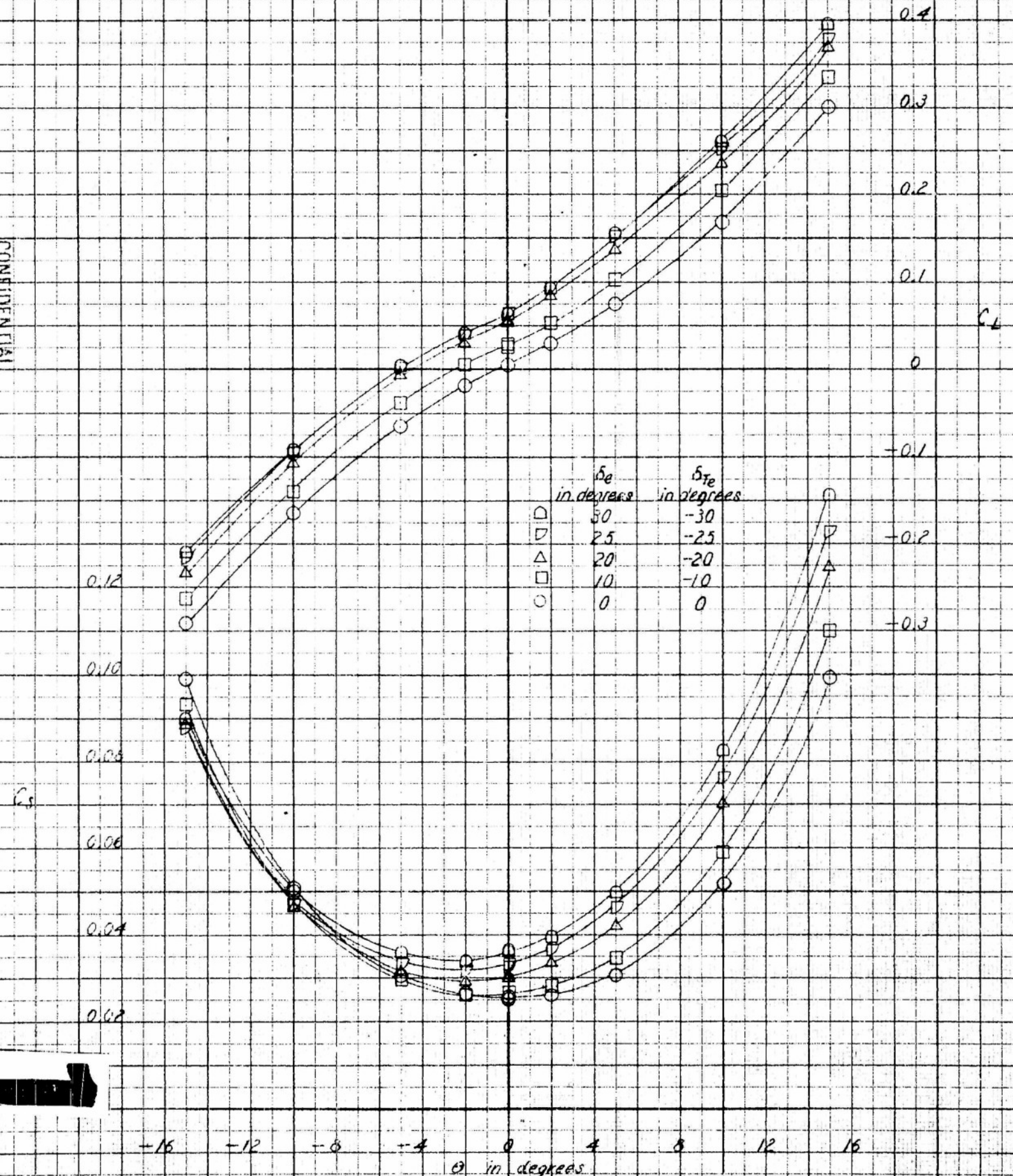
53+

PC 5 May 52

AERO 0066



CONFIDENTIAL



2

CONFIDENTIAL

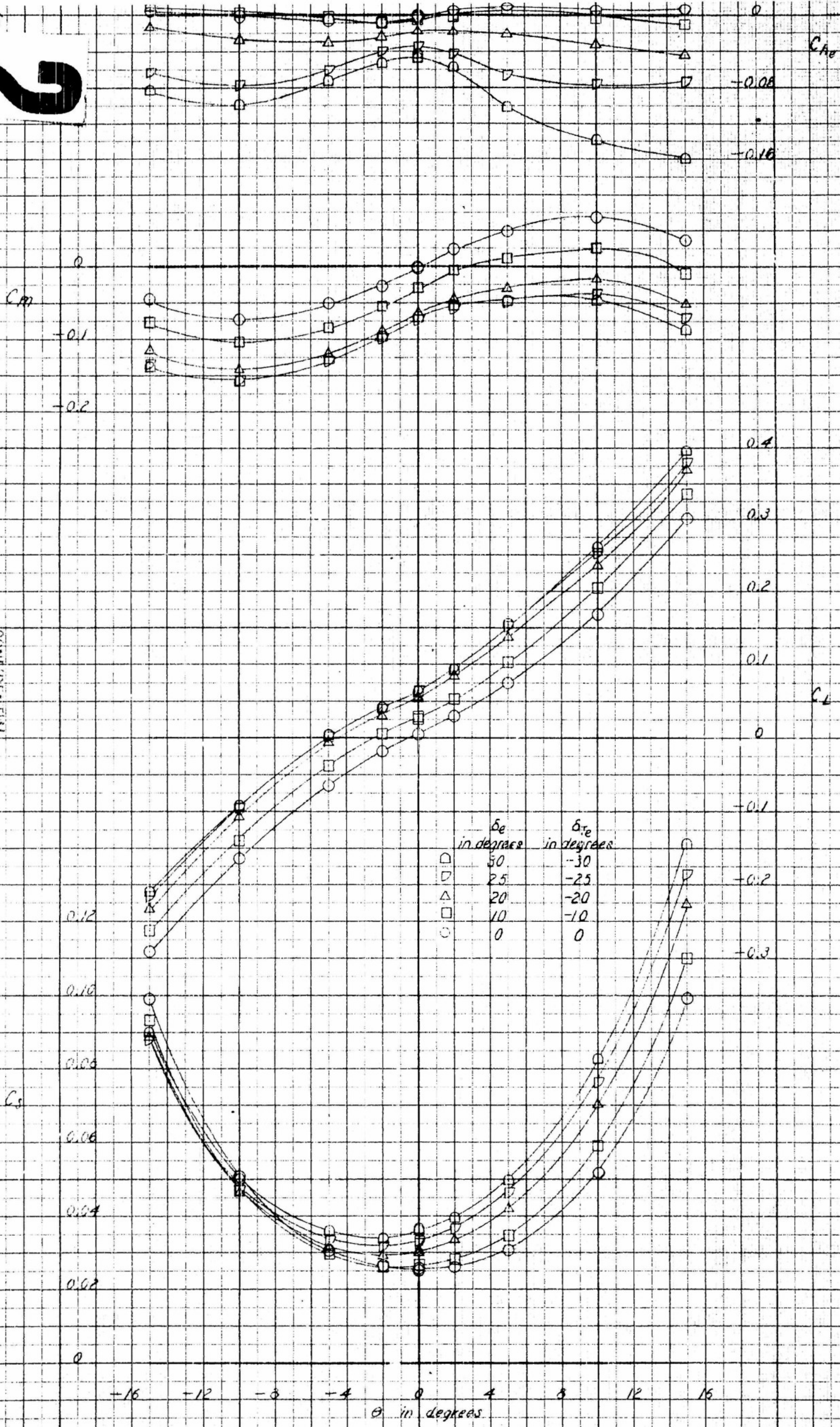


FIGURE 13-2

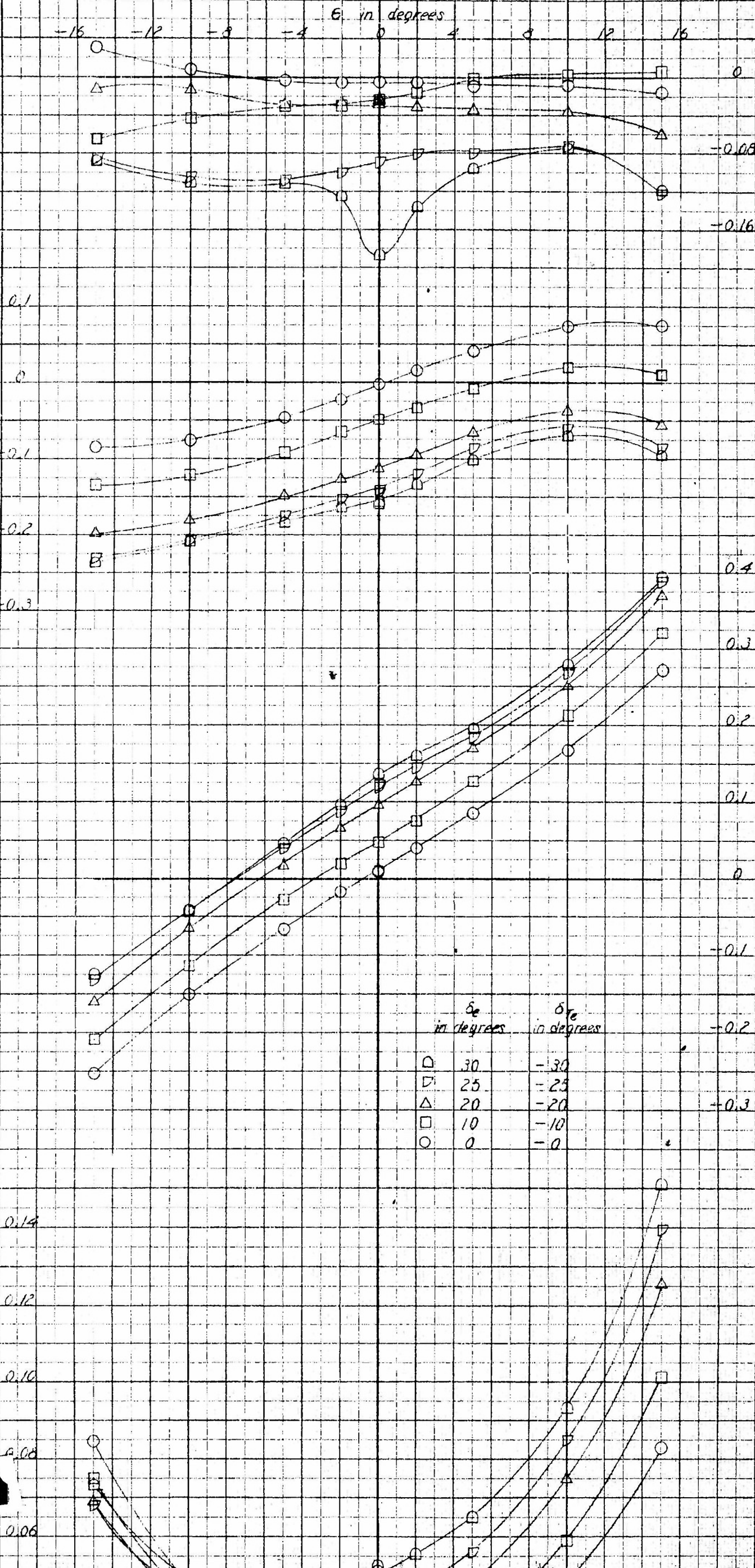
Figure 13-Effect of Elevator and Tab on Longitudinal Characteristics of a 1/48-Scale Model XZS26-1 Airship (a) Configuration BC/HVc

CONFIDENTIAL

PC 5 May 52

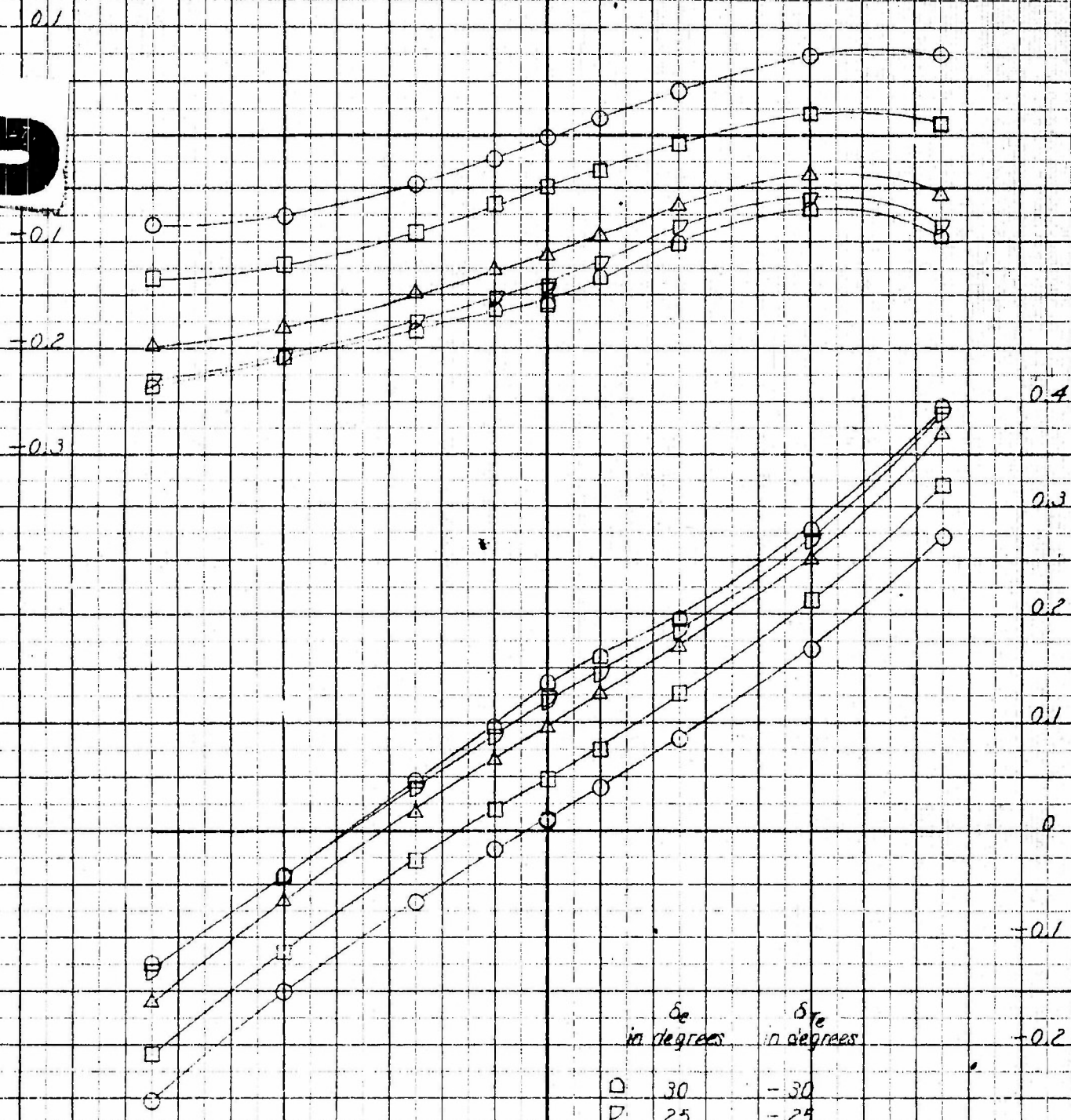
AERO B&B

CONFIDENTIAL



2

CONFIDENTIAL



C_L

0.14
0.12
0.10
0.08
0.06
0.04
0.02
0

-16 -12 -8 -4 0 4 8 12 16
 θ in degrees

Figure 13 (Continued)
(b) Configuration $BC(HV)_x$

FIGURE 13 b

CONFIDENTIAL

14M 6 May 52

AERO 866

CONFIDENTIAL

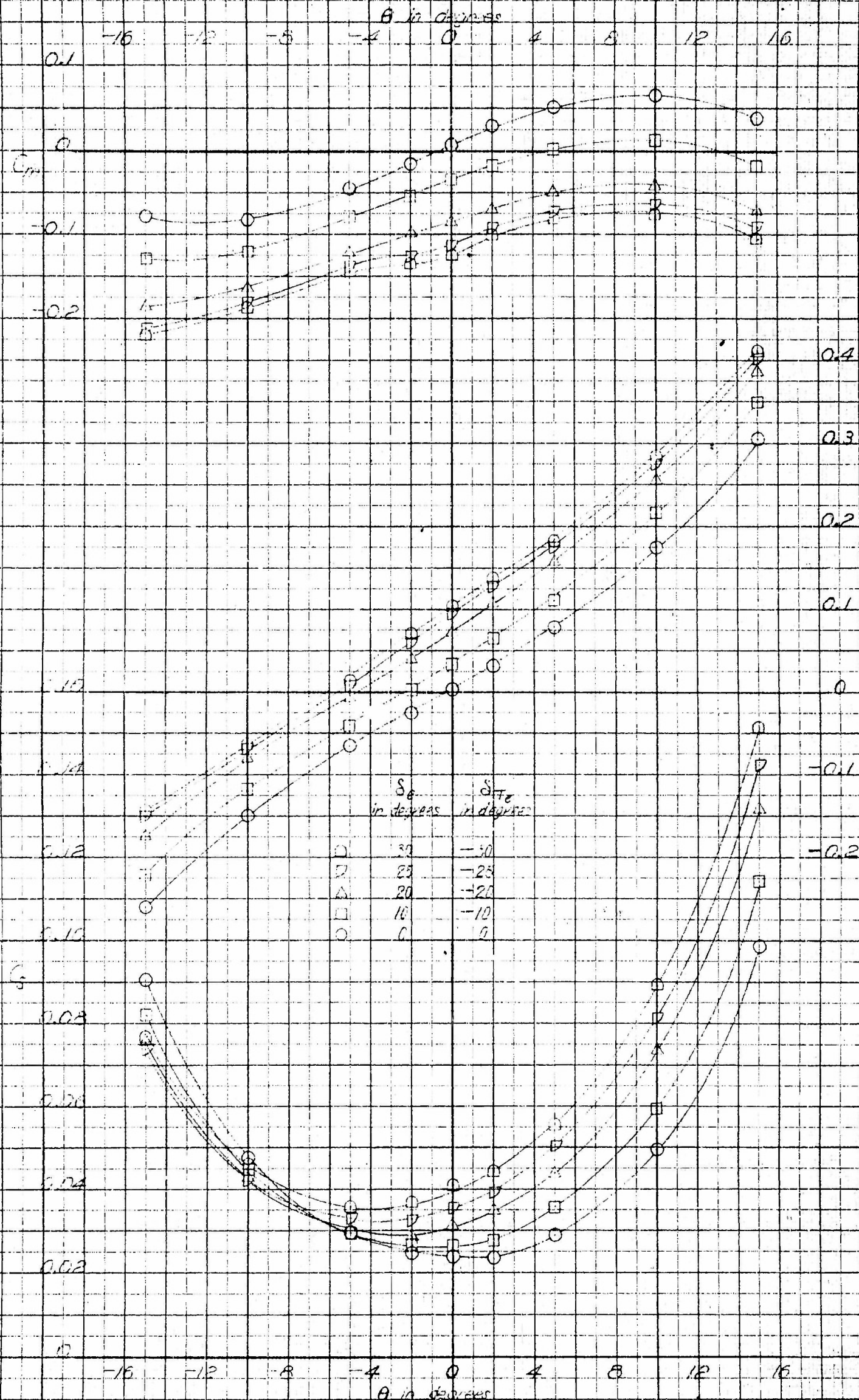


FIGURE 13.C

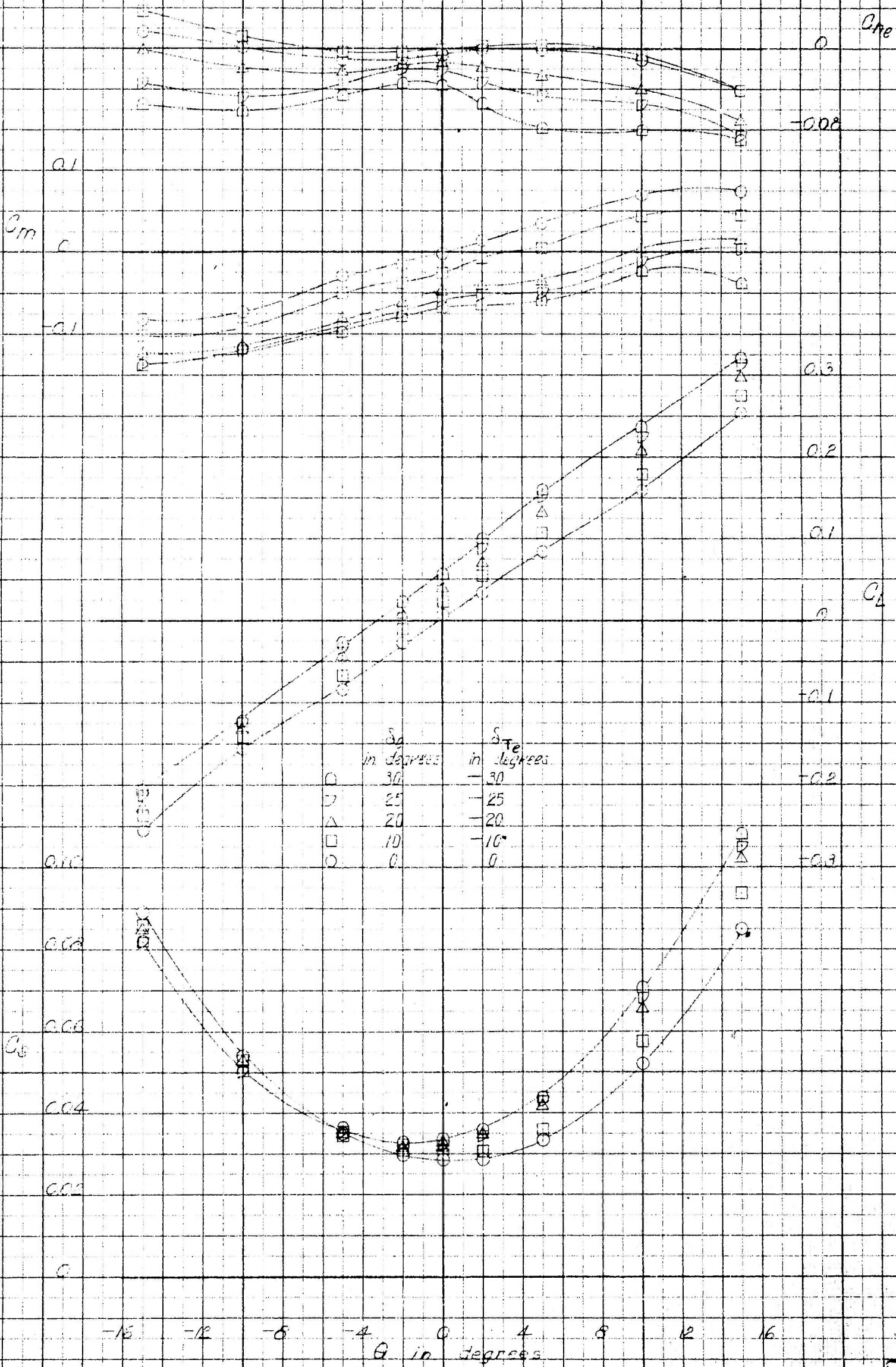
Figure 13 (Continued)
(c) Configuration BC(HV)A

CONFIDENTIAL

14.8 May '52

AEROBGS

θ in degrees



CONFIDENTIAL

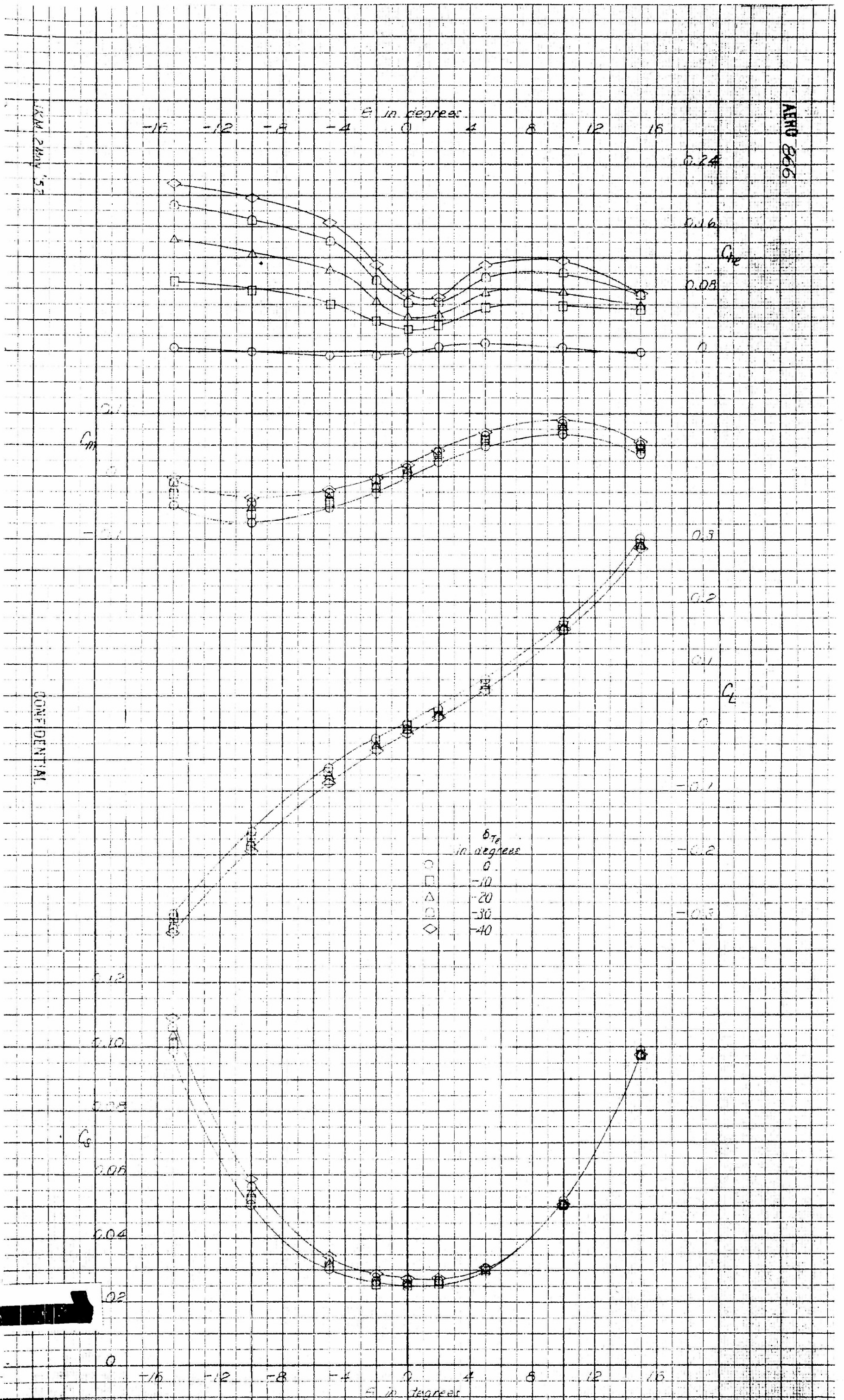
FIGURE 13 d

Figure 13 (Concluded)
(d) Configuration BC(HV)M

CONFIDENTIAL

CONFIDENTIAL

CONFIDENTIAL



CONFIDENTIAL

2

CONFIDENTIAL

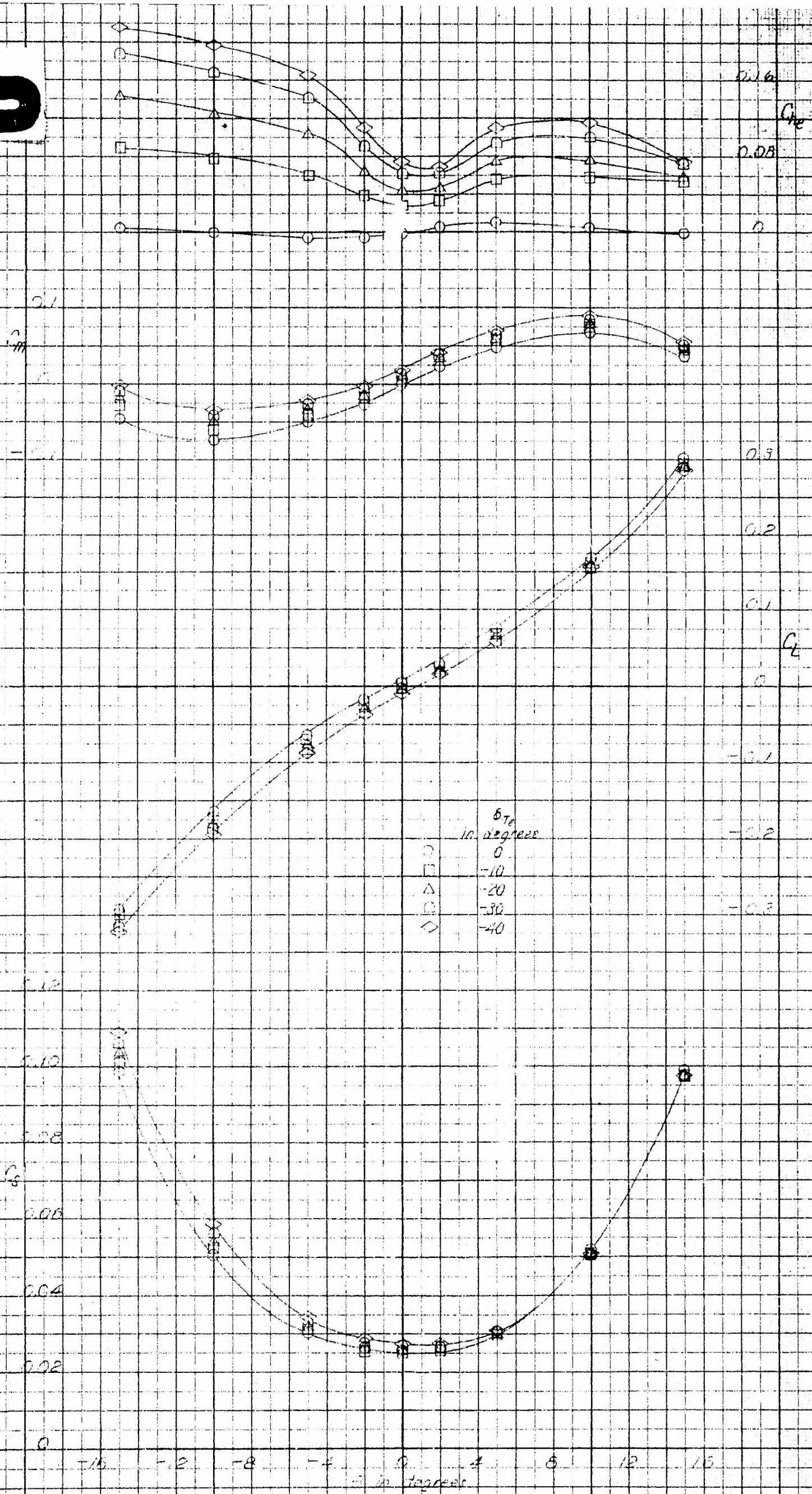


FIGURE 14 a

Figure 14 - Effect of Tab Deflection on Longitudinal Characteristics of
a 1/48-Scale Model XZS26-1 Airship
(a) Configuration BC(HV)0, $\delta_e = 0^\circ$

CONFIDENTIAL

MM 5103, 152

AERO 856

CONFIDENTIAL

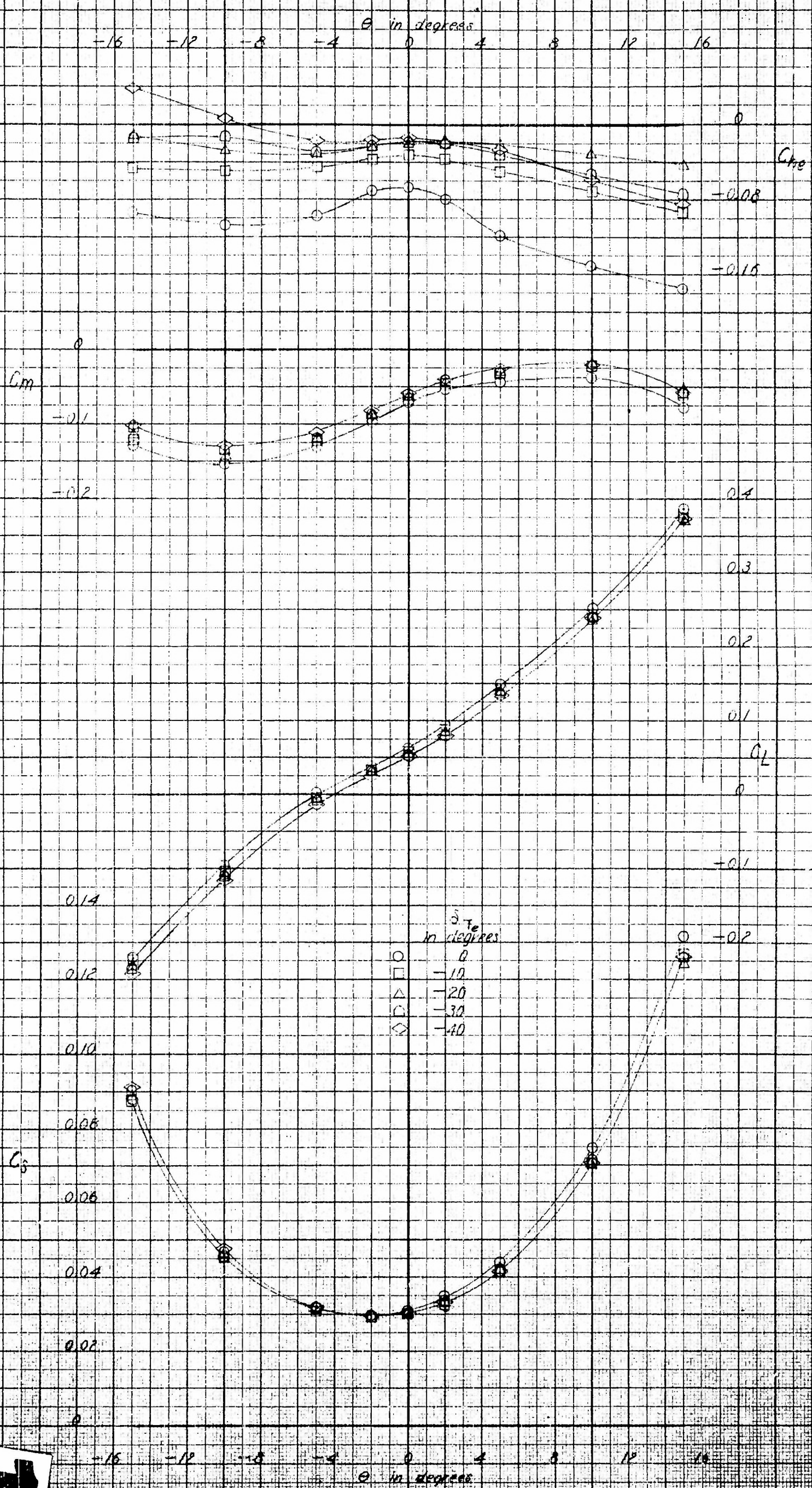
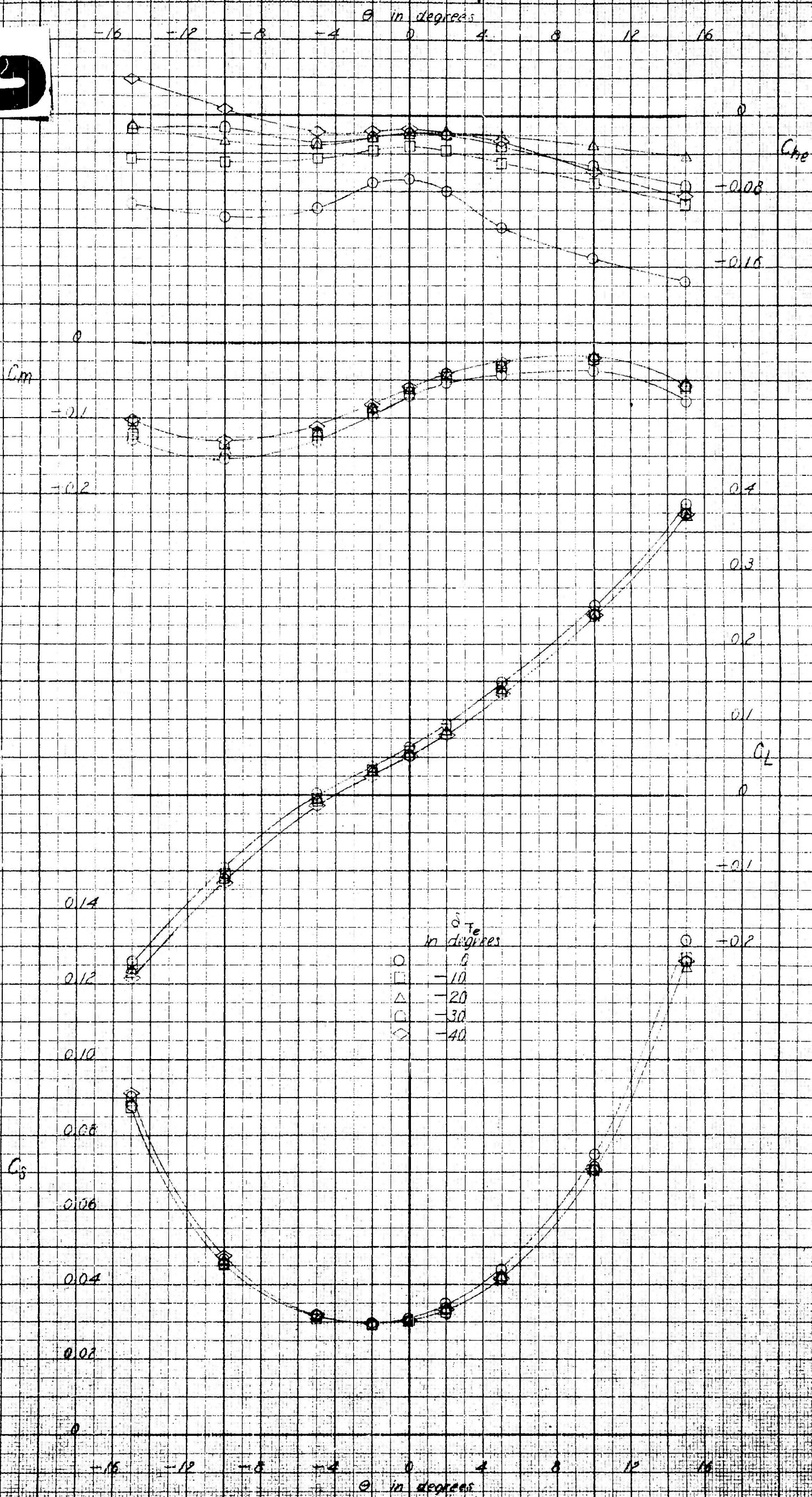


Figure 14 (Continued)



2

AERO 856



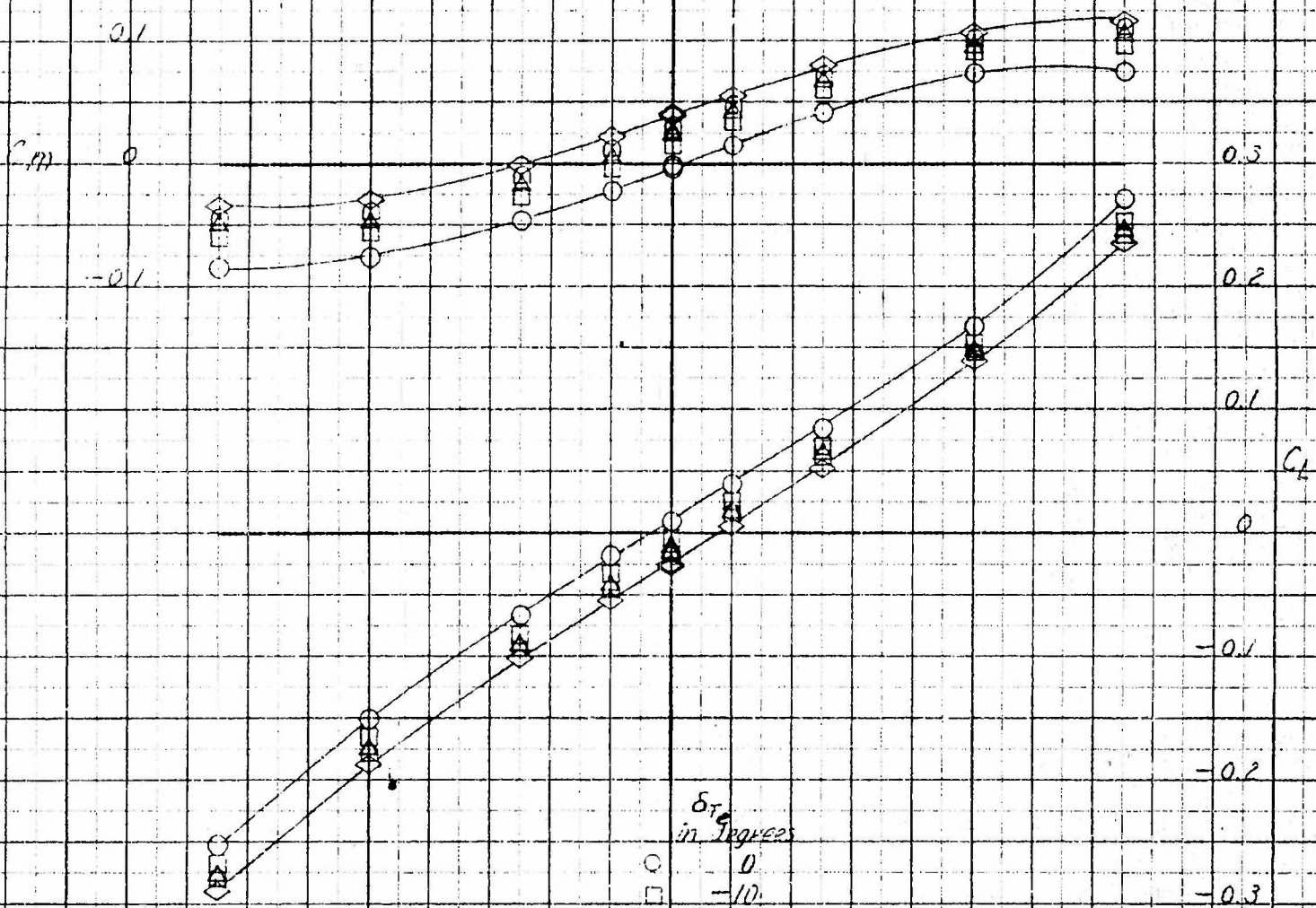
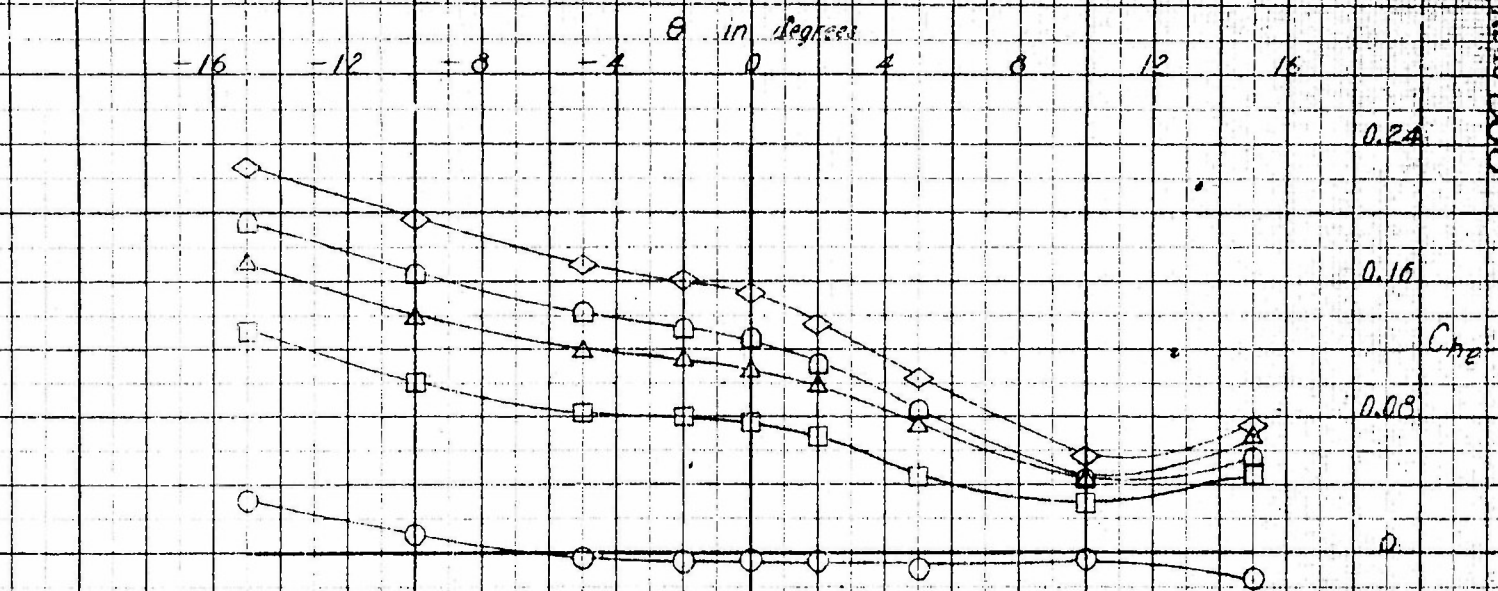
CONFIDENTIAL

CONFIDENTIAL

Figure 14 (Continued)
(b) Configuration BC/HVc, $\delta_e = 70^\circ$

25 May '52

AERO 2866



CONFIDENTIAL

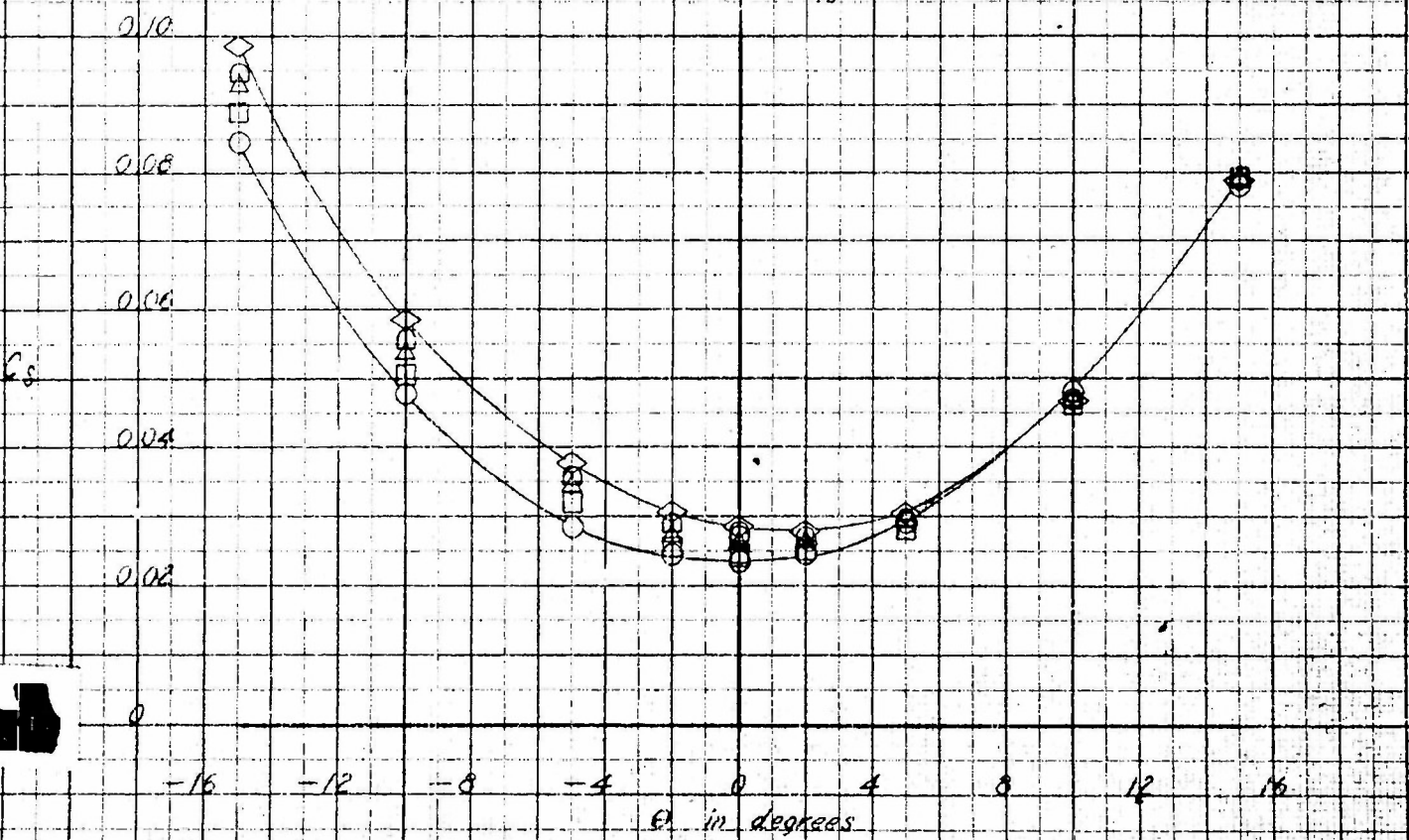
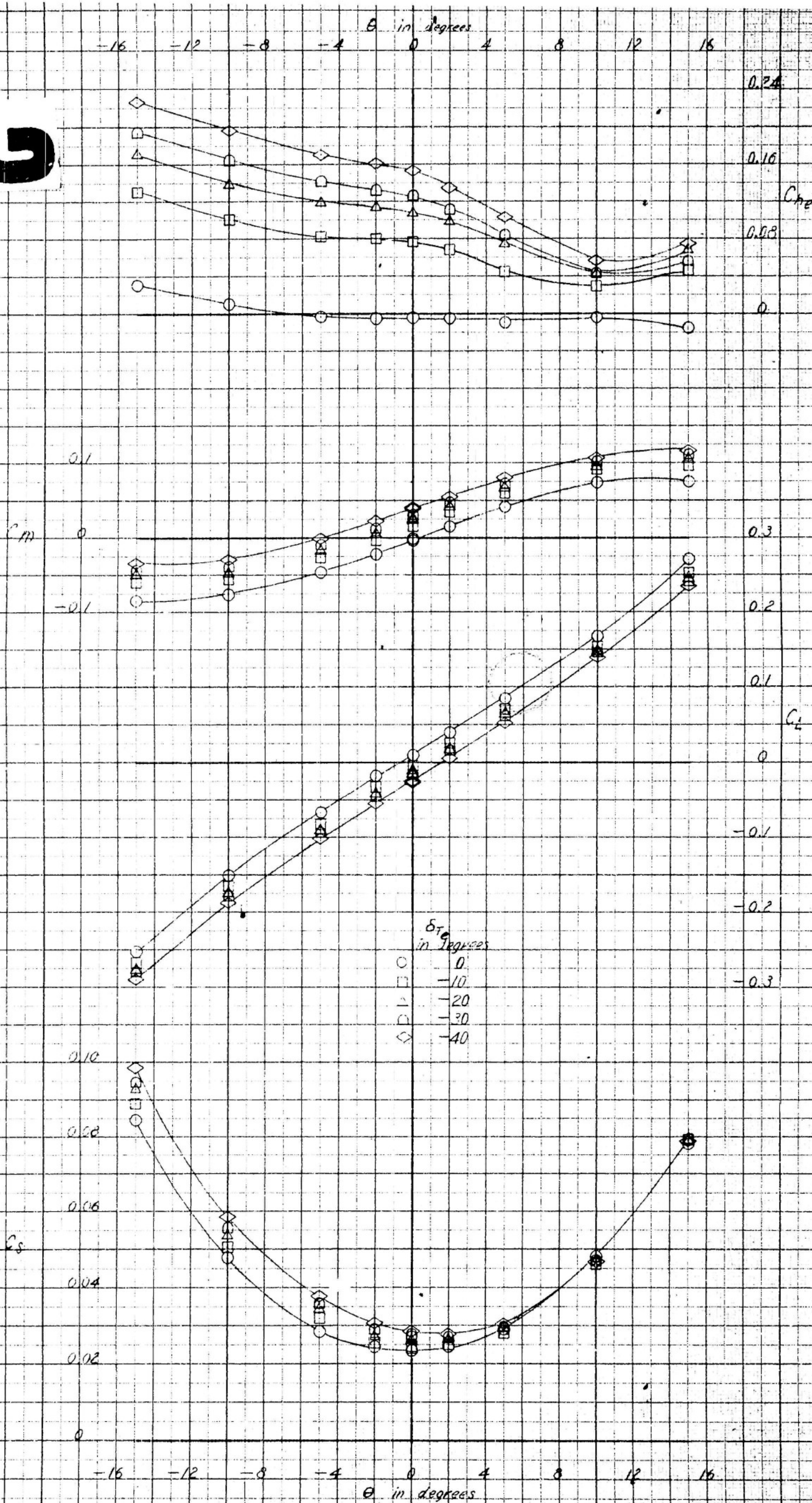


Figure 14 (Continued)

FIGURE

CONFIDENTIAL

2



CONFIDENTIAL

FIGURE 14 C

Figure 14 (Continued)

(c) Configuration BC(HV)_x, $\delta_e = 0^\circ$

CONFIDENTIAL

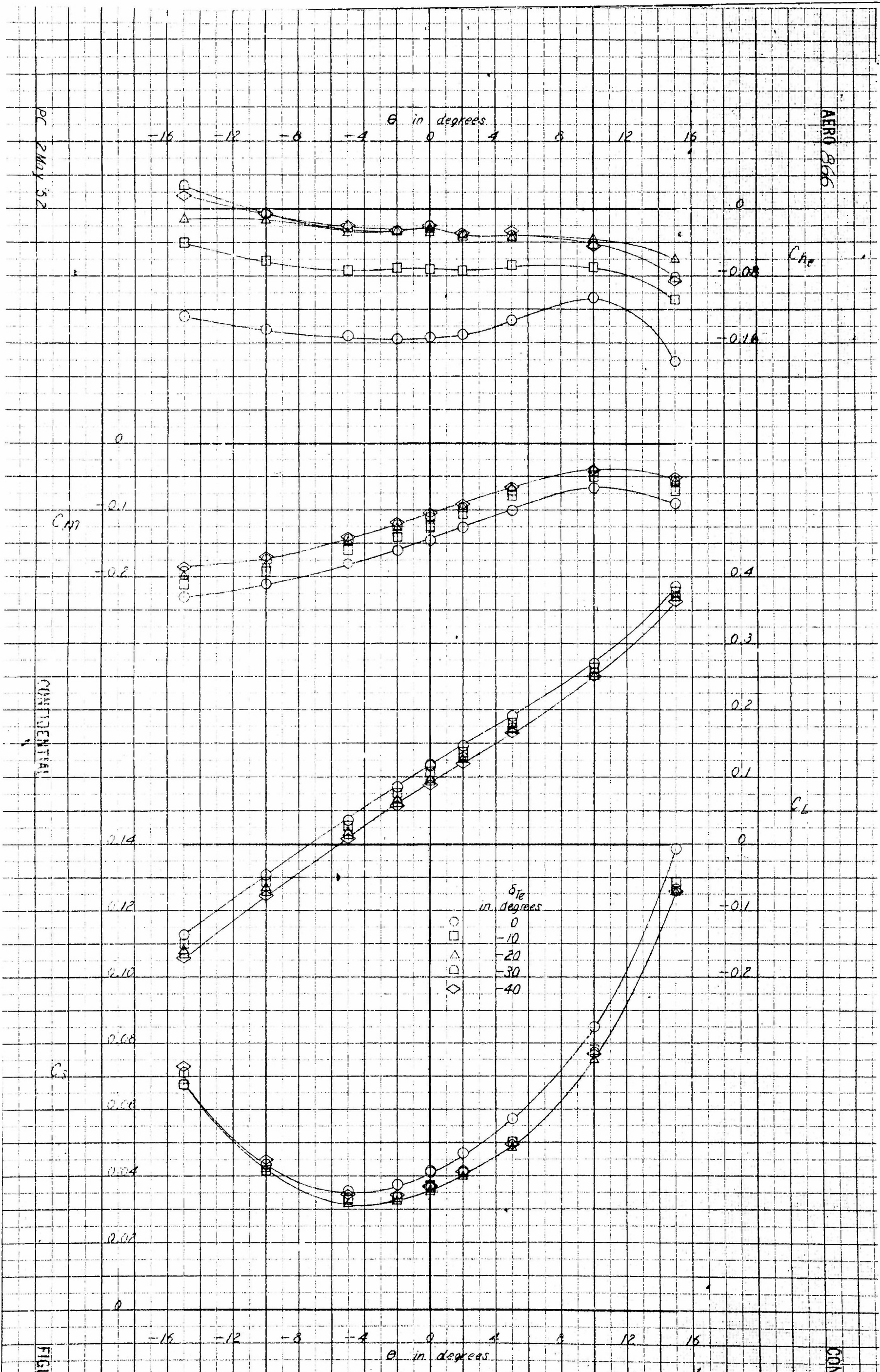
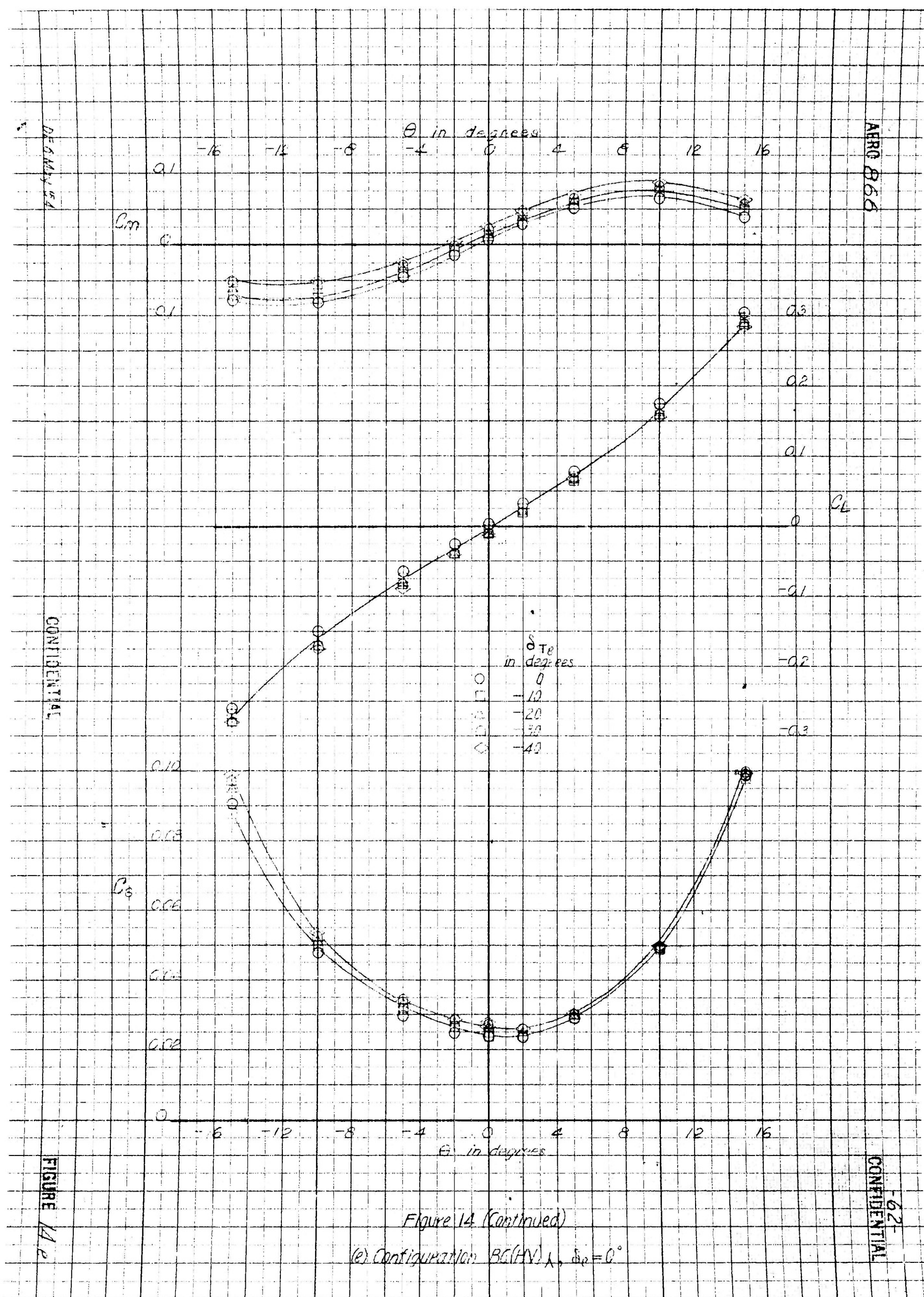


FIGURE 14.d

Figure 14 (Continued)
 (d) Configuration BC(HV)_x, $\delta_e = 20^\circ$



UHM 6 MAY '52

AERO 666

CONFIDENTIAL

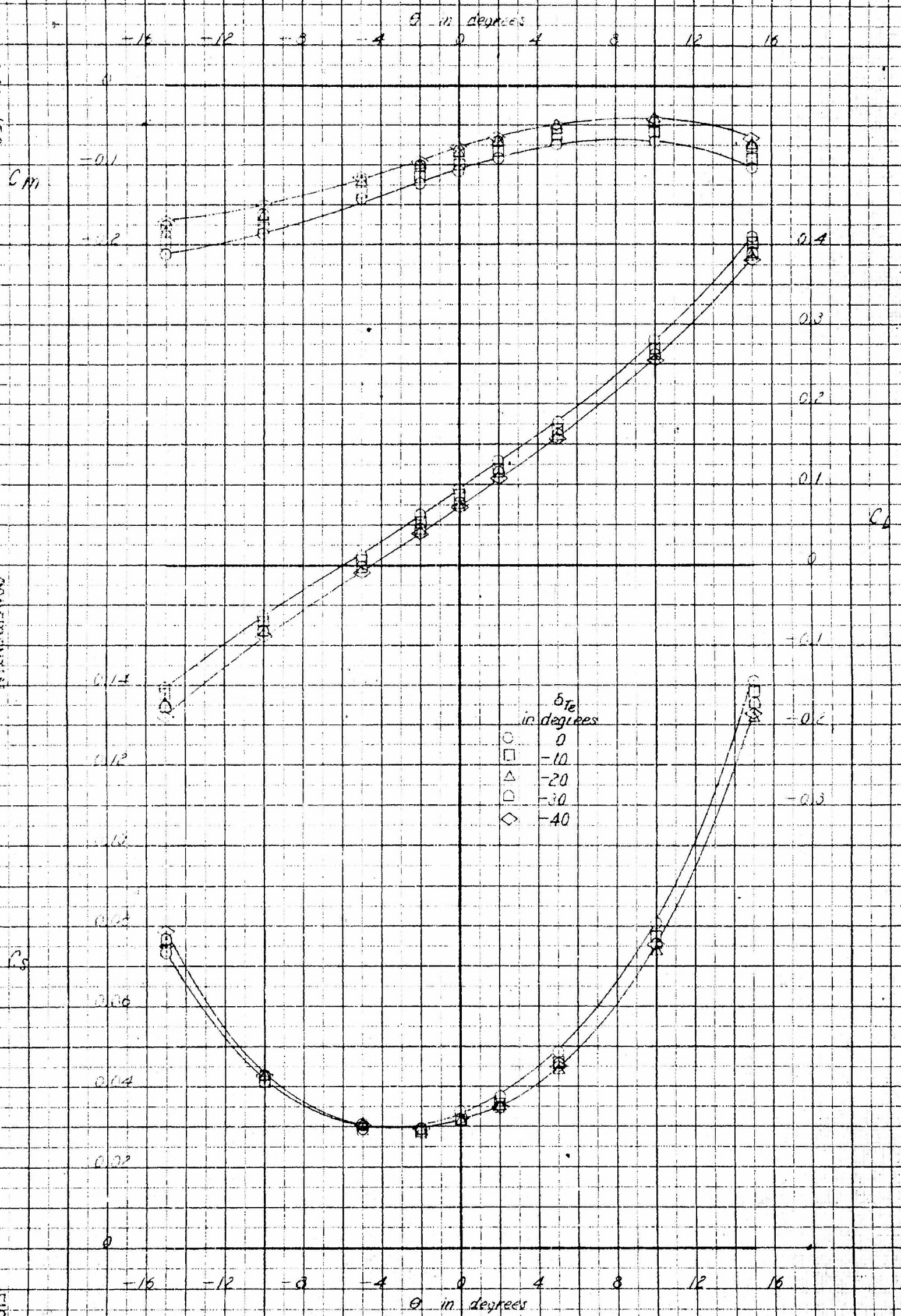


FIGURE 14f

Figure 14 (Continued)
(f) Configuration BC(HV)₁, $\delta_e = 20^\circ$

CONFIDENTIAL

-63-

JKM 9 May 52

AERO 866

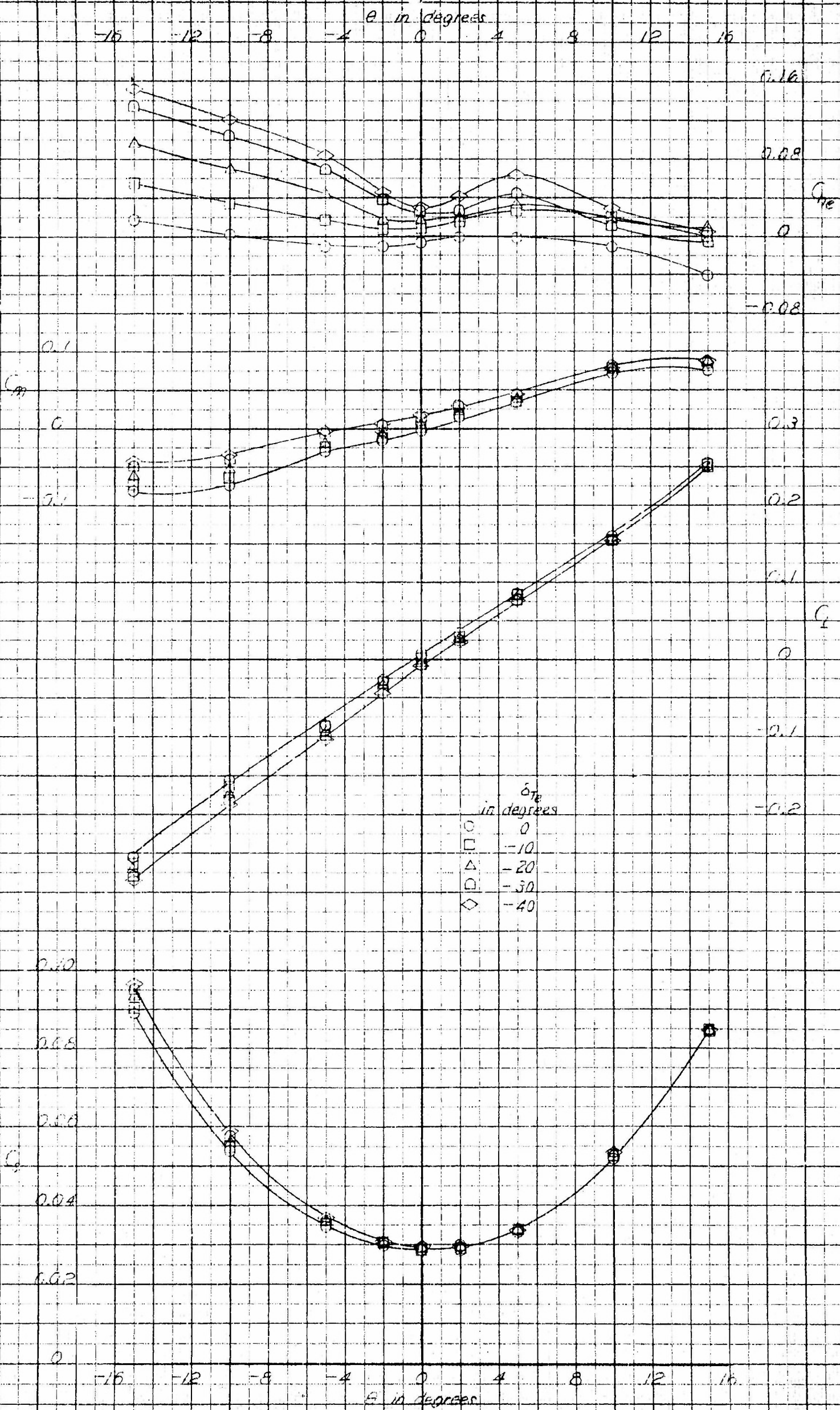


FIGURE 14.9

Figure 14 (Continued)
(g) Configuration BC(HV)₄, $\delta_e = 0^\circ$

CONFIDENTIAL

PL 9 MAY 52

AERO 565

CONFIDENTIAL

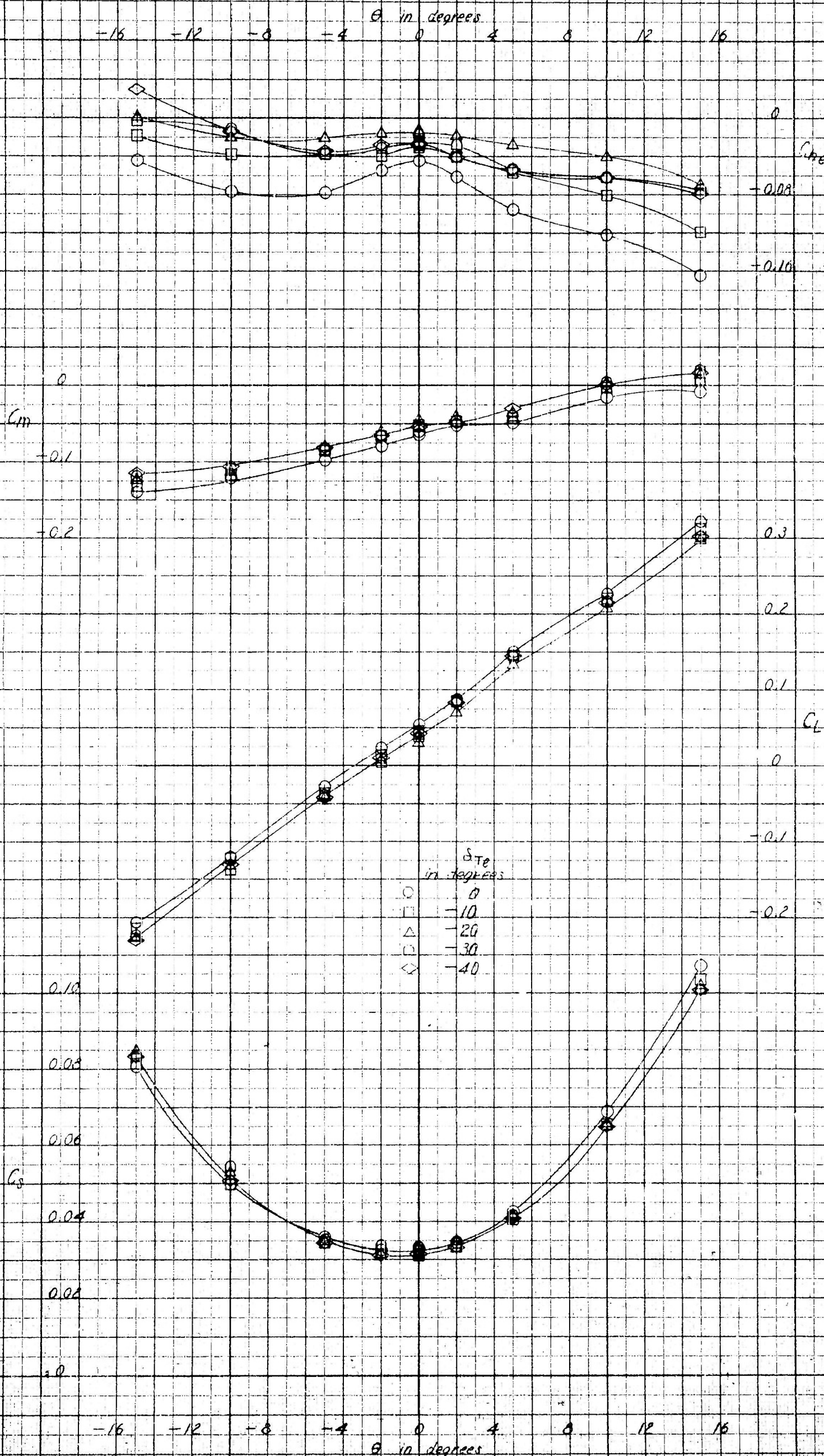


Figure 14 (Concluded)

(b) Conflavation $Re(HV)$, $S_n = 20$

CONFIDENTIAL

2

AERO 566

CONFIDENTIAL

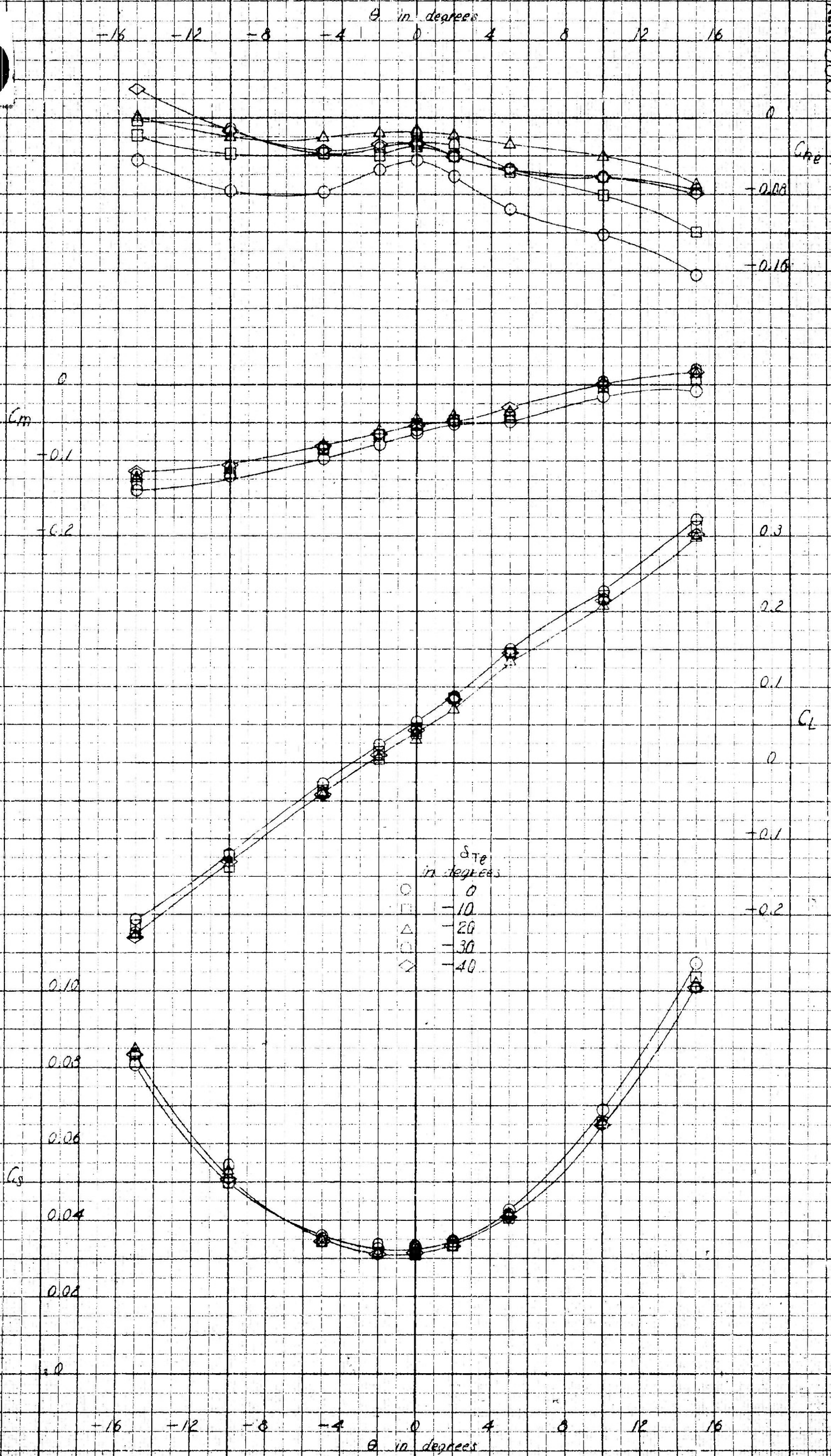


FIGURE 14 h

Figure 14 (Concluded)
(h) Configuration BC(HV)_{4h}, $S_e = 20^\circ$

CONFIDENTIAL

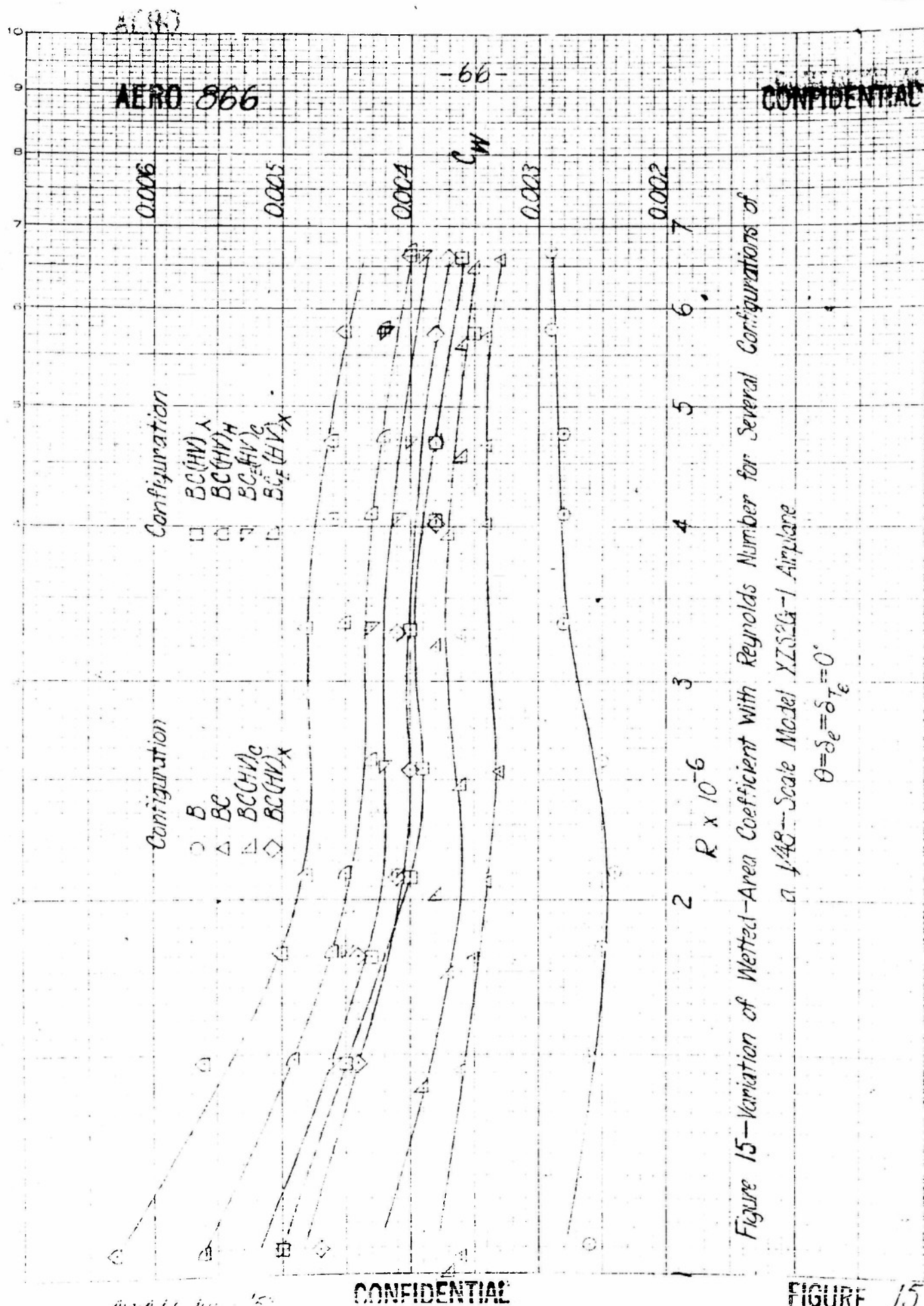


Figure 15—Variation of Wetted-Area Coefficient With Reynolds Number for Several Configurations of

a 1/48--Scale Model YZSG-1 Airplane

$$\theta = \delta_e = \delta_T = 0^\circ$$

a Axial Distance
 L Total Length
 r Radius at Point of Interest
 r_0 Maximum Radius

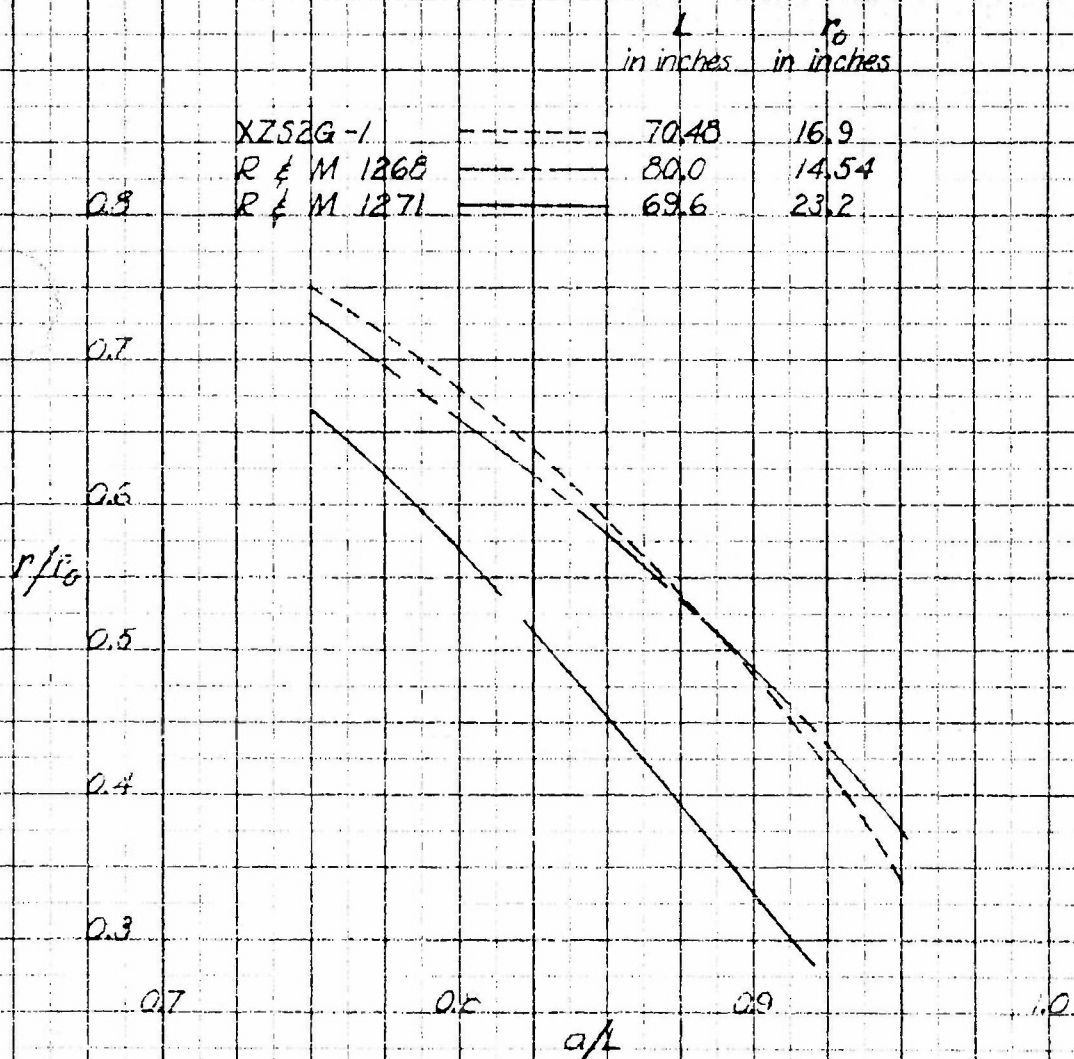


Figure 16—Comparison of Body Geometry of Several Airship Envelopes

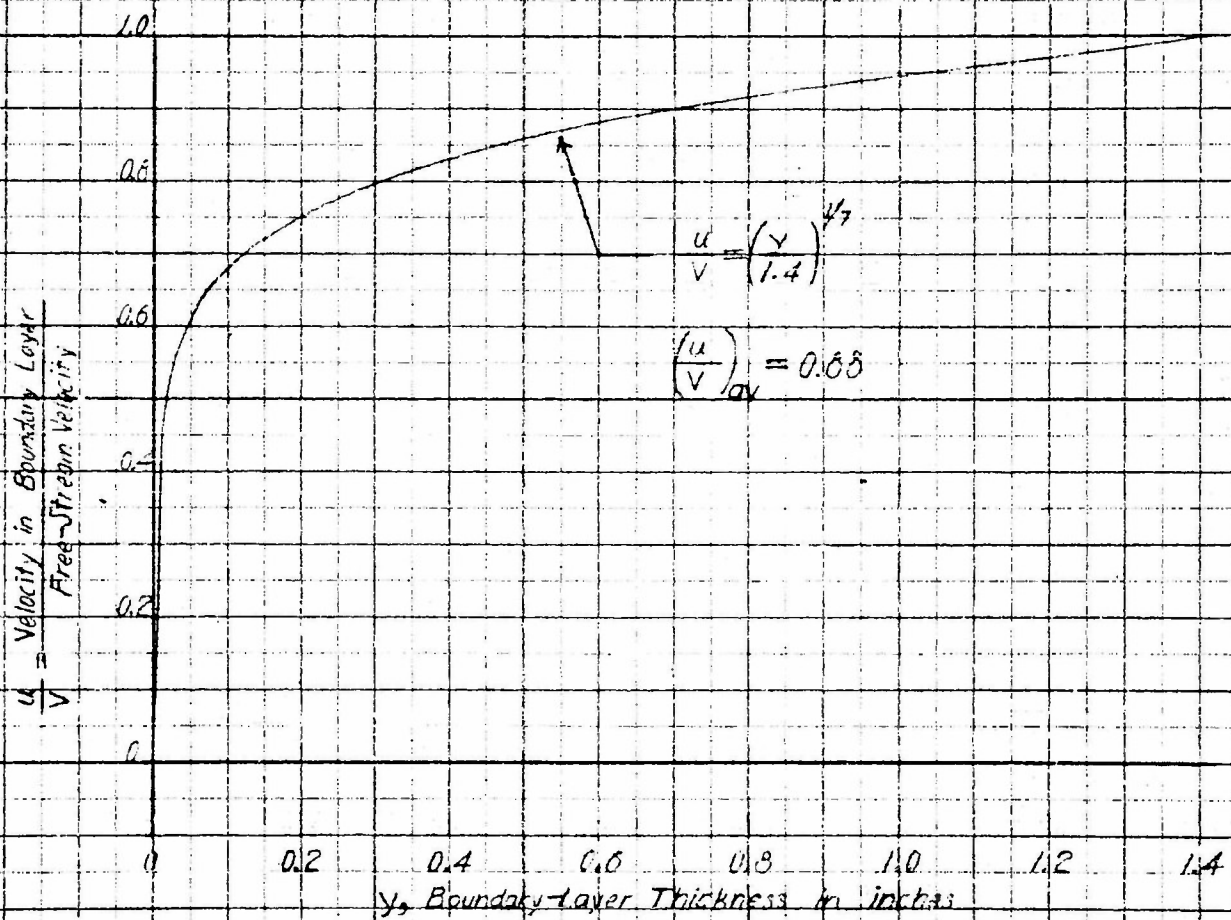


Figure 17-Velocity of Air in Boundary Layer of an Airship

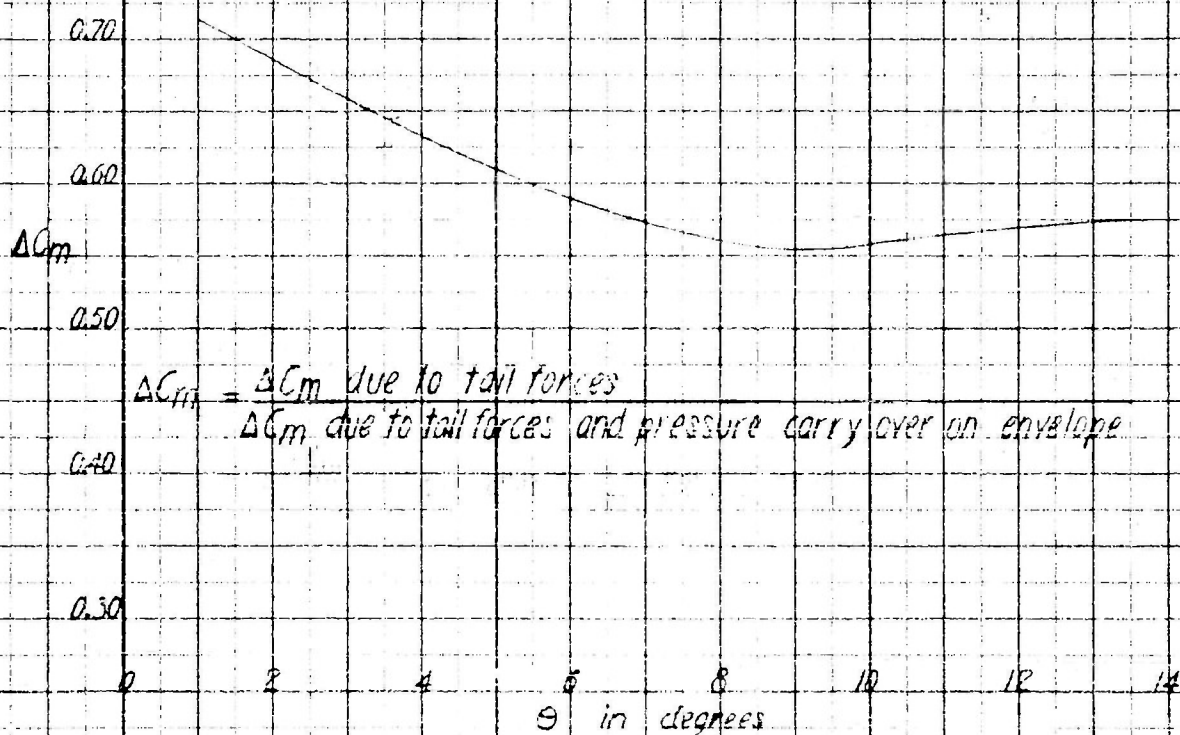


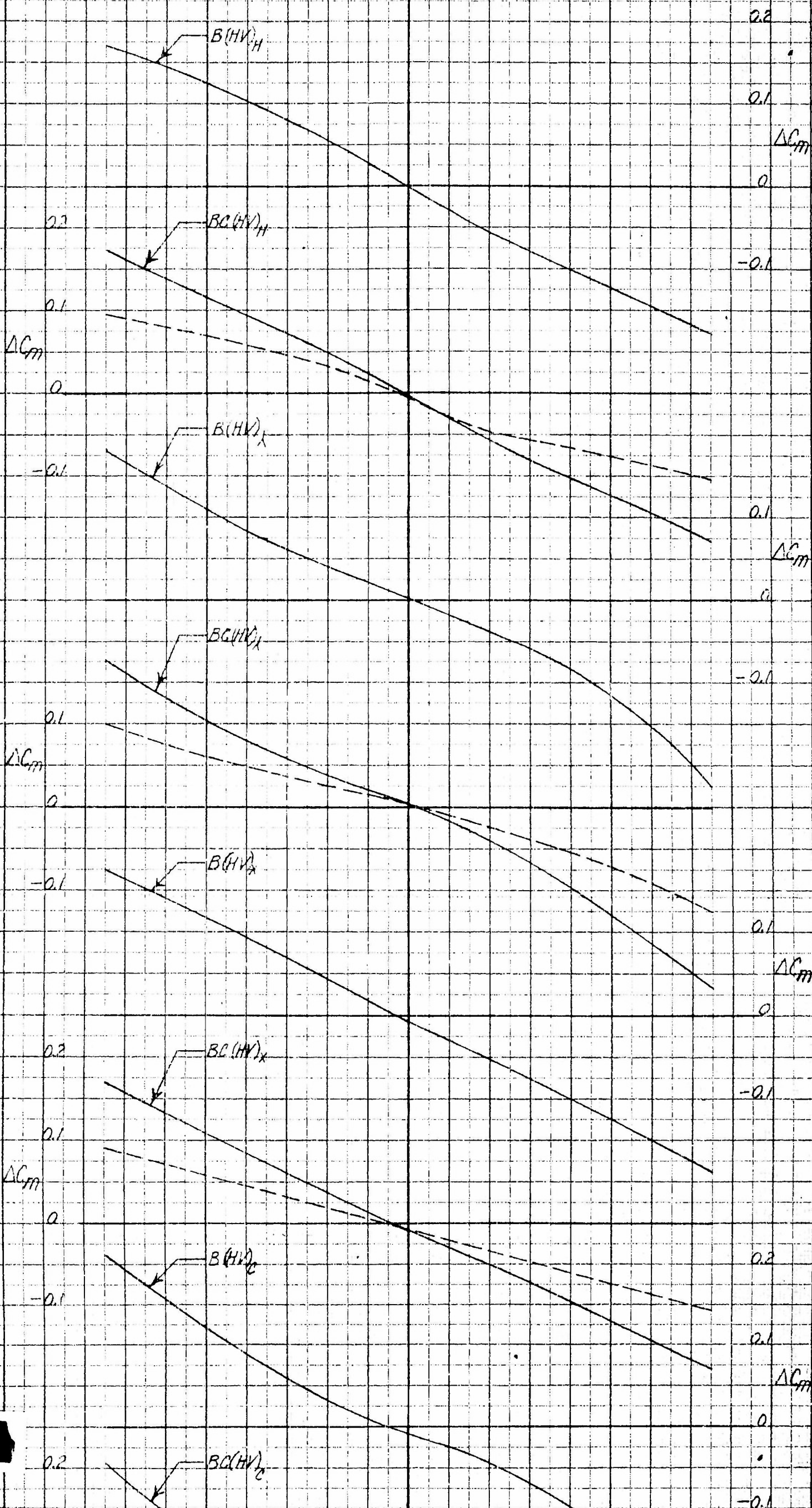
Figure 18- Pitching Moment Directly Attributable to the Tail of an Airship

AERO 866

θ in degrees

-16 -12 -8 -4 0 4 8 12 16

AVIA 16 JUL 1952



CONFIDENTIAL

CONFIDENTIAL

2

CONFIDENTIAL

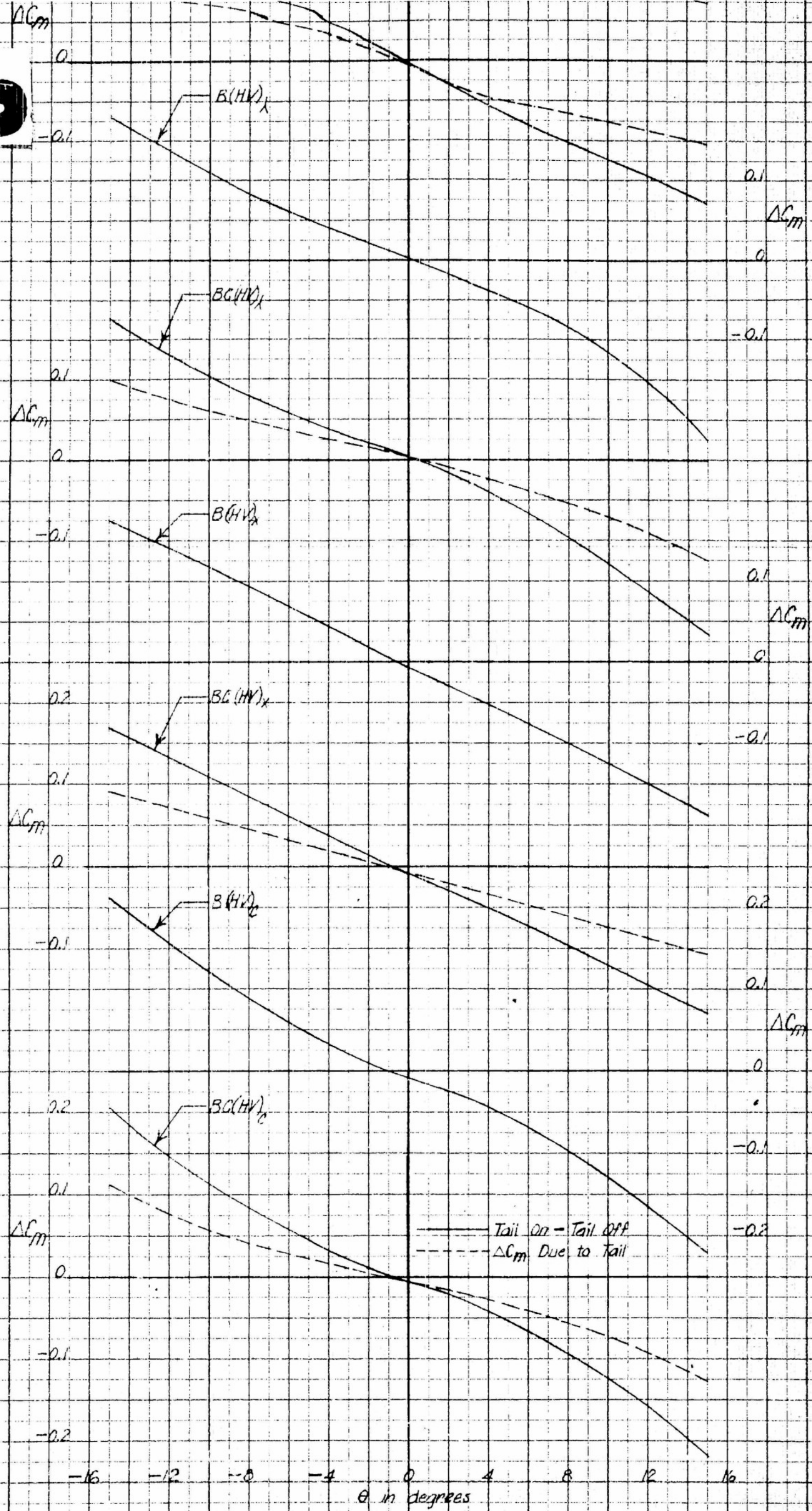


FIGURE 19

Figure 19 - Pitching Moment Due to Tail on a 1/48 Scale Model XZS2G-1 Airship
 $\delta_e = \delta_T = 0^\circ$

CONFIDENTIAL

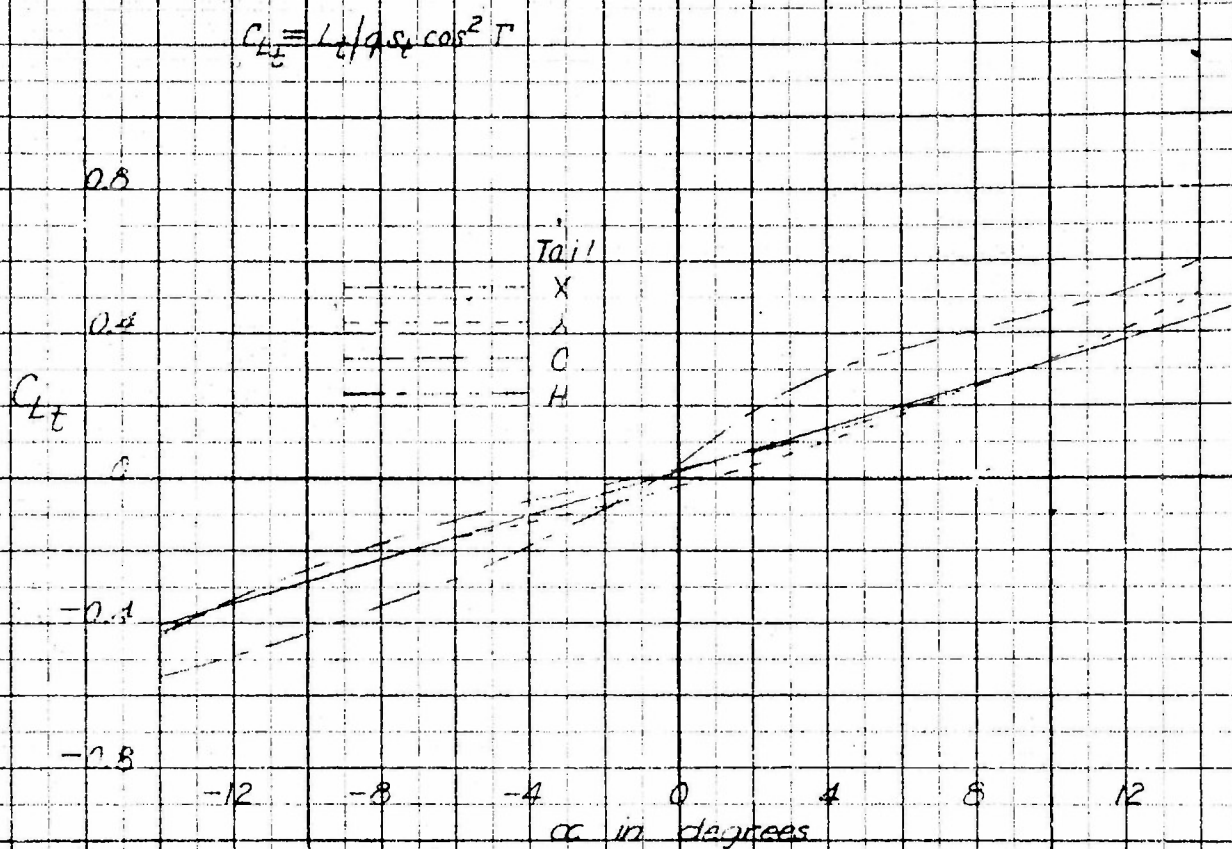


Figure 20—Tail-Lift Coefficients for the Various Tails
on a 1/48-Scale Model XZS26-1 Airship

$$\delta_e = \delta_{T_e} = 0^\circ$$

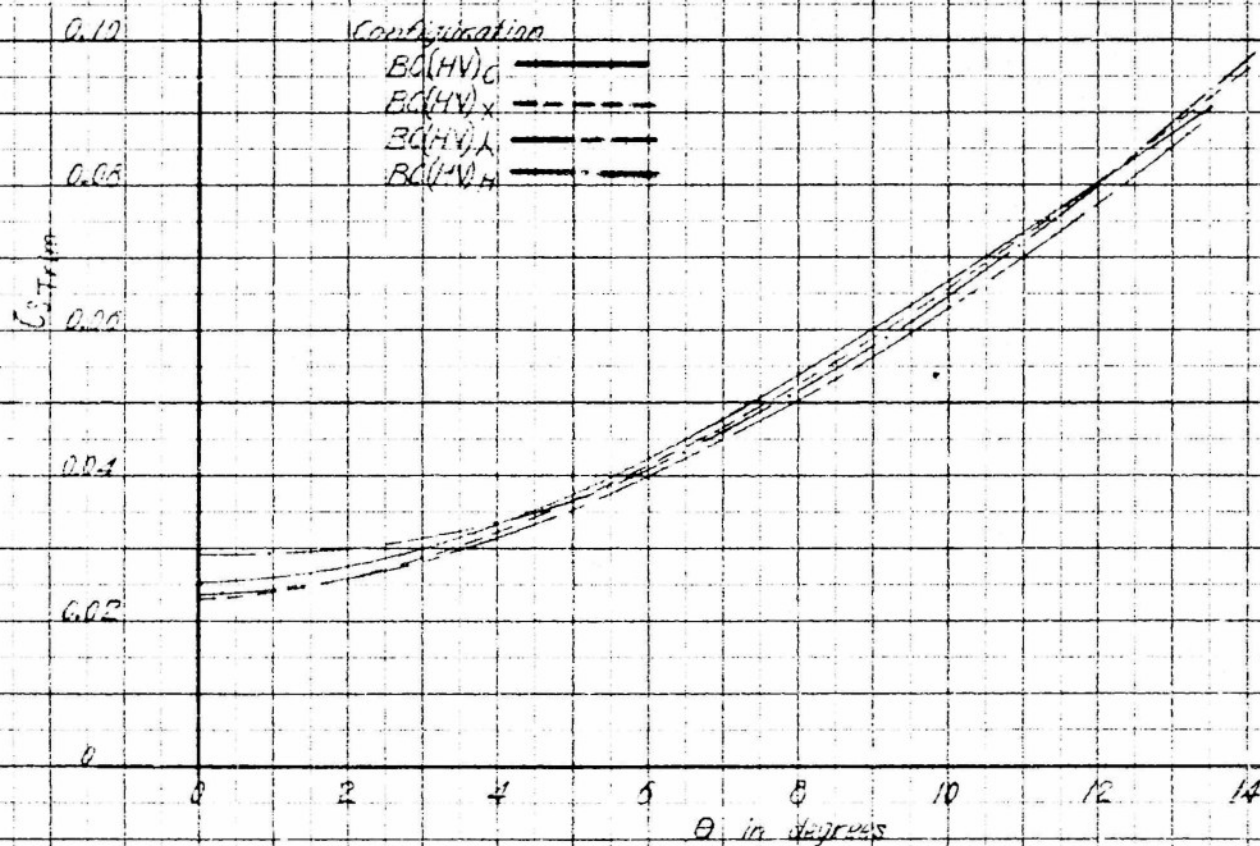


Figure 21-Variation of Drag With Pitch for Trim Condition of a
1/48-Scale Model XZSEG-1 Airship

$$\delta_{\theta} = 0^{\circ}$$

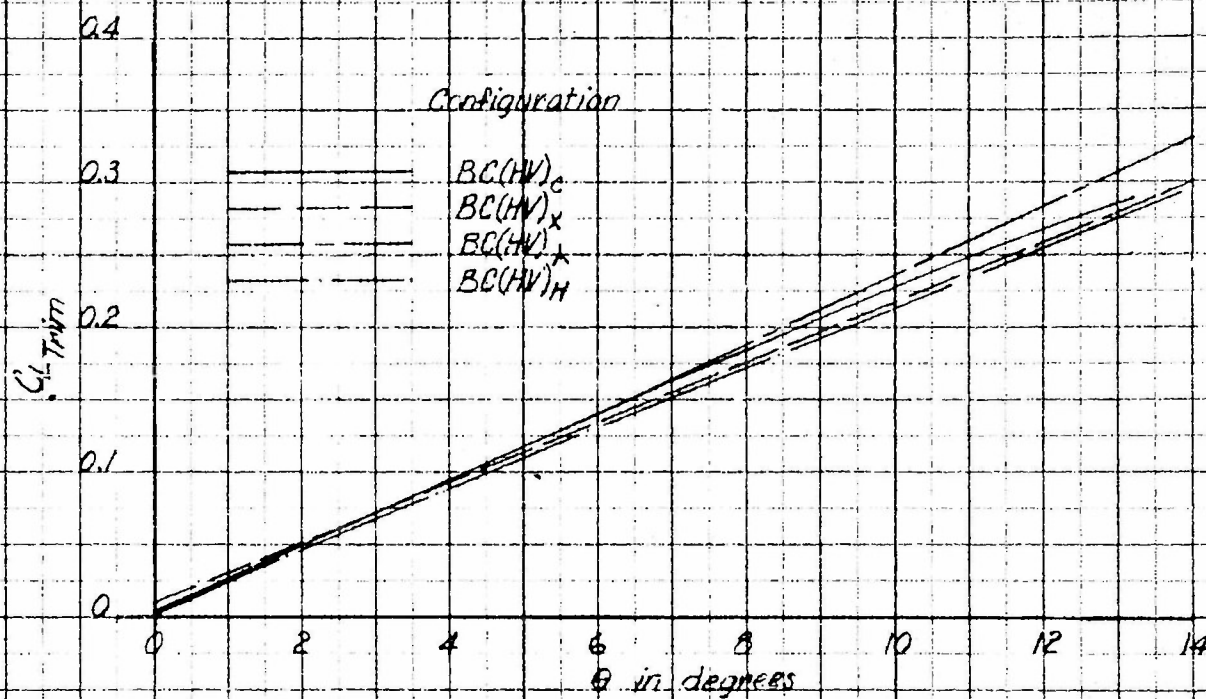


Figure 22-Variation of Lift With Pitch for Trim Condition of a 1/48-Scale

Model XZS2G-1 Airship

$$\delta T_e = 0^\circ$$

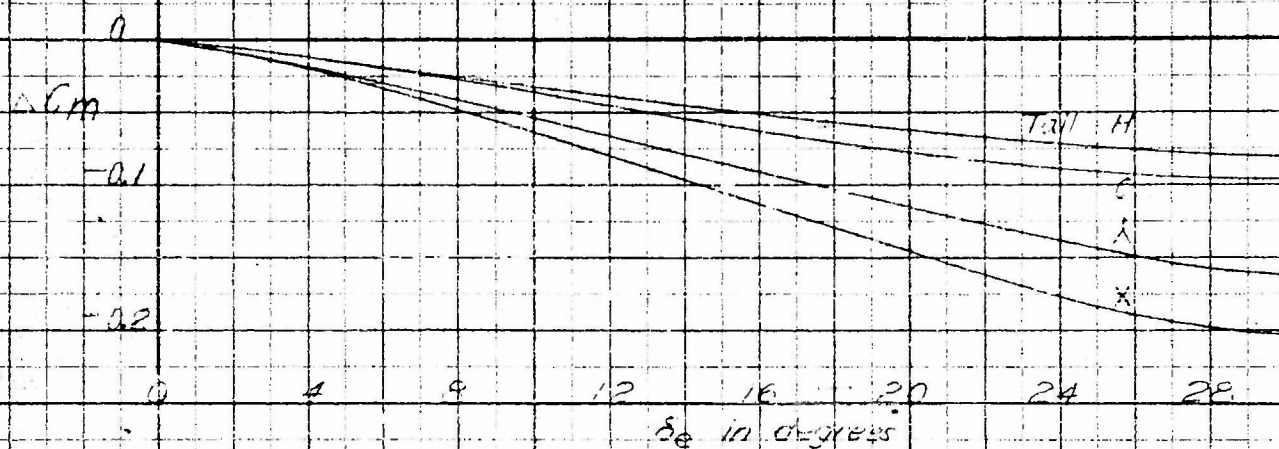


Figure 23 - Pitching Moment Due to Elevator Deflection

on a 1/48-Scale Model XZS2G-1 Airship

(a) Can Off, $\theta = \delta_{Te} = 0^\circ$

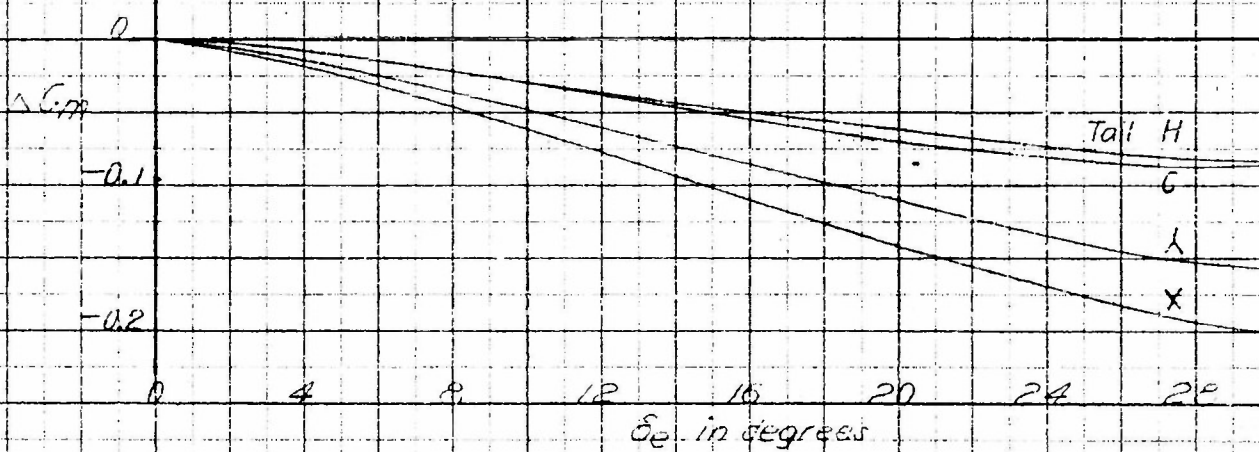


Figure 23 (Concluded)
(b) Car On, $\theta = \delta_{Te} = 0^\circ$

Configuration
 BC17V1F
 BC17V1C
 BC17V1X
 BC17V1X

$\delta = -5^\circ$
 $\delta = 0^\circ$
 $\delta = -5^\circ$
 $\delta = 0^\circ$

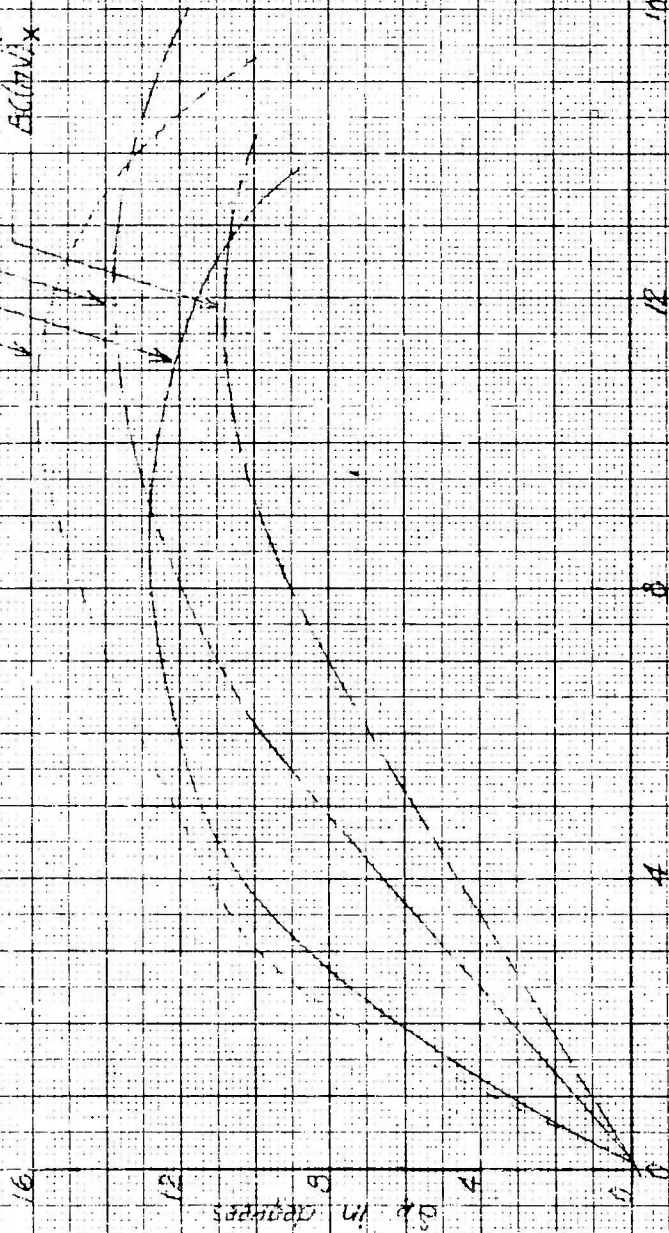


FIGURE 24 - Elevator Angle Required for Trim over V48 - Scale Model XZ526-1 Aircraft

AERO 866

-77-

CONFIDENTIAL

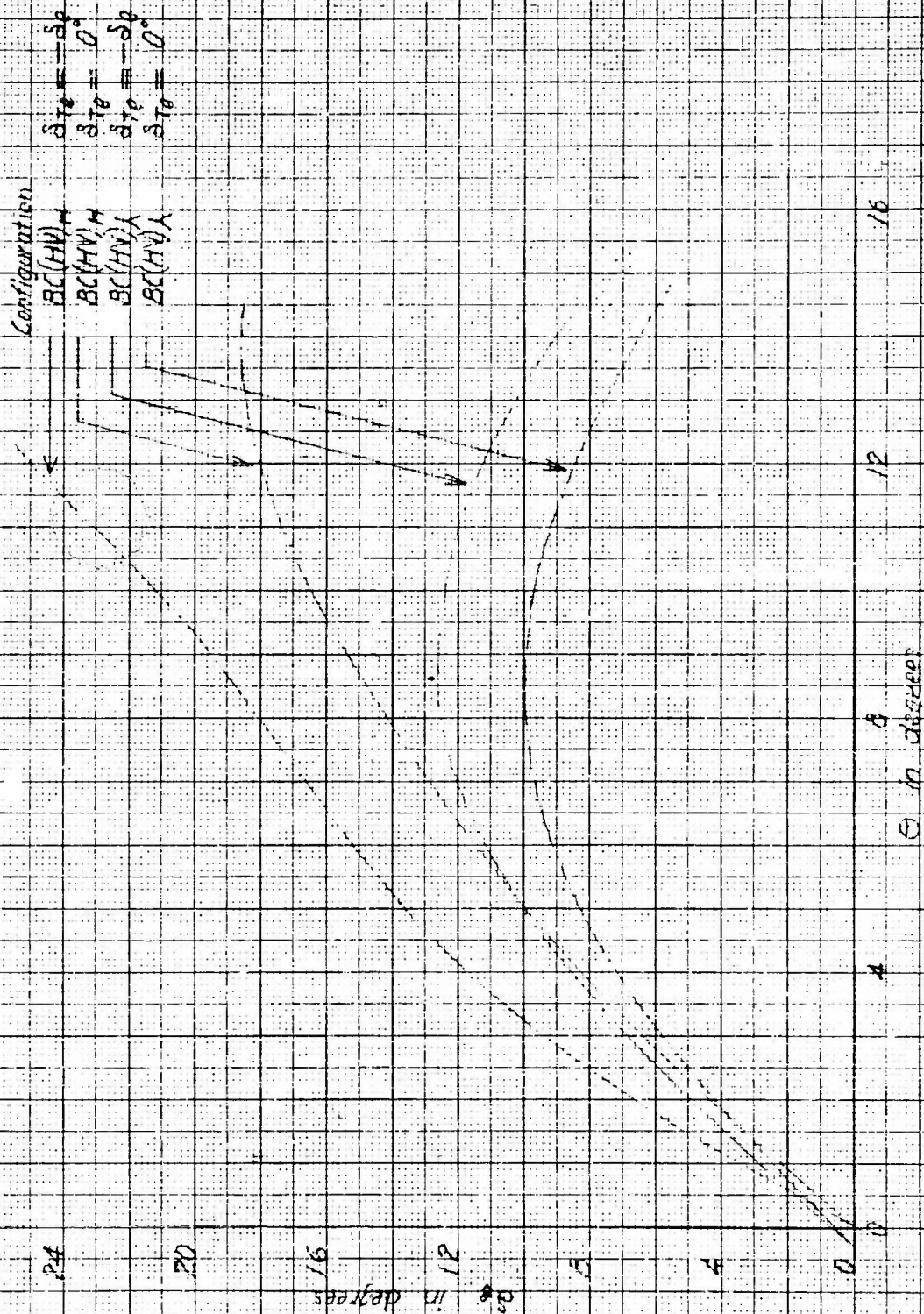
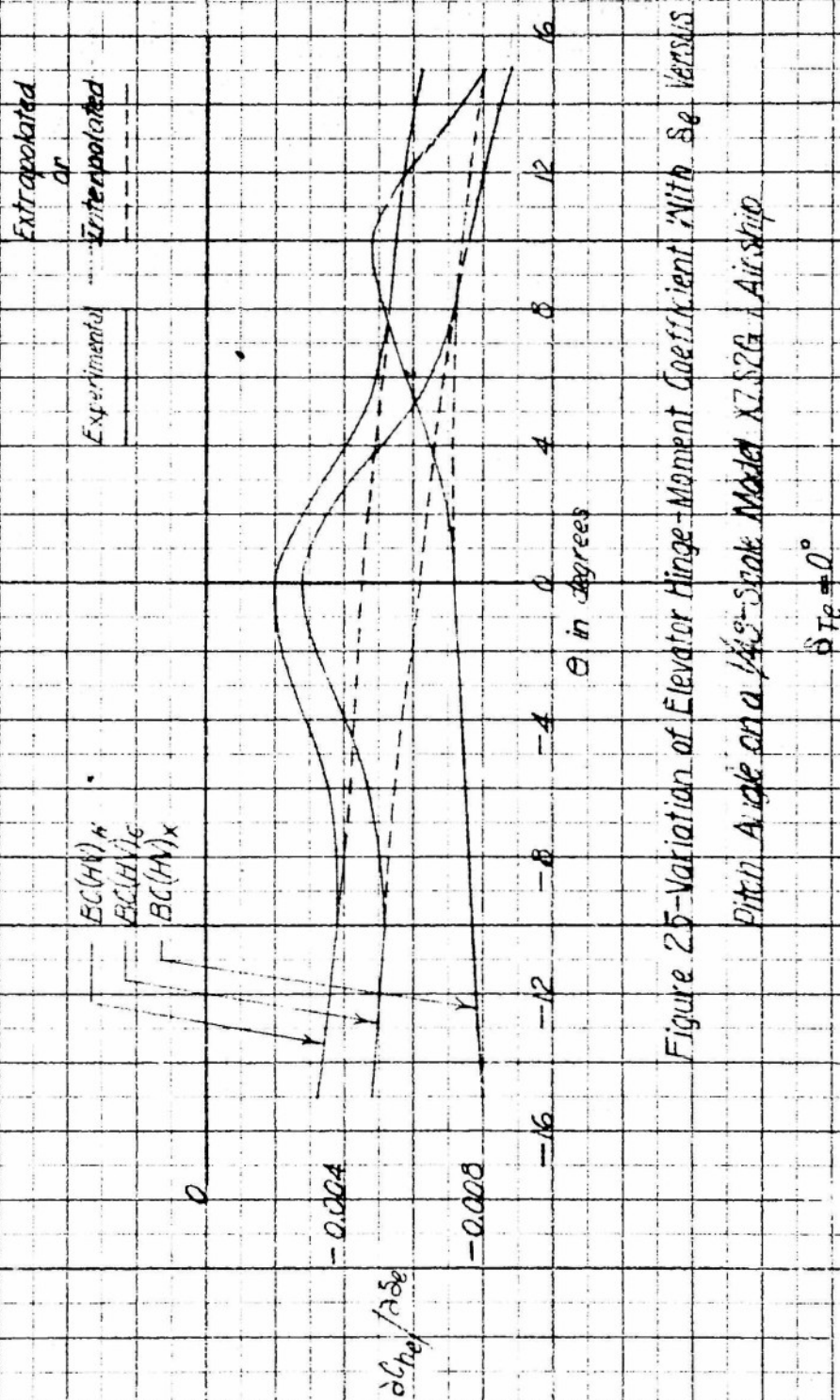


Figure 24 (Concluded)

ANA 16 June 52

CONFIDENTIAL

FIGURE 24 (concl)



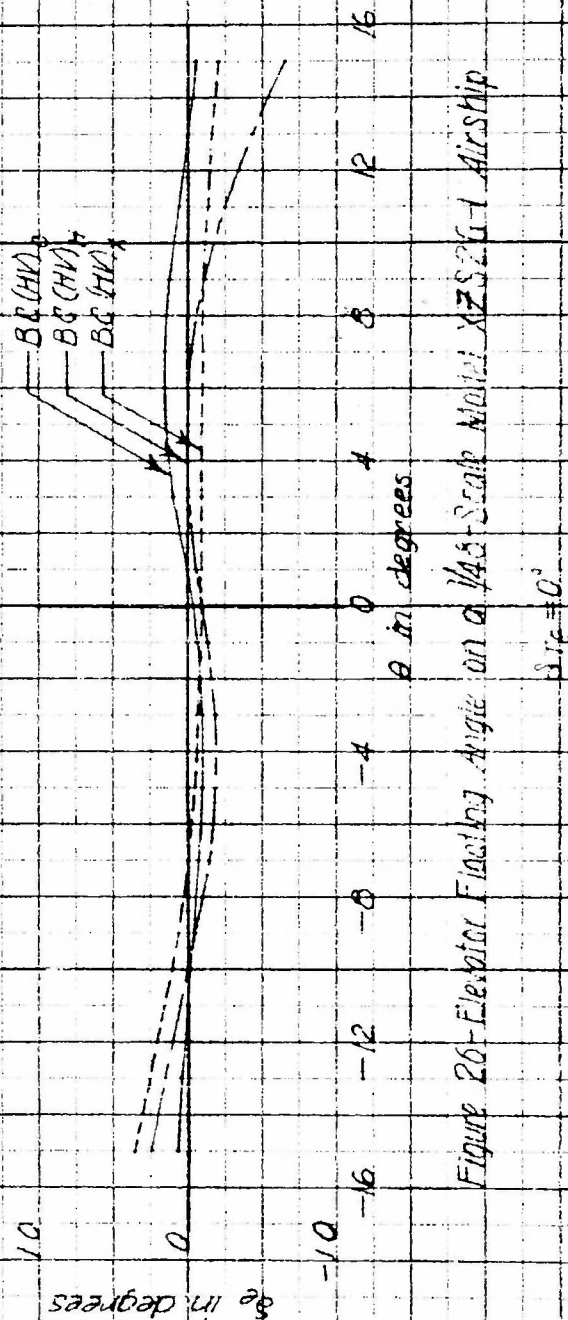


Figure 26-Elevator Finishing Angle on a 1/45 Scale Model XF5G-1 Airship

AERO 805

-80-

CONFIDENTIAL

Configuration
 $\delta T_e = -\delta e$
 $\delta T_e = -\delta e$
 $\delta T_e = -\delta e$
 $\delta T_e = 0$
 $\delta T_e = 0$
 $\delta T_e = 0$

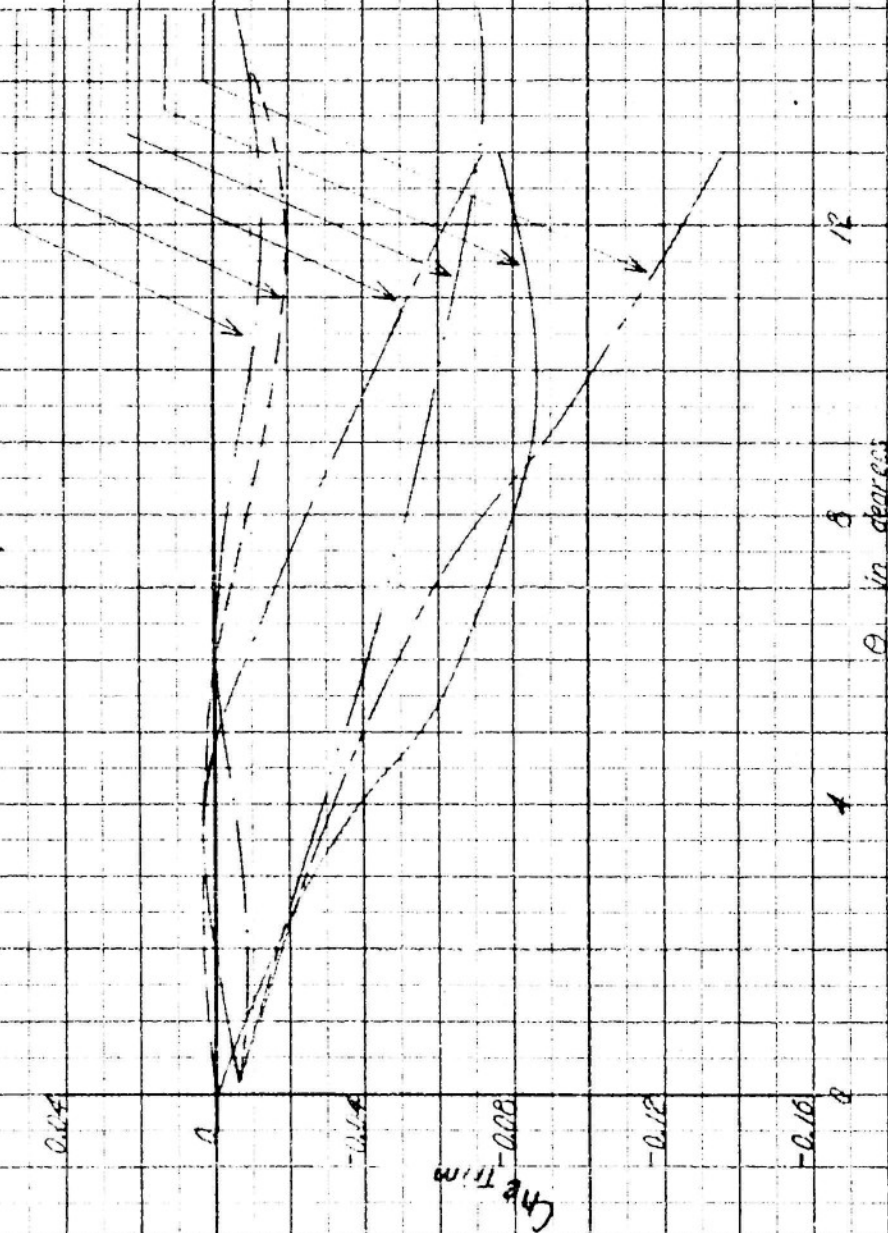
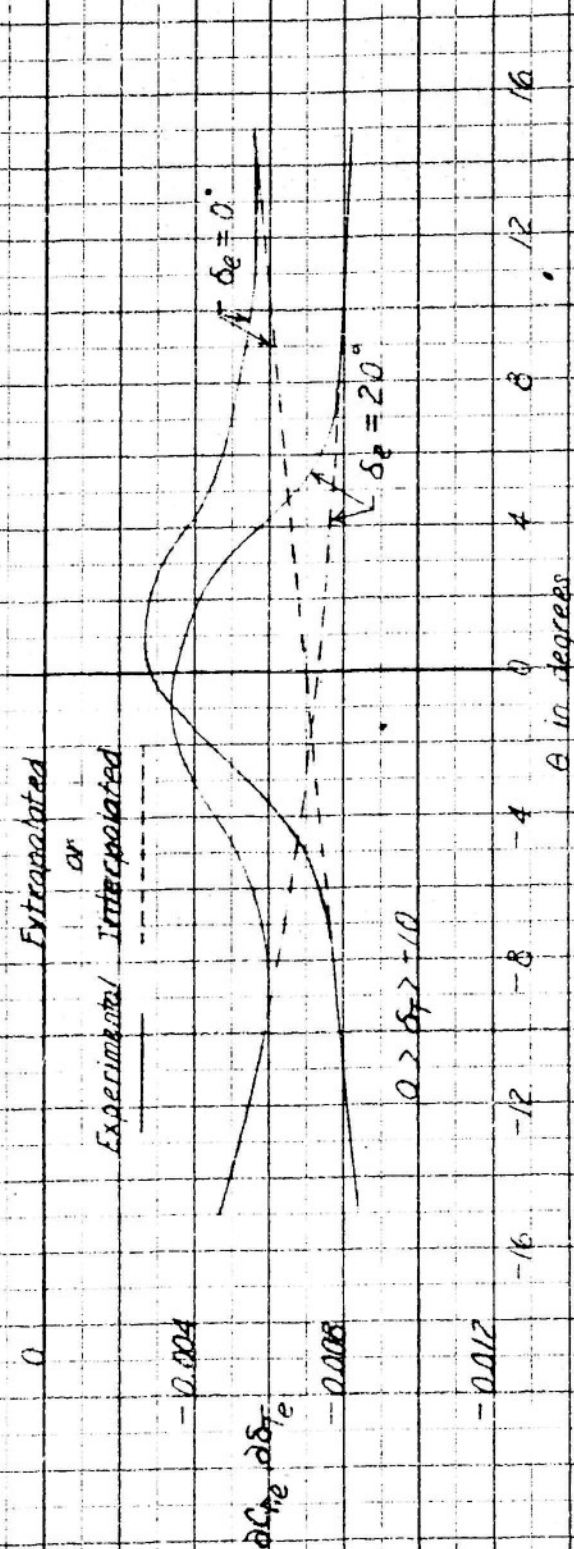


Figure 27-Elevator Hinge Moment Required for Trim on a 1/48-Scale Model XZ526-1 Airship

APR 17 June 52

CONFIDENTIAL

FIGURE 27

Figure 28 - Variation of Elevator Hinge - Moment Coefficient With δ_e

Versus Pitch Angle on a 1/4 Scale Model at 7.523 - 1 Airship

(a) Configuration BCFH46

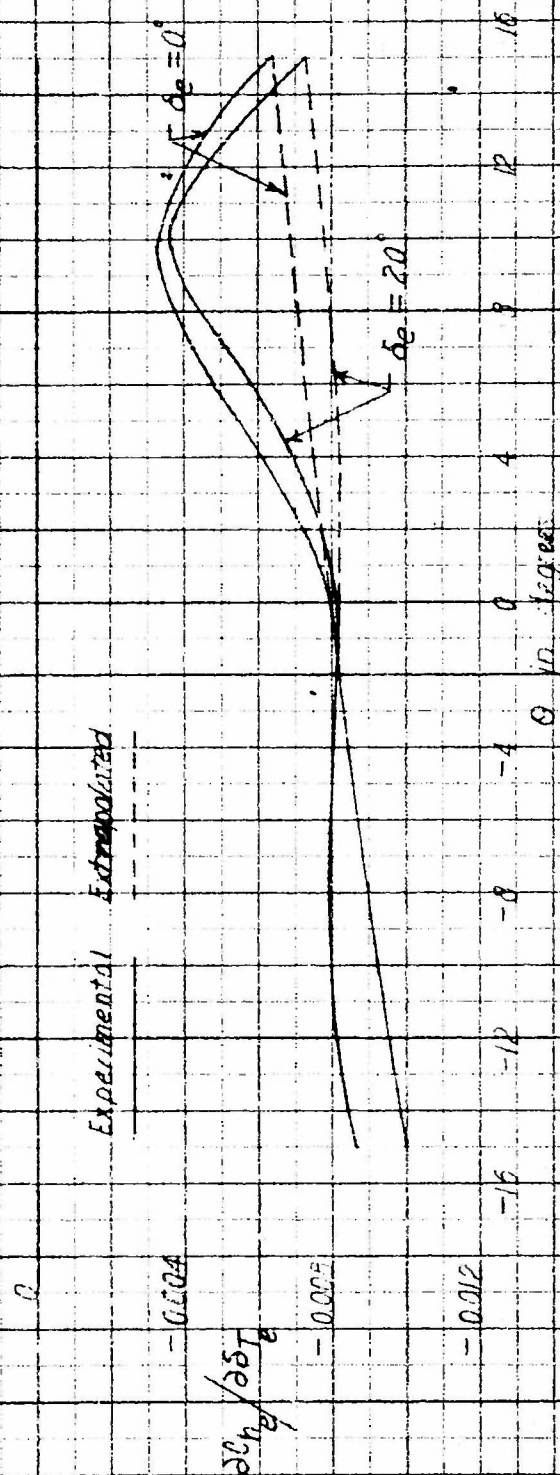


Figure 28 (Continued)
(b) Configuration BC/HVX

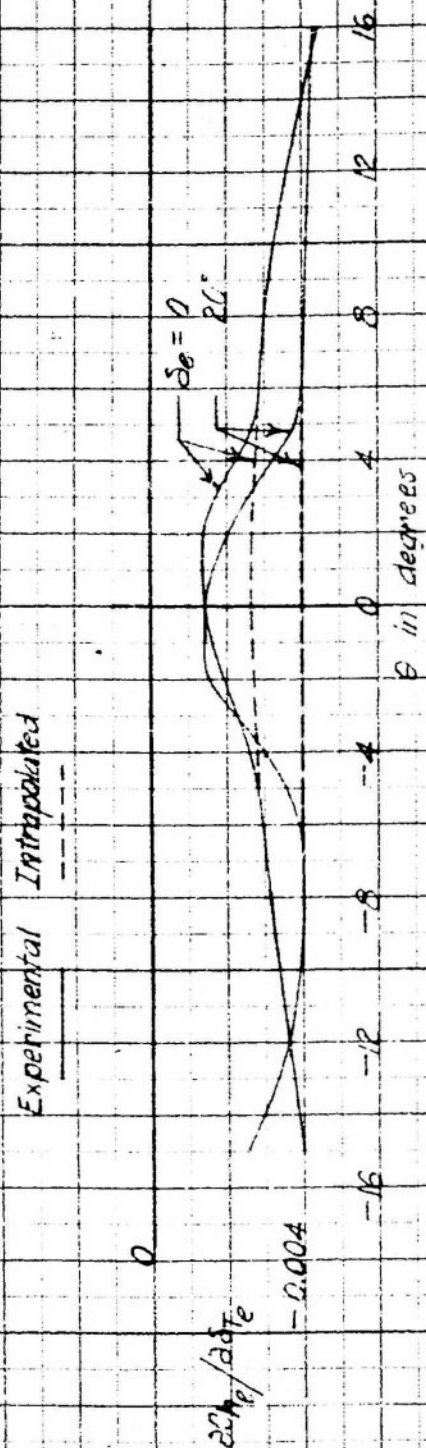


Figure 28 (continued)

Configuration BC (H/V)

<p>DTMB Aero Rpt 366 Pt I</p> <p>David W. Taylor Model Basin</p> <p>WIND-TUNNEL TESTS OF A 1/48-SCALE MODEL OF THE X-2526-1 AIRSHIP WITH VARIOUS TAIL CONFIGURATIONS. PT. I: LONGITUDINAL AND DRAG CHARACTERISTICS, by Arnold W. Anderson & Samuel J. Flickinger, Jr. Sep 1954. 83 p. incl. illus. 15 refs. (Aerodynamics Lab. Aero Test A-283. TED TMB AD-3113)</p> <p>CONFIDENTIAL</p> <p>Tests made to investigate aerodynamic characteristics of four basic tail-envelope configurations & effect on characteristics of two car-radome combinations. They included force-coefficient results on entire model due to model pitch, elevator deflection, and elevator-tail deflection. Elevator hinge moment data were also taken for above variations.</p>	<p>CONFIDENTIAL</p> <p>1. AIRSHIPS (GOODYEAR 2526-1) 2. RADOMES</p> <p>I. Anderson, Arnold W. II. Flickinger, Samuel J. III. DTMB Aero Test A-283</p>	<p>DTMB Aero Rpt 866 Pt I</p> <p>David W. Taylor Model Basin</p> <p>WIND-TUNNEL TESTS OF A 1/48-SCALE MODEL OF THE X-2526-1 AIRSHIP WITH VARIOUS TAIL CONFIGURATIONS. PT. I: LONGITUDINAL AND DRAG CHARACTERISTICS, by Arnold W. Anderson & Samuel J. Flickinger, Jr. Sep 1954. 83 p. incl. illus. 15 refs. (Aerodynamics Lab. Aero Test A-283. TED TMB AD-3113)</p> <p>CONFIDENTIAL</p> <p>Tests made to investigate aerodynamic characteristics of four basic tail-envelope configurations & effect on characteristics of two car-radome combinations. They included force-coefficient results on entire model due to model pitch, elevator deflection, and elevator-tail deflection. Elevator hinge moment data were also taken for above variations.</p>	<p>CONFIDENTIAL</p> <p>1. AIRSHIPS (GOODYEAR 2526-1) 2. RADOMES</p> <p>I. Anderson, Arnold W. II. Flickinger, Samuel J. III. DTMB Aero Test A-283</p>
<p>DTMB Aero Rpt 366 Pt I</p> <p>David W. Taylor Model Basin</p> <p>WIND-TUNNEL TESTS OF A 1/48-SCALE MODEL OF THE X-2526-1 AIRSHIP WITH VARIOUS TAIL CONFIGURATIONS. PT. I: LONGITUDINAL AND DRAG CHARACTERISTICS, by Arnold W. Anderson & Samuel J. Flickinger, Jr. Sep 1954. 83 p. incl. illus. 15 refs. (Aerodynamics Lab. Aero Test A-283. TED TMB AD-3113)</p> <p>CONFIDENTIAL</p> <p>Tests made to investigate aerodynamic characteristics of four basic tail-envelope configurations & effect on characteristics of two car-radome combinations.</p>	<p>CONFIDENTIAL</p> <p>1. AIRSHIPS (GOODYEAR 2526-1) 2. RADOMES</p> <p>I. Anderson, Arnold W. II. Flickinger, Samuel J. III. DTMB Aero Test A-283</p>	<p>DTMB Aero Rpt 366 Pt I</p> <p>David W. Taylor Model Basin</p> <p>WIND-TUNNEL TESTS OF A 1/48-SCALE MODEL OF THE X-2526-1 AIRSHIP WITH VARIOUS TAIL CONFIGURATIONS. PT. I: LONGITUDINAL AND DRAG CHARACTERISTICS, by Arnold W. Anderson & Samuel J. Flickinger, Jr. Sep 1954. 83 p. incl. illus. 15 refs. (Aerodynamics Lab. Aero Test A-283. TED TMB AD-3113)</p> <p>CONFIDENTIAL</p> <p>Tests made to investigate aerodynamic characteristics of four basic tail-envelope configurations & effect on characteristics of two car-radome combinations.</p>	<p>CONFIDENTIAL</p> <p>1. AIRSHIPS (GOODYEAR 2526-1) 2. RADOMES</p> <p>I. Anderson, Arnold W. II. Flickinger, Samuel J. III. DTMB Aero Test A-283</p>

UNCLASSIFIED

UNCLASSIFIED